DEVELOPMENT OF A NOVEL IN VITRO MODEL SYSTEM TO CHARACTERIZE THE ROLE OF ACTIVITY IN MOTOR NEURONS DURING DEVELOPMENT AND DISEASE

by

Erin K. Aubrey

Submitted in partial fulfilment of the requirements
for the degree of Master of Science

at

Dalhousie University
Halifax, Nova Scotia
April 2016

Experience is simply the name we give our mistakes
-*Oscar Wilde*

TABLE OF CONTENTS

LIST OF TABLES

LIST OF FIGURES

ABSTRACT

Neural activity modulates motor axon guidance and synaptic function during development. Differences in neural activity also contribute to the demise of specific motor neuron subtypes in amyotrophic lateral sclerosis (ALS). Studying the cellular mechanisms underlying these activity-dependent processes is complicated due to the inability to precisely activate motor neurons separate from other cell types. Here, we resolve this issue by generating embryonic stem cell-derived motor neurons (ESCMNs) expressing channelrhodopsin-2 (ChR2). ChR2 ESCMNs depolarize and fire single action potentials when pulsed by light. Chronic light activation of ChR2 ESCMNs (0.025 Hz for 2 days) increases neurite outgrowth, mediated by enhanced expression of polysialylated NCAM (PSA-NCAM). ChR2 ESCMNs expressing SOD1G93A, a mutation causing ALS, form neuromuscular junctions in vitro, but unlike wild-type counterparts, fail to maintain functional connections over time. Together, this thesis introduces a novel model system to study cellular mechanisms underlying activity-dependent modulation of motor neuron development and disease.

LIST OF ABBREVIATIONS USED

ACh	Acetylcholine
AChR	Acetylcholine receptor
ALS	Amyotrophic lateral sclerosis
AP	Action potential
BDNF	Brain-derived neurotropic factor
BMP	Bone morphogenetic protein
BTX	Bungarotoxin
CAM	Cell adhesion molecule
CNTF	Ciliary neurotrophic factor
Cre	Causes recombination
DIV	Days in vitro
dTC	D-Tubocurare
E	Embryonic day
eGFP	Enhanced green fluorescent protein
Endo-N	Endoneuraminidase-N
EPP	Endplate potential
ESC	Embryonic stem cell
ESCMN	Embryonic stem cell derived motor neurons
FACS	Fluorescence activated cell sorter
FES	Functional electrical stimulation
FGF	Fibroblast growth factor
FGFR1	Fibroblast growth factor receptor
FN	Fibronectin
GABA	Gamma-aminiobutyric acid
GDNF	Glial cell-derived neurotrophic factor
GF	Growth factor
GFP	Green fluorescent protein
Hb9	Homeobox gene 9
hESCMN	Human embryonic stem-cell derived motor neuron
HH	Hamburger Hamilton
HMC	Hypaxial motor column
ICM	Inner cell mass
Ig	Immunoglobulin
iPSC	Induced pluripotent stem cell
LMC	Lateral motor column
m	Quantal content
mEPP	Miniature endplate potential
MC	Motor column
MMC	Medial Motor column
MMCMNs	Medial motor column motor neurons
MN	Motor neuron
MND	Motor neuron disease
MU	Motor unit

NCAM	Neural cell adhesion molecule
NMJ	Neuromuscular junction
ns	Not statistically significant
PBS	Phosphate buffered saline
PMC	Preganglionic motor column
pMN	Motor neuron progenitor domain
PSA	Polysialic acid
RA	Retinoic acid
SAG	Smoothened agonist
SC	Spinal Cord
Shh	Sonic hedgehog
SOD1	Superoxide dismutase 1
SV2	Synaptic vesicle protein 2
TTX	Tetrodotoxin
WT	Wild-type
YFP	Yellow fluorescence protein

ACKNOWLEDGEMENTS

Thank you to Dr. Victor Rafuse for taking me into your lab and teaching me to be curious. I would also like to thank my committee members; Dr. Ying Zhang, Dr. Jim Fawcett and Dr. Bill Baldridge. Thank you to Dr. Angelo Iulianella for years ago for giving me my first chance to experience research. To the Department of Medical Neuroscience I would like to thank all the students, faculty and staff who made it a great environment to work in every day.

Thank you to the members of the Rafuse Lab (both past and present) for providing guidance, support and wisdom – without you this would not have been possible. Cindee Leopold, to whom I owe a great deal for her technical expertise and without whom I would have been completely lost, for even longer. Steve Whitefield thank you for all your help.

To my family thank you for your constant support and patience with me. Thank you to my friends, even to those further away, for always being there or on the other end of the phone at the end of the day.

Finally, I would like to thank Jamie Murphy for his love, support and enormous amounts of patience with me throughout this journey.

CHAPTER 1: INTRODUCTION

Neural activity modulates motor axon guidance and synaptic function during development. Differences in neural activity also contribute to the demise of specific motor neuron subtypes in amyotrophic lateral sclerosis (ALS). Studying the cellular mechanisms underlying these activity-dependent processes is complicated due to the inability to precisely activate motor neurons separate from other cell types. Activity-dependent processes can be studied in a simplified environment using the model introduced in this thesis. I will first give a brief background surrounding motor neuron development, motor neuron disease, the role of activity in development and disease, in vitro modeling and optogenetics.

Development of Spinal Motor Neurons

Over a century ago, Sherrington described motor neurons as the final common pathway in the induction of movement, bridging the nervous system to skeletal muscle (Albright et al., 2000). Since then the spinal motor neuron has become the most extensively studied cell in the mammalian nervous system, responsible for innervating skeletal muscle and inducing contractions (Kernell, 2006, reviewed by Chipman et al., 2012). Motor neurons and every cell in the body originate from three principle germ layers. The ectoderm, the outer most layer, gives rise to all major tissues of the central and peripheral nervous system along with the epidermis. Neural induction in the ectoderm results in the formation of the neural tube, a structure that gives rise to the brain and spinal cord. Rostral-caudal poles are established along the axis of the neural tube. Caudalization of the neural tube occurs when surrounding somites secrete the morphogen

all-*trans*-retinoic acid (RA) (Durston et al., 1998; Muhr et al., 1999; Wilson and Edluns, 2001). The caudalizing effects of RA was demonstrated in studies using *Xenopus* embryos where RA treatment, during neural tube formation, was shown to promote enlarged spinal cord formation at the expense of forebrain development (Durston et al., 1989).

Dorsal-ventral polarity is also established within the neural tube. Sonic hedgehog (Shh) is a morphogen released from the floor plate and the notochord resulting in patterning of ventrally located progenitor domains (Placzek et al., 1991; Yamada et al. 1993; reviewed by Alaynick et al., 2011). Both the notochord and the floor plate were shown to induced ectopic expression of motor neuron genesis when placed near the dorsal region of the developing chick spinal cord (Yamada et al., 1991, Placzek et al., 1991; reviewed by Chipman et al., 2012).

Along the dorsal-ventral (D-V) axis in the developing spinal cord at embryonic day 9.5 (e9.5) in the mouse there are 12 defined progenitor domains (reviewed by Alaynick et al., 2011). Each domain is responsible for the generation of particular post-mitotic cells and is defined by the expression of specific transcription factors (Jessell 2000, Briscoe and Ericson, 2001; Lee and Pfaff, 2001). The most ventral domain next to the floor plate is p3 defined by both Nkx2.2/2.9 and gives rise to V3 interneurons (Briscoe et al., 1999; Goulding et al., 2002). Dorsal to this is the motor neuron progenitor domain (pMN). Within pMN, Shh acts to up- regulate transcription factors that direct the expression of motor neuron factor consolidating genes such as Islet 1, Lhx3 and NeuN and Hb9 (Arber et al., 1999; Briscoe and Ericson, 2001; Novitch et al., 2001). The domains more dorsal to pMN give rise to interneurons that have various functions such as

processing sensory information (reviewed by Alaynick et al., 2011; Davis-Dunsenbery et al., 2014). Taken together, these results suggest that RA and Shh signaling are important morphogens directing differentiation of neural progenitors into motor neurons.

Later in development, motor axons exit the spinal cord via the ventral roots and project to specific muscle target(s). Motor neurons are divided into subtypes based on their anatomical origin and adult function (Landmesser and Morris 1975; Landmesser 1978a, b). Anatomically, vertebrate motor neurons are topographically arranged along the rostral-caudal axis into two discrete motor columns (Landmesser 1978 a, b; reviewed by Landmesser 1980; Sockanathan et al., 2003). The medial motor column (MMC) contains motor neurons that innervate dorsal epaxial muscles. Epaxial muscles are responsible for maintaining posture (Tsuchida et al., 1994). Limb muscles are innervated by motor neurons from the lateral motor column (LMC) (Landmesser, 1978 a, b; Hollyday 1980). These motor neurons can be subdivided into either medial LMC (LMC_M) that project to ventrally derived limbs or lateral LMC (LMC_L) that project to dorsally derived limbs (Landmesser, 1978; Hollyday 1980). Indeed, this dorsal-ventral (D-V) pathfinding choice represents one of the earliest binary decisions motor axons must take in order to subsequently innervate their correct muscle targets. Errors in this decision making process will unquestionably lead to motor axons mistargeting to incorrect muscles (see below).

Cell adhesion molecules

Cell adhesion molecules (CAMs) are a subset of cell surface macromolecules found throughout the body that control cell-cell interactions during nervous system development. CAMs can influence neuronal adhesion, migration, neurite outgrowth,

fasciculation, synaptogenesis and intracellular signaling (Fields and Itoh, 1996). CAMs have been implicated in activity dependent development; such that a neural impulse could regulate all of the processes listed above (Fields and Itoh, 1996; Rutishauser and Landmesser, 1996).

One of the first adhesion molecules to be associated with the development of the nervous system is the neural cell adhesion molecule or NCAM (Rutishauser et al., 1982). NCAM was first identified in the laboratory of Dr. Gerald Edelman, where it was shown to promote cell-to-cell adhesion and the appropriate organization of the chick retina (Thiery et al., 1977; Buskirk et al., 1980). Two of the main NCAM isoforms are comprised of a transmembrane intracellular domain of varying lengths. The third isoform is attached to a glycophosphatidylinositol anchor. All NCAM isoforms attach to two fibronectin domains (FN) and five Ig domains (Cunningham et al., 1987). The extracellular portions are relatively similar for all NCAM isoforms, all of which possess the ability to bind to other cell adhesion molecules via the Ig domains (Frei et al., 1992; Zhou et al., 1993; Horstkorte et al., 1993; Milev et al., 1994; Anderson et al., 2005). NCAM exists in three major isoforms throughout the nervous system and are named according to their molecular weights (kDa); NCAM180, 140, and 120 (Cunningham et al., 1987). Each isoform contributes differently to NCAM mediated functions (Edvardsen et al., 1993; Leshchyns'ka et al., 2003; Polo-Parada et al., 2004; Hata et al., 2007). Although all NCAM isoforms are expressed at the mouse NMJ (Rieger at al., 1985; Hamshere et al., 1991; Rafuse and Landmesser, 1996), NCAM 180 kDa and 140 kDa are expressed by motor axons (Rieger et al., 1985; Polo-Parada et al., 2005) while NCAM 120kD is predominately expressed by glial cells (Nobel et al., 1985; Bhat and Silberberg,

1986). Extracellular binding affinities can be altered by adding or removing NCAM from the cell surface via either exocytic or endocytoic mechanisms (Thelen et al., 2008; Yap et al., 2010; Chernyshova et al., 2011). In addition, the adhesive properties of NCAM can be modulated through the addition of polysialic acid (PSA) to its extracellular domain (Rutishauser and Landmesser 1996).

PSA is synthesized in the Golgi apparatus and is added to NCAM by posttranslational modification via polysialyltransferase enzymes PST (PST-1/ST8SiaIII) or STX (ST8SiaII) (Rutishauser, 1996). Each enzyme alone is sufficient to add chains of PSA to NCAM, although PSA synthesized by PST produces greater chain length then that produced by STX (Rutishauser, 1996). Furthermore, both enzymes can work cooperatively to produce a higher degree of polysialylation than either alone (Rutishauser, 1996). In the presence of Mn^{2+}, Mg^{2+}, or Ca^{2+} both enzymes are more efficient, where PST is more sensitive to changes in calcium concentration than STX (Rutishauser, 1996).

Chains of PSA attach to the fifth Ig domain of NCAM (Crossin et al., 1984). PSA on NCAM regulates cell-adhesion underlying synaptic plasticity (Muller et al., 1996; Eckardt et al., 2000; Dityatev et al., 2004), peripheral pathfinding (Tang et al., 1992; Franz et al., 2005) and terminal arborization (Landmesser et al. 1990; Rafuse and Landmesser, 2000). PSA can be experimentally removed from NCAM with endoneuraminadase (EndoN). Shortly after exiting the neural tube limb-innervating motor neurons up-regulate PSA and display a robust defasiciculation in the plexus region (reviewed by Rutishauser and Landmesser, 1996). Motor axons branch off from the primary nerve trunk and rearrange themselves into muscle specific fascicles. When

EndoN was used to remove PSA at this time during development, this rearrangement and defasciculation was prevented (Landmesser et al., 1990; Tang et al., 1992). Axons remained associated with each other and grew in parallel to the muscle thus compromising their ability to seek out correct muscle targets (reviewed by Rutushauser and Landmesser, 1996). Unpolysialyated NCAM can bind several molecules to influence the kinetics of outgrowth, specifically fibroblast growth factor receptors (FGFR) binding to the FN domain or glial derived neurotrophic factor (GDNF) molecules at the third Ig domain (Paratcha et al., 2003; Anderson et al., 2005; Kiselyov et al., 2005; Nielson et al., 2009; Chernyshova et al., 2011).

Activity in Motor Development

Early neuronal activity has been proposed to modulate several fundamental aspects of neural development such as the specification of function, transmitter identity, axon branching and connectivity within neural circuits (Borodinsky et al., 2004; Crisp et al., 2011; Landmesser et al., 2010; Marek et al., 2010; however see Myers et al., 2005; Varoqueaux et al., 2005; Benjumeda et al., 2013). For example, propagating waves of spontaneous, highly rhythmic electrical activity occurs along the neuraxis in the developing spinal cord in birds and mammals. These waves of activity cause near synchronous activation of motor neurons on either side of the spinal cord and occur as motor axons make their initial pathfinding decisions while exiting the neural tube (reviewed by Hanson et al., 2008). While the precise function of this rhythmic activity is not known, *in ovo* studies indicate that it is involved in motor axon pathfinding. This was shown by decreasing the frequency of depolarizing waves with picrotoxin, a $GABA_A$ receptor blocker. When the frequency of synchronous activation was slowed by

picrotoxin motor axons made D-V pathfinding errors as they entered the limb. These errors were correlated with a decreased expression of PSA-NCAM (Hanson and Landmesser, 2004). Recently, the same group demonstrated that pathfinding errors seen with the chronic picrotoxin treatment were not a result of altered $GABA_A$ receptor signaling (Kastanenka and Landmesser, 2010). They did so by electroporating the channelrhodopsin-2 (ChR2) gene into the neural tube of chick embryos, that were chronically treated with picrotoxin, in order to restore the normal frequency of synchronous activation using light pulses. When this was done they found that D-V pathfinding errors were prevented and PSA-NCAM levels remained that of the control values (Kastanenka and Landmesser, 2010).

When the frequency of the bursting was increased, by chronically treating chick embryos with the GlyT1 glycine transporter inhibitor, sarcosine (Eulenburg et al., 2005), D-V pathfinding was not altered, however, anteroposterior (A-P) pathfinding errors did occur (Hanson and Landmesser, 2006). Motor axons were able to target their correct muscles when activity was returned to normal levels if the errors had occurred in the plexus region (Hanson and Landmesser, 2006). In order to control for non-specific effects of sarcosine (used to increase bursting frequency) ChR2 was electroporated in ovo in order to depolarize motor neurons at twice the control frequency (Kastanenka and Landmesser, 2013). In this case, motor axons made appropriate D-V pathfinding decisions, but were unable to make pool-specific decisions (Kastanenka and Landmesser, 2013). Together, these results demonstrate that the developing neuromuscular system is highly sensitive to alternations in the patterns of spontaneous bursting. In a broader sense, these studies highlight the risk associated with drug intake during pregnancy that could

alter neuronal activity (e.g. nicotine from cigarettes) causing inappropriate formation of specific neuronal circuitries resulting in developmental defects.

The Neuromuscular Junction

The neuromuscular junction (NMJ) is a tripartite synapse comprised of a motor nerve terminal, muscle fibre and terminal Schwann cells (tSCs) (reviewed by, Sanes and Lichtman, 1999). During the formation of the NMJ the motor axon must transition from a growing cell responding to guidance signals to a highly specific structure transmitting electrochemical information. Transmission at the NMJ begins within minutes after motor axons contact muscle fibres (reviewed by, Sanes and Lichtman, 1999). However, this early form of transmission has low efficacy due to lack of nicotinic acetylcholine receptor (AChR) receptor density and low amounts of transmitter within each vesicle being released.

Muscle fibres are initially innervated by multiple motor axons at single endplates postnatally, but as the synapse matures all but one axon is eliminated. Neural activity influences this process such that blocking or increasing neural activity slows or speed up withdrawal of polyneuronal innervation, respectively (reviewed by: Sanes and Lichtman et al., 1999). During the same time period (1-2 weeks postnatally in mice) the morphology of AChRs at the endplate transitions form a small plaque like cluster to a large pretzel-shaped structure (reviewed by: Sanes and Lichtman, 1999). The cellular mechanisms governing this process are poorly understood, however the kinetics of AChR subunit stabilization, maturation and turn-over are all influenced by pre- and post-synaptic activity (Avila et al., 1989; Bezakova et al., 2001).

Neurotransmission

As pre and post-synaptic terminals mature the efficacy of neurotransmission improves. Neurotransmission at the NMJ begins when the motor neuron becomes depolarized above the threshold needed to fire an action potential. The action potential causes voltage-dependent calcium channels to open and calcium ions to flow into the cell. This influx of calcium causes synaptic vesicles to dock and fuse with the presynaptic membrane. Vesicles at the NMJ contain the excitatory neurotransmitter acetylcholine (ACh), an excitatory neurotransmitter at the NMJ. ACh released from vesicles into the synaptic cleft bind to nicotinic AChR on the muscle fibres leading to a depolarizing post-synaptic potential. When this reaches threshold an action potential is triggered that propagates down the muscle fibre leading to increased levels of calcium that activate subsequent muscle contraction.

Pioneering studies done in the laboratory of Dr. Bernard Katz in the 1950s were the first to demonstrate the phenomena of quantal neurotransmission (Kandel, 2000). Using the frog NMJ as a model system, they determined that presynaptic terminals package neurotransmitters into discrete quantal units. Additionally, they demonstrated that each quantal unit is released in a probabilistic manner into the cleft mediated by an action potential driven presynaptic calcium current (reviewed by: Kandel, 2000). Several years later it was found that the quantal units were packaged in synaptic vesicles and as a result of presynaptic excitation these vesicles function in an exo-endocytic cycling manner (Miller and Heuser, 1980). Quantal analysis can be performed to determine the amount of transmitter released from a single vesicle (quantal size), or the number of vesicles fusing with the presynaptic membrane as result of an action potential (quantal

content) (reviewed by Kandel: 2000). Single quanta are spontaneously released and can be recorded post-synaptically in the form of miniature end plate potentials (mEPPs) (reviewed by: Kandel, 2000). When multiple vesicles fuse presynaptically the resultant release of ACh opens several AChRs in the muscle membrane at the endplate. The resulting excitatory postsynaptic potential is known as an end plate potential (EPP). Normally, the EPP is large enough to trigger voltage gated sodium channels in the muscle membrane thereby converting the EPP into an action potential. The action potential is subsequently propagated along the T-Tubule network causing a release of calcium leading to excitation-contraction coupling in the skeletal muscle fibre (reviewed by: Kandel, 2000).

Motor Neuron Disease

Human neurodegenerative diseases represent a broad spectrum of progressive disorders that are without a cure and are marginally treatable. They cause degeneration and eventually death of nerve cells resulting in difficulties in movement (ataxias) or mental function (dementias). Motor neuron diseases (MNDs) are a subset of neurodegenerative diseases where motor neurons, or the nerves controlling them (e.g. upper motor neurons), degenerate. Amyotrophic Lateral Sclerosis (ALS) is a fatal adult-onset MND where motor neurons innervating skeletal muscle fibres progressively degenerate resulting in muscle weakness, paralysis, and ultimately death by respiratory failure (Cleveland and Rothstein, 2001). The disease progresses in a highly selective manner by first targeting motor neurons innervating limb muscles followed by muscles necessary for speech and respiration. Currently there is no cure for ALS. The only FDA approved treatment, Riluzole, increases lifespan by a few months (Bensiman et al., 1994;

Lacomblez et al., 1996; reviewed by Cleveland and Rothstein, 2001). Most treatments offered to patients are generally palliative in nature. Due to the lack of treatments patients with ALS usually succumb to the disease 2-5 years after diagnosis (Cleveland and Rothstein, 2001; Czaplinski et al., 2006). The majority of ALS cases are sporadic (~90%) with an unknown cause. The remaining ~10% of cases are referred to as familial ALS and are due to known inherited mutations. The first genetic mutation identified was that encoding the Cu/Zn binding superoxide dismutase (SOD) 1 enzyme. This mutation accounts for ~20% of familial ALS cases (Rosen et al., 1993; reviewed by Hedgeus et al., 2008). There are over 100 known mutations of SOD1 that result in ALS symptoms (reviewed by Biollee et al., 2006). One of these is the SOD1G93A mutation that results from an amino acid substitution at position 93 (alanine replaced by glycine) (Gurney et al., 1994).

Transgenic rodents with the SOD1G93A mutation develop similar pathophysiology traits observed in patients with ALS. For example, SOD1G93A mice have progressive motor neuron degeneration starting at P90-P100 until they die between P120-140 (Gurney et al., 1994). ALS transgenic mouse models display dysfunction at the NMJ due to a retraction of the presynaptic terminals prior to cell death (Frey et al., 2000; Fischer et al., 2004), suggesting ALS causes axonal 'die-back' in addition to motor neuron cell death. Even when motor neurons are genetically prevented from dying in SOD1G93A mice, motor axons still degenerate at the NMJ resulting in the phenotypic paralysis and death (Gould et al., 2006). Studies have shown that the transplantation of motor neurons to locations of degeneration in mice can restore function motor function to denervated muscles when activated exogenously with electrical stimulation (Yohn *et al.,*

2008). Furthermore, it has been shown that transplantation of ESCMNs in vivo drastically decreased abnormal locomotor behavior in animal models of ALS (Deshpande et al., 2006).

An important physiological and clinical aspect of ALS is the selective vulnerability of different motor neuron populations (or motor units) to the disease (reviewed by: Kanning et al., 2010; Frey et al., 2000**;** Hegedus et al., 2007; 2008). A motor unit is defined as single motor neuron and all the muscle fibres it innervates (Henneman and Mendal, 1991; Burke, 1994). Mammalian motor units can be broken down into three main subclasses, slow (S), fast fatigue-resistant (FR) and fast fatigable (FF), based on the speed of contraction of the innervated muscles and resistance to fatigue during prolonged activation. In general, S motor units are fatigue resistant and produce relatively little force while fast-fatigable units are more forceful but rapidly fatigue (reviewed by; Frey et al., 2000; Purves et al., 2001). Motor units are recruited in a systematic order during force production such that smallest, most fatigue-resistant S units are recruited before the larger, more fatigable fast units (Henneman et al., 1965). As such, S motor units are activated more often than fast units and tend to be associated with postural muscles. In ALS, FF motor units are the first to die followed by FR and finally S (Hegdus et al., 2008; Gordon et al., 2010). Increasing neuromuscular activity has been shown to preserve vulnerable FF motor units in SOD1G93A mice, as they are converted to slower, less forceful, fatigue resistant motor units (Gordon et al., 2010). This study demonstrated the beneficial role activity can play in ALS, as the more active motor units are less vulnerable to the disease.

Activity in Motor Disease

When patients receive an ALS diagnosis it is not well understood whether healthcare professionals should prescribe an exercise regimen to keep the muscles active or instead patients should commence a more sedentary lifestyle. Consequently, the issue of activity and how much to exercise is a concern for ALS patients. It has been proposed that weaker muscles are more vulnerable to damage from over-exertion as they are already functioning in a strained state at maximal limits (Coble 1985). Healthcare professionals have discouraged exercise activity in the past due to a concern that overuse will lead to increased weakness (Sinaki 1978). Furthermore, epidemiological data shows a higher incidence of ALS diagnosis in those who have lived highly active lifestyles either through work (military, professional athlete) adding to the belief that enhanced exercise may hasten disease progression (Kurtzke 1991; Stickland 1996).

Clinical studies have shown that exercise can be beneficial for ALS patients. Specifically, patients subjected to stationary bicycling or treadmill walking, categorized as moderate aerobic exercise, had a decrease in muscle spasticity while the rate of disease progression did not change (Dal-Bello-Haas et al., 2007; Pupillo et al., 2014; Dal Bello-Haas and Florence, 2013*)*. This demonstrates that exercise can potentially keep ALS patients' muscles and nerves healthier longer. Animal studies using the SOD1G93A mouse subjected to moderate activity (treadmill or swimming) showed decreased disease progression and allowed for muscles to remain functional longer (Kirkinezos et al., 2003; Kasper et al., 2005; Deforges et al., 2009; Veldink, 2003). However, another study in male mice showed that high endurance exercise was detrimental (Mahoney, 2004). As

studies have demonstrated beneficial and harmful effects of exercise in ALS, more research is required to tease out the correct correlation between the two.

In vitro modeling, bringing it all together

The phrase 'in vitro' is derived from the Latin term meaning "in glass". In vitro studies model biological processes in a minimalized experimental condition where complicating variables can be eliminated or controlled. For example, in vitro modeling with embryonic stem (ES) cells allows for insight into the mechanisms of development and human disease. ES cells possess the ability to renew themselves through the process of cell division and, under physiological and experimental conditions, can be directed differentiated into any cell type in the body (e.g. motor neuron, red blood cell or muscle fibre). In 2002, Tom Jessell's group demonstrated that mouse ES cells can be directed to differentiate into motor neurons by exposing them to morphogens (Wichterle et al., 2002). Successful differentiation of motor neurons was achieved by first aggregating ES cells into three-dimensional structures termed, embryoid bodies (EBs). After two days in vitro (DIV), the EBs were then treated with RA and a smoothened agonist (SAG; an activator of Shh signaling pathway) (Wichterle et al., 2002). Similar to endogenous motor neuron differentiation, the differentiated ES cell-derived motor neurons (ESCMNs) expressed ventral progenitor domain transcription factors such as the homeodomain gene Hb9. Hb9 is homeobox gene essential for motor neuron generation and is expressed by post-mitotic motor neurons (Arber et al., 1999; Thaler et al., 1999; Wichterle et al., 2002). Identification of differentiated motor neurons was possible because the ES cells were derived from a transgenic mouse with enhanced green fluorescent protein (eGFP) reporter gene upstream of the HB9 promoter. This allowed for quantification showing

that 20-30% of cells within the EBs were GFP^+ and therefore successfully differentiated into motor neurons (Wichterle et al., 2002).

More recent work has shown that interneurons are present within the EBs, based on patterns of neural activity recorded as a result of glutamate application (Miles et al., 2004; Chipman et al., 2014). Glial cells expressing glial fibrillary acidic protein (GFAP) are also present within differentiated EBs (unpublished observations, Rafuse laboratory). Two different motor neuron subtypes were present when ESCMNs were created. The majority of motor neurons were characteristic of MMC motor neurons (epaxial innervating) due to co-expression of LIM homeodomain proteins Islet 1 and Lhx3. Another small percentage was identified as the LMC_L subtype (dorsal limb innervating) due to their expression of LIM homeodomain proteins Lhx1 (Wichterle et al., 2002; Tsuchida et al., 1994).

ESCMNs have since been shown to exhibit many characteristics typical of endogenous motor neurons such as the development of mature electrophysiological firing properties (Miles et al., 2004). Further, ESCMNs project axons to muscles lining the vertebral column after being transplanted into the neural tube of chicken embryos indicating that the ES cells specifically differentiate into MMC motor neurons when treated with RA and SAG (Wichterle et al., 2002; Soundararajan et al., 2006; Soundararajan et al., 2007; Soundararajan et al., 2010). When plated on muscle fibres in vitro ESCMNs form functional and anatomically mature NMJs after several weeks (Miles et al., 2004; Guo et al., 2011; Umbach et al., 2012; Chipman et al., 2014). Lastly, when ESCMNs were transplanted into the distal end of a transected peripheral nerve in mice

they restored contractile force by forming functional NMJs with denervated muscle fibres (Yohn et al., 2008).

The interest in developing ESCMNs is to not only to investigate motor neuron development but to also for developing in vitro models to study motor neuron diseases such as ALS. Mouse ES cell lines have been developed that contain human mutant SOD1 constructs for modeling ALS in vitro to investigate underlying molecular and cellular disease mechanisms. Work from Kevin Eggan's laboratory demonstrated that ESCMNs derived from mice expressing the human SOD1G93A mutation are prone to early death compared to control ESCMNs (Di Giorgio et al., 2007). This study demonstrates it is possible to recapitulate ALS disease pathology in a dish. ESCMN in vitro models of ALS can be used as tools to identify potential therapeutic targets. For example, Yang and colleagues used ESCMNs derived from mice to perform a small molecule screen to identify therapeutic candidates for ALS patients (Yang et al., 2013). Using a model system with mouse ESCMNs is an excellent preclinical tool as it allows for results to be attained efficiently with a low cost and high yield before moving to human models.

Optogenetics

Over the past 100 years, neural circuits have been studied, in part, by recording from one group of cells while electrically stimulating another (Kandel *et al.,* 1961; Kendel *et al*., 2000). While this approach has been instrumental in providing a foundation of knowledge on how the nervous system functions, it has a major limitation in that electrical stimulation is non-specific. Consequently, specific neural subtypes cannot be

selectively activated, particularly if they are interspersed with other neuronal subtypes within a specific region of the nervous system.

Optogenetics solves this limitation. Optogenetics is the expression of opsins in specific cell types using targeting genetics (Boyden et al., 2005; Boyden, 2011). Opsins were initially studied because of their fascinating biophysical properties of transducing photons into electrical current (reviewed by, Deisseroth, 2015). However, since their initial characterization, three main classes of microbial opsins have now been adapted to optically control cellular functions. Bacteriorhopsins (the first discovered, pumps protons out of the cell) and halorhodopsins (pumps chloride ions into the cell), both channels cause hyperpolarization when activated in neurons make them less likely to fire action potentials. Therefore, these two opsins typically act in an inhibitory nature within a neural system (Spudich, 2006; Han, 2012; Zhang et al., 2011). The third opsin, known as channelrhodopsin, is a non-specific light-gated cation channel causing depolarization when activated by light (Spudich, 2006; Han, 2012; Zhang et al., 2011).

This thesis uses ChR2, the opsin underlying phototaxis in the green alga *Chlamydomonas reinhardtii* (Nagel et al., 2003). Since its initial discovery, ChR2 has been expressed in neurons where it has been shown to induce depolarization when the cells are illuminated by light (Boyden et al., 2005; Li et al., 2005; Nagel et al., 2005). This technique has been widely embraced within the neuroscience community because it offers a way to precisely, and noninvasively, activate specific neuronal populations in vitro, ex vitro and in ovo (Boyden et al., 2005). Since its initial discovery just over a decade ago there have been numerous discoveries utilizing optogenetics to research behavior, physiology and pathology. Although the majority of optogenetic studies use

rodents, or cells harvested from them, other model systems have been used including: nematodes (Flavell et al., 2013), fruit flies (Ramdya et al., 2015), song birds (Roberts et al., 2012), zebrafish (Thiele et al., 2014) and nonhuman primates (Lu et al., 2015).

The kinetics of native ChR2 channels are slower than voltage-gated sodium channels typically activated in neurons to generate action potentials. For example, the time constants of ChR2 opening and closing are 10 and 11 ms, respectively (Bamann et al., 2008; Mattis et al., 2012). This is slow compared to the 1-2 ms time constant for voltage-gated sodium channels (Kandel *et al*., 2000). Consequently, light pulse frequencies that are too high (10 to 50 Hz) will result in ChR2 channels that do not close, preventing membrane repolarization and subsequent action potentials (Liske *et al.,* 2013). Native ChR2s were also found to desensitize quickly and required very bright light for activation. To circumvent this issue, a genetically modified version of the original ChR2 was created that possesses an H134R variant allowing for larger photocurrents, greater light sensitivity and less desensitization (Nagel et al., 2005; Lin et al., 2009; Guanudin et al., 2009; Lin 2011; Madisen et al., 2012). This variant was consequently selected to be used in this thesis.

The in vitro model introduced in this thesis integrates optogenetics and stem cell biology that allows for the study of the NMJ by precise activation of motor neurons with ChR2 expressing ESCMNs. Harnessing optogenetics to specifically stimulate motor neurons in our system allows us to characterize and quantify the effects of activity on motor neurons early in their development and as they form functional NMJs. In order to model disease in vitro we created ChR2 ESCMNs expressing the SOD1G93A mutation. Our in vitro model system allows for rapid drug screening of molecules that could slow

disease progression and increase function at the NMJ (suggested by Chipman et al., 2012; Vitaline et al., 2011). Finally, as ALS is a complex disease we believe that this reduced system can be used to study pathophysiologies that are specifically related to motor neuron dysfunction as it pertains to the NMJ.

Summary of Objectives

Overall Project Aim: To develop a novel *in vitro* model system to characterize the role of activity in motor neurons during development and in disease.

Hypothesis 1: An in vitro model system can be used to characterize the role of activity in axon growth and the underlying cellular mechanisms.

Chapter 3:

Aim 1: To develop stem cell derived light activated motor neurons.

Aim 2: To characterize the firing properties of motor neurons in response to light stimulation and depolarizing current in vitro.

Aim 3: To characterize the role of activity on growth and development of motor neurons.

Hypothesis 2: An in vitro model system can be used to understand the role of activity in synapse stability in ALS.

Chapter 4:

Aim 4: To develop a co-culture system comprised of stem cell derived light activated motor neurons, both WT and expressing SOD1 and chick muscle fibres.

Aim 5: To characterize how activity can modulate synaptic connectivity at the neuromuscular junction in healthy and diseased motor neurons.

CHAPTER 2: METHODS

Generation and Differentiation of mouse ChR2 ESCMNS and SOD1 ChR2 ESCMNs

Two transgenic mouse lines were used to create the stem cell derived ChR2 expressing motor neurons: an Ai32 mouse (Jacksons Labs Bar Habour, ME), that expresses a loxP-flanked STOP cassette inhibiting the downstream transcription of ChR2(H134R)-EYFP fusion gene (Nagel *et al.,* 2005) crossed with a HBG3 mouse expressing Cre recombinase under the control of HB9 regulatory sequence (a kind gift provided by Dr. T. Jessell, Columbia University, New York NY) (Figure 3.1A), they will be referred to as ChR2 ESCMNs. The second cell line created by first breeding a Cre^{+}/ ChR2(H134R) (Hb9:eGFP)/ $SOD1^{+}$ mouse, with a Cre^{+}/ $ChR2^{-}$ / $SOD1^{-}$ mouse ultimately yielding a $Cre^{+}/ChR2^{+}/SOD1^{+}$ embryonic stem derived cell line (Figure 4.1). The cells will be referred to as the SOD1 ChR2 ESCMN cell line from this point onward.

Embryonic Stem (ES) Cells were isolated from the inner cell mass (ICM) of mouse blastocysts using standard techniques. Pregnant females were sacrificed on the 3rd day of pregnancy when embryos are at the 8-16 cell stage. The uterine horn was extracted and placed in warmed M2 media (Sigma M7167). Blastocysts were flushed from the uterine horn and transferred to a 4 well plate containing a confluent monolayer of mitomycin C treated (Sigma) primary mouse embryonic fibroblasts (PMEF). The ICM was allowed to expand for approximately 4 days then fed every two days with ESC media containing DMEN (Gibco 11995-073), ESC grade fetal bovine serum (FBS; 15% by volume; Millipore ES-009-B), penicillin/streptomycin (1% by volume; Gibco 5140-122), 2-mercaptoethanol (1% by volume; Millipore ES-007-E), non-essential amino acids (1%

by volume; Millipore TMS-001-C) and ESGRO LIF (leukaemia inhibitory factor; 1000u/ml; Millipore ESG1106). After 4 to 6 days of ESC media changes, the ICM was mechanically separated from the blastocyst using a tungsten needle and 2.5% trypsin. Cells were further dissociated into smaller clumps and transferred onto a 4 well plate containing PMEF and ESC media where they were allowed to expand into ES cell colonies and then passaged to avoid confluency (Figure 3.1B).

Isolated ES cell colonies were differentiated into motor neurons as described previously (Wichterle *et al.,* 2002; Miles *et al.,* 2004; Soundararajan *et al.,* 2006, Chipman *et al.,* 2014). In brief, ES cells were grown as aggregated cultures in DFK-10 media to form free floating embryonic bodies. DFK10 medium consisted of DMEN (Gibco 11995-073) and Ham's F-12 medial (Specialty Media) in a 1:1 ratio supplemented with knock-out serum replacement (10% by volume; Invitrogen, Burlington Ontario, Canada), penicillin/streptomycin (1% by volume; Sigma, St. Louis, MO), N2 supplement (2.4% by volume; Invitrogen), glucose (4500mg/l), L-glutamine (200mM), heparin (1u/l; Sigma), and β-mecaptoethanol (0.1mM; Sigma). After two days, the embryonic bodies were treated with a smoothened agonist and retinoic acid (RA) (1M; Sigma, St Louis, MO) and cultured as free-floating cells for an additional 5 days. GFP expression was monitored as an assessment of differentiation and only embryonic bodies with robust GFP expression were used for the co-cultures.

Outgrowth Assays: Dissociation and stimulation protocol

Immediately following differentiation protocol the Ai32 ChR2 embryoid bodies were dissociated into a single cell suspension using TrypLE (Invitrogen) (Figure 3.2A). Prior to plating, cells were washed in Hanks Balance Salt Solution (HBSS, Gibco) and

resuspended in DFK10 media. Cells were counted and plated at a low density, 15,000 cells/well, in a 24-well plate coated with matri-gel (Invitrogen). Matri-gel was utilized to visualize the affect of the optical stimulation on the MNs growing without contacting other cells within the EB (interneurons, glial cells and other motor neurons). The low-density cultures were grown in DFK10 media with GDNF (10ng/µl, Gibco) and CNTF (5ng/µl, Gibco) in a 37°C incubator with 5% CO2 for the duration of the experiment (Figure 3.2). Cultures were moved into either the stimulation incubator or dark isolation incubator ~4 hours after plating or once the dissociated cells had adhered to the coverslips to ensure they did not fall to the sides of the wells. Once the dissociated cells were adhered to the coverslips, if they were in an experimental condition where they were treated with either TTX [25µM] or 1µl of EndoN. This was done before being moved into either stimulation condition.

Cultures in the stimulated condition were moved to an incubator where blue LED lights (470 nm; SP-04-B4, Luxeon Star LEDs, Brantford Ontario) connected to a Arduino based programmable control unit were mounted on top of the culture plate. Cells were stimulated with an exposure of 100 ms at a frequency of either 0.1hz or 0.025hz for 48 hours (Figure 3.2B, C). The frequency of 0.025Hz was initially chosen as it mimicked the endogenous frequency of the propagating waves of spontaneous activity during development in the chick that occur every 40 seconds (Kastanenka and Landmesser, 2010). The cells in the non-stimulated condition where moved to a separate incubator without lights, in a dark room and remained in the dark until they were fixed ensuring no exposure to ambient light for the entire 48 hours (Figure 3.2D).

Whole Cell Patch Clamp Recordings

Whole cell patch clamp recordings were completed in a similar fashion as described previously by Borowska *et al*. (2013) and Toma et al. (2015). Coverslips chosen for analysis were either 24 hours, 48 hours, 1 week or 2 weeks *in vitro*. Embryoid bodies were dissociated and plated similarly to above, at 50,000 cells per well. Coverslips were place in a recording chamber with an oxygen Ringer's solution (111 mM NaCl, 3.08 mM KCl, 11 mM glucose, 25 mM $NaHCO_3$, 1.25 mM $MgSO_4$, 2.52 mM $CaCl_2$, and 1.18 mM KH_2PO_4, pH 7.4) at room temperature for 30 minutes to adjust to conditions prior to the start of recordings. Recordings were completed on GFP positive MNs were visually identified using a DAGE-MTI IR-1000 CCD camera mounted on an Olympus BX51WI microscope, while being continuously perfused in Ringer's solution oxygenated with 95% O_2/5% CO_2.

Recordings were done in current-clamp mode using a MutliClamp 700B amplifier (Molecular Devices). pCLAMP 10.3 (Molecular Devices) controlled a Digidata 1400A board (Molecular Devices) that was used to filter out analog signals at 10kHz. Patch-clamp recording pipettes were filled with a solution containing, 128 mM K-gluconate, 4 mM NaCl, 0.0001 mM $CaCl_2$, 10 mM HEPES, 1 mM glucose, 5 mM Mg-ATP, and 0.3 mM GTP-Li (pH 7.2) each with a resistance of 5-8MΩ. To ensure consistent measuring conditions cells were all held at -60mV with an alternating current (AC). Cells were stimulated by either current injections delivered in increments of 1 or 10pA or by turning on fluorescent blue light through the microscope. Data was obtained by Clampex 10.3 (Molecular Devices) and analyzed by Axoscope 10.2 software (Molecular Devices). Further statistical analysis and graphs were generated with Sigma Plot 11 software (Systat Software).

Immunofluorescence, Imaging and Analysis

Cultures were fixed for staining in a 4% formaldehyde (Fisher Scientific, Houston, TX) solution in PBS (1x) for 10 minutes at room temperature, after which they were washed three times for 10 minutes with PBS (1x). ESCMNs were immunolabelled with a combination of antibodies as described in Table 2.1. Antibodies were diluted in PBS overnight at 4 degrees in the presence of 10% blocking serum and 0.3% Triton X-100 (Sigma). The co-cultures were then washed 3 times for 10 minutes in PBS before application of the secondary antibodies (Table 1.2), which were applied for 1 hour at room temperature (RT). Tetremethylrodamine conjugated α-Bungarotoxin (α-BTX; 1:500, Invitrogen) was added in some cases along with the secondary antibody to label nicotinic acetylcholine receptors of neuromuscular junctions. Co-cultures were washed and mounted in 50% glycerol/PBS mixture containing 0.03mg/ml ρ-phenylenediamine. Dissociated MNs or co-cultures were digitally photographed using a wide-field fluoresce microscope equipped with a broad focal plane lens (Lecia Microsystems, Bannockburn, IL, USA attached to a digital camera; C4742; Hamamatsu, Japan).

Preliminary quantification and morphological analysis of captured images were done on IPLab software (Version 4.0; BD Biosciences). Cell counts were done using IPLab software, by counting 3 different sections on each slide and taking an average of the 3 values, this was used to determine cell survival or the number of GFP^+ cells present. Videos and images taken of co-cultured ESCMNs and muscle fibres, for the purpose of demonstrating that ChR2 is functional within the MNs, was done using a Photometrics Cool Snap HQ^2 camera mounted on a Zeiss Axio Examiner D1 microscope, through 3i Software: Slidebook 6 (64 bit).

Outgrowth Measurements and Analysis

MNs selected for quantification were required to show positive staining for both β–Tubulin (be a neural cell) and GFP (specifically, a motor neuron expressing ChR2) (Table 2.1). The MNs were also required to be growing individually on the coverslip making no contact with other MNs or other cell types present (identified by β–Tubulin, Table 2.1 and hoeschst, Sigma 33258). Once MNs were selected, length measurements were taken using ImageJ using the tracing function and the total length was quantified by adding up each neurite length (Figure 3.6 - blue dotted line). The displacement was quantified by drawing a straight line from the cell body to the end of the longest neurite branch (Figure 3.6 – red dotted line). Intuitively, the number of neurite branches was quantified by counting the number of neurite branches traced (Figure 3.6 - green numbers). The statistical analysis and plots created where done on Sigma Plot 11 (Systat Software).

Western blotting: adhesion molecule expression, SOD1 expression

After 48 hours of being plated in either the stimulated condition (0.025hz) or the non-stimulated condition the cell lysates were collected by lifting the cells from the coverslips using TrypLE 10X (Invitrogen), spun down, resuspended, and sonicated in extraction buffer as described previously by Chipman *et al.* (2014). Once in the extraction buffer (10% glycerol, 1% NP40, 2% Tris, 2.75% NaCl in double distilled water, with a cocktail of protease inhibitors [Complete Mini, Roche Diagnostics, Mannheim Germany]), cells were sonicated for 10 seconds, placed on ice for 10 minutes, and then centrifuged for 30 minutes at 20,000g at 4°C. Pellets where then discarded and the supernatants were assayed for protein content using Pierce™ BCA Protein Assay Kit

(ThermoFisher Scientific). Results were read on a BioSpec-Mini (Shimadzu Biotech). Samples were then diluted in 5X SDS sample buffer (0.5M Tris [pH 6.8], 10% glycerol, 25% SDS, 10% 2-mercaptoethanol and 1% bromophenol blue diluted in distilled water). If polysialic acide (PSA) was being removed from samples with EndoN (generous gift from Urs Rutishauser), they were first diluted with distilled water and 1µl of EndoN was added. They were then incubated at 37°C for one hour before adding the sample buffer. Two different protocols were used: (i) samples were heated for 5 minutes at 95°C (Crown *et al.,* 2005) or (ii) were stored at 4°C overnight (Black *et al.,* 2009). The second method we found to produce more clear bands of PSA-NCAM, ensuring no PSA was cleaved due to the heating process.

Equal amounts of protein were loaded into each lane. Samples when then separated on a 6% acrylamide gel and transferred onto a polyvinylidene fluoride (PVDF) Immobilon-P membrane (Immun-Blot PVDF, BioRad, 162-0177). After being rinsed with Tris-buffered saline (TBS-T), membranes were blocked in 5% non-fat milk then probed overnight at 4°C with anti-NCAM primary antibody diluted in 5% milk solution (Table 2.1). After overnight incubation period, membranes were washed 3x10minutes in TBS-T before being probed for an hour at room temperature (RT) with secondary antibody diluted in 5% milk solution (Table 2.2). Following incubation in secondary antibody, membranes were washed 3x10minutes in TBS-T. Once washed, chemiluminescence was applied to membranes for 1 minute (SuperSignal West Pico Chemiluminesents Substrate, Thermo Scientific, Rockford Il), the membranes were developed on Kodak film (X-OMAT Blue Film XB, Kodak, Rochester, NY) and visualized using an x-ray processor.

Band intensity analysis was performed using ImageJ software, following the same methods as outline by the University of Queensland (2016). Quantification was graphed using Sigma Plot 11 software (Systat Software). Western blotting was used, as outline above, this time to determine the successful expression of SOD1 in the newly created SOD1 ChR2 cell line. The WT cell line that was used as a negative experimental control was the ChR2 ESCMN line that is lacking SOD1 expression (Figure 4.1B, lane one) and a $SOD1^{G93A}$ positive mouse ear clip was used as a SOD1 positive control (Figure 3.1B, lane three). The primary antibody used to identify misfolded SOD1 was the D3H5 antibody (Table 2.1), a generous gift from Jean-Pierre Julien's lab (Patel *et al.,* 2013).

Co-culture of ESCMNs and embryonic chick myotubes

ESCMNs were plated on chick myotube cultures for analysis of functional NMJs (Figure 4.1C, Figure 4.3). Myoblasts where harvested from the external adductor muscle of E12 White Leghorn chick embryos and cultured as previously described (Rafuse and Landmesser, 1996). Briefly, external adductor muscles were dissected from stage 38 White leghorn chicks and mechanically dissociated in Ham's F-10 media containing 10% horse serum (Invitrogen), 5% chicken embryo extract and 1.26mM $CaCl_2$. 105 myotubes were plated on coverslips in 24-well cell culture plates and fed after two days in culture with Ham's F-10 media (as described above). ESCMNs were plated on the chick myotubes three days after plating the myoblasts (Figure 4.1C). 1 hour prior to ESCMN plating, F-10 media was replaced with Neurobasal media (Invitrogen) supplemented with 2mM L-glutamine (Invitrogen) and penicillin/streptomycin (Invitrogen), GDNF (glial-derived neurotrophic factor) (20 ng/ml; Upstate Biotechnology, Lake Placid, NY) and CNTF (ciliary neurotrphoic factor) (10 ng/ml; Upstate Biotechnology). Co-cultures were

fed every 2 days for up to a week with neurotrophic supplemented Neurobasal formulation. For co-cultures grown for longer than one week, neurotrophic factors were omitted from the Neurobasal formulation (Figure 4.1C). After at least 5 days *in vitro,* both WT and SOD1 ESCMNs were tested for ChR2 expression using an inverted fluorescent microscope (Zeiss Axio Scope Vert.A1). Visual inspection was completed by pulsing blue light from the scope fluorescence box over the cultures while watching for an immediate muscle contraction.

Intracellular recordings of ESCMN-chick muscle fibre co-cultures

Sharp electrode intracellular electrophysiology was utilized at 2 weeks in vitro to assess neurotransmission in the ChR2 ESCMMs co-culture system as previously described by Chipman *et al.* (2014) and Miles *et al.* (2004). Experiments were performed at RT in a recording chamber using a solution containing 50% phenol red free Neurobasal (Invitrogen)/50% hibernate low fluorescence solution (Brain Bits, Springfield, IL). A rhodamine conjugated non-blocking antibody, mAB35, was applied 1 hour prior to recording to live stain for acetylcholine receptors to identify post-synaptic endplates. MNs leading to NMJs were identified by the endogenous GFP signal from the ChR2 ESCMNs (Figure 4.3A). N-Benzyl P-Toluenesulfonamide (BTS) [100μM] (Aldrich Chem: S949760) was used to paralyze the muscle to block contractions (by blocking the actin-myosin interface) to avoid movement of recording electrode. NMJs were located by co-localization of rhodamine and GFP staining, visualized through a Photometrics Cool Snap HQ^2 camera mounted on a Zeiss Axio Examiner D1 microscope, using 3i Software: Slidebook 6 (64 bit) (Figure 4.3A). Motor neurons where stimulated optically with the blue florescence light from the microscope using the time-lapse capabilities of the

Slidebook software, thus allowing for parameters such as pulse width and frequency to be modified with each recording.

Micropipettes used were filled with 3M KCl and had a tip resistance between 10 and 50mΩ. Responses were recorded using a MultiClamp 700B amplifier (Molecular Devices), controlled by pCALAMP10.3, obtained by Clampex software (version 10.2, Molecular Devices) and analyzed by AxoScope software (version 10.2, Molecular Devices). Statistics and graphing was generated with SigmaPlot 11 software (Systat Software). In some cases, TTX [25µM] (Alomone Labs: T-550) was added to the recording chamber to block evoked responses, EPPs (Figure 4.4G). Additionally, all the remaining spontaneous events, mEPPs, were blocked with a bath application of D-tubocurarine [50µM] (Sigma: T2379) (Figure 4.4H). All cells that were used for recording had a resting membrane potential that varied from ~ -20mV to -74mV, these being similar to previously recorded post-synaptic membrane potentials in iPSCMN chick-muscle co-cultures (Toma, *et al.,* 2015). Quantal content was determined by the equation previously described (del Castillo and Katz, 1954a, b, c); quantal content (*m*)= average amplitude of evoked endplate potential (EPP)/average amplitude of miniature or spontaneous endplate potential (mEPP).

The Contraction Index: a measure of *in vitro* behavior.

The Index

An *in vitro* 6 point scoring system (0-5) was created to grade the degree of muscle contraction a motor neuron is able to elicit after a single blue light pulse, called the Contraction Intensity Index (CI score) (Figure 4.4). Scoring begins on the fifth day *in vitro*, as this is the approximate time point at which MN-muscle connections begin to

become functional NMJs in our system. Scoring is done using an inverted fluorescent microscope under 10X magnification (Zeiss Axio Scope Vert.A1). When scoring co-cultures with embryoid bodies plated on muscle, the EB must be centered in the field of view (FOV). This creates an easy visualization of the muscle fibres sprawling out beneath (Figure 4.4).

A 0 on the scale is defined as when a light pulse is administered and there is no immediate corresponding contraction from the muscle (Figure 4.4A). A CI score of 1 or 2 represents a light pulse resulting in either one or two muscle fibres immediately twitching (respectively) (Figure 4.4A). A CI score of 3 is when approximately ⅓ of the muscle fibres in the FOV contract (together being a small sheet of muscle compared to single fibres twitching) (Figure 4.4A). A 4 on the CI scale is almost the entire field of muscle twitching in response to the light pulse, but there is a distinct region that is not reactive (Figure 4.4A). A 5 intuitively so, is the entire sheet of muscle in your FOV contracting as result of the light pulse, this can be so powerful that the EB in the center of the FOV is being pulled around the culture.

In order to assess the degree of contraction elicited from an individual motor neurons synapsing on a muscle fiber autonomous from other cells within the EB, CI scoring can be done with dissociated cells. ESCMNs are dissociated as described above (Figure 3.2) and plated on muscle fibres that are harvested and plated the same manner as outlined above. The scores equate the same, however instead of being able to find a central point of the culture in your FOV around the EB, 3 distinct areas on the coverslip are tested by flashing a flight pulse. The area that elicits the highest score is the score assigned to that culture.

Stimulation protocol

Co-cultures used for CI scoring that are stimulated either in EB or dissociated form are moved into light or dark conditions approximately 4 hours after plating or once the cells/EBs have adhered to the muscle. Cultures were stimulated in the incubator using LED lights (blue 470nm; SP-04-B4, Luxeon Star LEDs, Brantford, Ontario) connected to an Arduino based programmable control unit mounted on top of the culture plate, as previously described in Chapter 2 (Figure 3.2).

Immunofluorescence Post-Scoring

Co-cultures were fixed and stained using the same protocol outlined above. For anatomical quantification (see below), co-cultures were stained using antibodies for GFP, a neuronal marker, and AcH receptors were used (Tables 2.1).

Analysis and statistics

Anatomical analysis was done with images captured on an upright fluorescence microscope (Lecia Microsystems, Bannockburn, IL, USA attached to a digital camera; C4742; Hamamatsu, Japan) through IPLab software (Version 4.0; BD Biosciences). Analysis was done using ImageJ using intensity analysis of highlighted regions of neurite outgrowth, synaptic vesicles, and AChR. An area was highlighted to measure 3 different anatomical features in the cultures (the center of the EB is excluded so that the size of the EB cannot skew the quantification) (Figure 3.5A, yellow dotted region). Particle counting function was used to count the number and average size of threshold regions of staining. Statistical analysis of values and graphing was done using Sigma Plot 11 (Systat Software).

Table 2.1 Primary Antibodies

Antiserum	Host Species	Dilution	Clonally	Source
β-Actin	Mouse	1:500		Santa Cruz Biotechnology, Dallas, TX
B-Tubulin	Mouse	1:2000IF	Monoclonal	BioLegend, San Diego, CA
D3H5	Mouse	1:500 WB	Monoclonal	Dr. Jean-Pierre Julien, Université Laval, QC
GFP	Rabbit	1:2000 IF	Polyclonal	Chemicon, Temecula CA
NCAM (CD56-rodent specific)	Mouse	1:10000 WB	Monoclonal	BD Biosciences, Franklin Lakes NJ
SV2	Mouse	1:50 IF	Monoclonal	DSHB, Iowa City, IA

IF-Immunofluorescence; WB-Western Blot

Table 2.2 Secondary Antibodies

Antiserum	Dilution	Conjugate	Source
Goat anti-rabbit IgG	1:500 IF	Alexa Fluor488	Invitrogen
Goat anti-mouse IgG	1:500 IF	Cy 3	Jackson Immunoresearch, Baltimore, PA
Goat anti-mouse IgG	1:500 IF	AlexaFluoro647	Invitrogen
Goat anti-mouse IgG	1:5000 WB	HRP	Chemicon, Temecula CA

IF-Immunofluorescence; WB-Western Blot

CHAPTER 3: THE ROLE OF ACTIVITY IN DEVELOPMENT

Introduction

With the use of stem cell biology we were able to create ESCMNs that express ChR2 that are comparable to other preexisting ESCMN populations. We report with current clamp recordings that ChR2 ESCMNs are able to depolarize and develop the ability to fire a single action potential in response to a single light pulse. Further, the ChR2 ESCMNs when injected with depolarizing current were able to develop the ability to fire characteristically of typical motor neurons.

With the knowledge that ChR2 ESCMNs depolarized and fire action potentials as result of light stimulation, we demonstrated that chronic light activation resulted in enhanced growth; this change can be eliminated when action potentials are blocked. Adhesion molecule expression was increased in ChR2 ESCMNs that were stimulated. Additionally when PSA was enzymatically cleaved from NCAM the increased growth seen in light-activated motor neurons was augmented. These findings suggest, that motor neuron growth early in development without post-synaptic targets can be enhanced by activity.

Contribution statement

I would like to acknowledge the laboratory of Dr. Ying Zhang and her student Dylan Deska-Gautheir for performing patch clamp experiments (analysis of patch clamp electrophysiology data was performed by myself) and Cindee Leopold and Simone Laforest for technical assistance with stem cell culture maintenance and mouse husbandry.

Results

ChR2 expressing ESCMNs are comparable to other ESCMNs populations.

In order to selectively activate (i.e. depolarize) motor neurons in a heterogeneous culture system containing multiple neuronal subtypes we first crossed mice expressing Cre recombinase under the control of the HB9 promoter with mice expressing a loxP-flanked STOP cassette upstream of the ChR2(H134R)-EYFP fusion gene (Nagel *et al.,* 2005) (Figure 3.1A). This breeding strategy generates mice with motor neurons expressing ChR2(H134R)-EYFP because Hb9 is a motor neuron specific transcription factor (Arber et al., 1999). Embryonic stem (ES) were harvested from the uterus of these animals 2.5 days after copulation and expanded on a feeder layer of mouse embryonic fibroblasts using standard stem cell expansion protocols (Wichterle et al., 2002). These ES cells, here termed Hb9ChR2 ES cells, were cultured to form free-floating embryoid bodies and then directed to differentiate into motor neurons using retinoic acid (RA) and a smoothened agonist (SAG) (Wichterle *et al.,* 2002; Miles *et al.,* 2004; Soundararajan *et al.,* 2007) (referred to as ChR2 ESCMNs throughout this thesis) (Figure 3.1B). After 5 days in vitro (DIV), we found that ~19% (mean: 18.67% ±3.76 SD) of the Hb9ChR2 ES cells differentiated into $EYFP^+$ MNs cells. This percentage of ChR2 ESCMNs is not significantly different from the number of $EGFP^+$ MNs (mean: 17.5% ±2.29 SD ; p=0.3292) generated from HBG3 mouse ES cells when treated with RA and SAG over the same time course. We used HBG3 ESCMNs as a comparator group because they express eGFP and have been extensively characterized by several labs including our own (Wichterle et al., 2002; Miles et al., 2004, Soundararajan et al., 2006, 2007, 2010, Chipman et al., 2014). To determine whether ChR2 MNs extend neurites comparable to HBG3 ESCMNs we cultured embryoid bodies containing both cell types on matrigel for

3-7 days DIV. Figure 3.3 shows that the overall outgrowth of neurites between the two types was comparable 3-7 days after plating. Together, these results indicate that Hb9ChR2 ES cells have the same capacity to differentiate into motor neurons as HBG3 ES cells and that motor neurons from both ES cell lines have comparable neurite growth patterns when grown *in vitro*.

ChR2 ESCMNs depolarize and fire single action potentials when activated by light.

To determine whether MNs expressing ChR2 depolarize and fire action potentials when exposed to light, we performed whole-cell current clamp recordings on cultured ChR2 MNs plated on matrigel for 24 hours (n=3), 48 hours (n=17), 1 week (n=3) and 2 weeks (n=1) (Figure 3.4). We found that ChR2 MNs had sustained membrane depolarizations lasting the entire length of the light pulses (~200 ms) at all time points examined (Figure 3.4). However, there were noticeable differences between the young (i.e. 14-48 hours) and old cultures (1-2 weeks). First, light activation failed to produce action potentials in ChR2 MNs when cultured for only 24 hours (Figure 3.4A, left panel). Light pulses elicited single action potentials at the onset of some light evoked depolarizations, 56% of the time, after 48 hours (Figure 3.4A). Single action potentials (and sometimes doublets) occurred at the onset of each light-induced depolarizations in ChR2 MNs cultured for 1 and 2 weeks (Figure 3.4B), even when the frequency of pulses increased to 2.5 Hz (Figure 3.4B, right panel). In addition to the emergence of action potentials, we found that the amount of depolarization induced by light increased from ~5mV at 24 hours to >15mV after 1-2 weeks (Figure 3.4). Together these results indicate that ChR2 MNs develop over time in culture such that by 1 week they generate single action potentials with each light-induced depolarization.

ChR2 ESCMNs develop firing patterns typical of MNs when injected with depolarizing currents.

Previous studies on ESCMNs derived from the HBG3 ES cell line showed that they fire repetitive action potentials when injected with a sustained depolarizing current after 4 DIV (Miles et al., 2004). To ascertain whether ChR2 ESCMNs similar firing properties we injected depolarizing currents into ChR2 MNs while performing whole cell patch clamp recordings at 24 hours (n=3), 48 hours (n=17), 1 week (n=3) and 2 weeks (n=1) *in vitro* (Figure 3.5). Similar to HBG3 ESCMNs (Miles et al., 2004), young ChR2 ESCMNs (i.e. 24 and 48 hour cultures) did not fire multiple action potentials when injected with a sustained depolarizing current, however they did elicit a single spike at the onset of the pulse (Figure 3.5A). In agreement with previous studies using ESCMNs (Miles et al., 2004), we also found that ChR2 ESCMNs exhibited repetitive firing during a sustained depolarization when cultured for 1 and 2 weeks and had maximum firing frequencies between 13-16 Hz when injected with 80 pA of current (Figure 3.5B). In addition, the amount of current required to evoke an action potential (or spike response seen in more immature cells) decreased as the cells matured in culture such that approximately 65 pA of current was needed in order to elicit a single spike at 24-48 hours while only 20 pA was required at 1 and 2 weeks (Figure 3.5-C, 1 Week). Finally, spike frequency adaptation typical of endogenous MNs (Granit *et al.,* 1963; Kernell and Monster 1982) was observed during sustained depolarizations at 1 and 2 weeks as evidenced by the instantaneous frequency versus time plot shown in Figure 3.5D. Taken together, this data indicates that ChR2 ESCMNs develop firing characteristics similar to previously described mouse ESCMNs (Miles et al., 2004), mouse iPSCMNs (Toma et al., 2015) and human ESCMNs (Takazawa et al., 2012) as well as endogenous

spinal MNs (Fulton and Walkton, 1986; Gao and Ziskind-Conhaim, 1998). The absence of repetitive firing during light-induced activation is likely due to 1) inactivation of Na channels during the sustained depolarization where additional action potentials would be prevented until the Na channels turn of after the light is turned off or 2) the neurons were not depolarized enough to elicit repetitive action potentials.

Light-activation of ChR2 ESCMNs enhances neurite growth and complexity.

Neural activity plays a role in the development of several neuron specific characteristics such as synaptic connectivity within neural circuits, neurotransmitter identity, axon guidance and axon-branching (Heeroma *et al.,* 2003; Borodinsky *et al.,* 2004; Myers *et al.,* 2005; Varoqueaux *et al.,* 2005; Hanson and Landmesser, 2003; 2005; 2006; Franz et al., 2005; 2008; Kastanenka and Landmesser, 2010; Marek *et al.,* 2010 Benjumeda *et al.,* 2013). However, the underlying cellular mechanism by which activity regulates these processes remains largely unknown (Hanson and Landmesser, 2008). To help unravel this mystery we sought to develop a reduced *in vitro* model system where the activity of MNs could be precisely controlled independently from the influence of neighbouring cells. As such, we cultured ChR2 ESCMNs at low density, 15,000 cells per well, on matrigel in 24-well plates fitted with light emitting diodes (LEDs; 470nm wavelength) controlled by a frequency pulse generator. The ChR2 ESCMNs were then cultured in the dark (n=183 cells) or activated by the LEDs at 0.025 (n=144 cells) or 0.1 Hz for 48 hours (n=19 cells) (Figure 3.6A). The cells were then fixed and anatomy characterized by quantification of total neurite outgrowth (Figure 3.6B; blue dotted-line), total displacement (Figure 3.6B; red dotted-line) and neurite branch number (Figure 3.6B; green numbers). Only ESCMNs not in contact with neighbouring cells were chosen for

quantification to reduce variables, such as neurite to neurite enhancement of growth that could complicate interpretation of the activity-dependent effects. Figure 3.5B shows how the ChR2 ESCMNs morphologies differed between the three conditions described above. The ChR2 ESCMNs stimulated at 0.025 Hz, 0.1 Hz or cultured in the dark had total neurite outgrowths (mean ±SD) equaling 612 ± 570 μm, 448 ± 260 μm and 143 ± 130 μm, respectively (Figure. 3.6C). Quantification showed that total neurite outgrowth was significantly less in the cultures grown in the dark compared to both light-activated groups (0.025 Hz $p<0.001$ and 0.1 Hz $p<0.001$; Mann-Whitney Rank Sum Test). ChR2 ESCMNs, light-activated at 0.025 Hz, 0.1 Hz, or cultured in the dark had total neurite displacements of 277 ± 260 μm, 230 ± 100 μm and 98 ± 115 μm, respectively (Figure. 3.6D). As with total length, both light stimulation paradigms resulted in greater displacement of the longest neurite from the cell body compared to MNs grown in the dark (0.025 Hz $p<0.001$ and 0.1 Hz $p<0.001$; Mann-Whitney Rank Sum Test). Finally, the total number of neurite branches was 4.2 ± 2.5, 4 ± 1.5 and 1.9 ± 1.5 for ChR2 ESCMNs stimulated at 0.025 Hz, 0.2 Hz and grown in the dark, respectively (Figure. 3.6E). Cells grown in the dark had significantly fewer neurite branches compared to both groups stimulated by light (0.025 Hz $p<0.001$and 0.1 Hz $p<0.001$; Mann-Whitney Rank Sum Test). Interestingly, in all three parameters quantified we found no significant difference between the stimulation frequencies used to activate the MNs. It should be noted that after 24 hours in culture (n=20) an increase in all three parameters measured was seen at a stimulation frequency of 0.025 Hz (total length: 547 ± 364 μm, displacement: 239 ± 163 μm, branches: 4.5 ± 2.4).

Activity induced changes in morphology are attenuated when action potentials are blocked.

Our whole cell current clamp recordings indicated that ChR2 ESCMNs depolarize when exposed to light and that this depolarization is sustained for the entire duration of the pulse (Fig. 3.4). In addition, we found that single action potentials were generated at the onset of each light-pulse, at 48 hours in culture, 56% of the time (Figure 3.4). The changes in growth observed in the light stimulated conditions could therefore be due to activation of growth promoting signaling pathways triggered by strong, sustained depolarizations or they could be regulated by signaling pathways activated by the emergence of action potentials. To distinguish between these two possibilities we treated dissociated ChR2 ESCMNs with tetrodotoxin [TTX; 25 μM] to block voltage gated Na channels and placed them in the dark for 48 hours or light-activated them hours at 0.025 Hz for the same time period. For comparison purposes cultures without TTX, as described previously in Figure 3.6, were similarly light-activated or placed in the dark. The TTX treatment eliminated the differences between stimulated and non-stimulated MNs with respects to total length and displacement (Figure 3.7A; n=7). Stimulated ChR2 ESCMNs had a greater total length than MNs grown in the dark as well as stimulated TTX treated MNs ($p=0.011$), and non-stimulated TTX treated MNs cultured in the dark ($p=0.022$) (Figure 3.7B). Similarly, stimulated ChR2 ESCMNs had a greater displacement than stimulated TTX treated MNs ($p=0.03$) and non-stimulated TTX treated ($p<0.001$) and untreated treated MNs grown in the dark ($p=0.019$) (Figure 3.7C). Although a trend was seen with a decrease in branching in TTX treated cultures it was not found to be significant (Figure 3.7D). Taken together, these results suggest that the morphological changes induced by light-activation resulted from the activation of

specific signaling pathways that were triggered by the presence of action potentials (however, see Discussion).

PSA-NCAM and NCAM protein levels are regulated by neural activity in ChR2 ESCMNs.

Previous studies have shown that distinct patterns of neural activity modulates the expression of axon guidance molecules such as neural cell adhesion molecule (NCAM) and its polysialic acid (PSA) moiety. For example, pharmacologically slowing spontaneous motor neuron bursting activity with picrotoxin in ovo significantly attenuates the expression of polysialylated NCAM (PSA-NCAM) on the growing motor axons as the extend out of the spinal cord (Hanson and Landmesser, 2004). This decrease in PSA-NCAM expression was correlated with motor axon guidance defects (Hanson and Landmesser, 2004). Furthermore, PSA-NCAM expression levels became normal and motor axon targeting defects eliminated in picrotoxin treated chick embryos when spontaneous activity patterns were restored using in ovo light-activation of ChR2 expressing spinal neurons (Kastanenka and Landmesser, 2010). Inspired by these studies, we next assessed whether the expression of PSA and/or NCAM in MNs is regulated by activity using our *in vitro* light-activated model system.

Protein homogenates were collected from ChR2 ES cell cultures that were stimulated for 48 hours at 0.025 Hz (100 ms light pulse width) or remained in the dark for the same time period. PSA and NCAM isoform expressions levels were then examined with SDS-PAGE combined with immunoblot analysis using an antibody that recognizes all NCAM isoforms. Half of the homogenates were treated with endoneuraminidase N (EndoN) to specifically remove the PSA moiety from the individual NCAM isoforms (Figure 3.8A, lanes 3 & 4) while the other half remained untreated to visualize PSA-

NCAM (Figure 3.8A, lanes 1 & 2). In the latter condition, PSA-NCAM appears as a broad band extending from ~250 kDa-180 kDa when separated on a 6% gel (Figure 3.8A; lanes 1 & 3). When PSA is removed from NCAM, two distinct bands are observed (Figure 3.8A, lanes 2 & 4), representing the neural specific 180- and 140kDa NCAM isoforms.

The light stimulated ChR2 ESCMNs showed a higher expression of both PSA-NCAM (lane 1) and NCAM (lane 2) then the non-stimulated cells (lane 3 and 4). Band intensity analysis, normalized by actin (i.e. protein loading control), was performed using ImageJ software (Figure 3.8B-D). The intensity of PSA-NCAM staining on the stimulated ChR2 ESCMNs was a three-fold higher than the un-stimulated cells (i.e. cells cultured in the dark; Figure 3.8B). There was a 2-fold increase seen in combined NCAM isoform expression in the stimulated cells (Figure 3.8C). When the individual NCAM isoforms were quantified separately, they both showed a 2-fold increase in the light condition; however, there was greater expression in the 140 kDa isoform in both conditions (140 kDa compared to the 180 kDa) (Figure 3.8D).

These results suggest that light-activation increases the expression of NCAM and PSA in cultured MNs. Because the increase in expression of PSA-NCAM is relatively more than the increase in NCAM, these results also suggest that light-activation triggers cellular responses that enhance polysialylation relatively more than the synthesis of additional NCAM molecules.

To investigate whether light-activated changes in motor neuron morphology is caused by the simultaneous increase in PSA expression we cultured ChR2 ESCMNs and light-activated them at 0.025 Hz for 48 hours as described above in the presence and

absence of EndoN (i.e. with and without PSA, respectively; Figure 3.9A). Parallel cultures were treated and untreated with EndoN and grown in the dark for comparison. Removal of PSA significantly reduced the total length of the ChR2 ESCMNs in the stimulated condition (Figure 3.9; n=24, Mann-Whitney Rank Sum Test, $p<0.001$). However, it did not completely abolish the affect of the light stimulation; the MNs stimulated without PSA had a total length significantly greater then the non-stimulated cells with and without PSA removed (Figure 3.9B; without PSA n=33; Mann-Whitney Rank Sum Test; both $p<0.001$). The removal of PSA in the non-stimulated condition did not have a significant affect to the total length of the ChR2 ESCMNs. Similar relationships were observed with total displacement where the removal of PSA in the light stimulated cells reduced the displacement significantly compared to cells with PSA that were stimulated (Figure 3.9C, Mann-Whitney Rank Sum Test; $p=0.018$). Yet, the ChR2 ESCMNs without PSA still had greater displacement then those non-stimulated with or without PSA (Figure 3.9C; Mann-Whitney Rank Sum Test; both $p<0.001$). Again the removal of PSA in the dark did not cause a significant difference in displacement between the two conditions. The loss of PSA did not decrease the number of neurite branches within the light-activated or dark conditions (Figure 3.9D), although MNs in both light-activated conditions had more branches the parallel cultures grown in the dark (Figure 3.9D). There was no significant difference seen in the stimulated ESCMNs with or without PSA. Interestingly, the stimulated ESCMNs without PSA had significantly more neurite branches than those cells that were in the dark with PSA (Figure 3.9D, Mann-Whitney Rank Sum Test $p=0.017$) and those without PSA (Mann-Whitney Rank Sum Test $p=0.012$). Furthermore, the MNs without PSA in the stimulated and non-

stimulated condition were also significantly different from each other (Figure 3.9D, Mann-Whitney Rank Sum Test p=0.015). Taken together, these results indicate that light-activation increases NCAM polysialylation and that this increase regulates, at least in part, growth of ChR2 ESCMNin culture.

Chapter 3 Figures

Figure 3.1. Illustrations showing the transgenic constructs of the mice bred to create the ChR2 ESCMNs, the methodology of the embryonic stem cell creation and differentiation of EBs into ESCMNs. **A**, Mice heterozygous for $HB9^{cre}$ were bred with mice having a floxP-flanked STOP cassette upstream of ChR2(H134R)-EYFP fusion gene. **B**, ES cells (termed Hb9ChR2 ES cells) were then isolated from the inner cell mass of blastocysts harvested from the pregnant females, 3.5 days post-coitus, and expanded on a feeder layer of mouse embryonic fibroblasts (illustration adapted from Landry and Zucker, 2004). **C,** ES cells were later cultured as a cell suspension for 48 hours where they formed aggregates termed EBs. To direct ES cells to differentiate into motor neurons the EBs were then treated with RA and SMo for 5 DIV. Cre-mediated recombination leads to deletion of the flanked sequences in HB9 expressing cells causing ChR2-EYFP to be expressed in the diffrenetiated ESCMN.

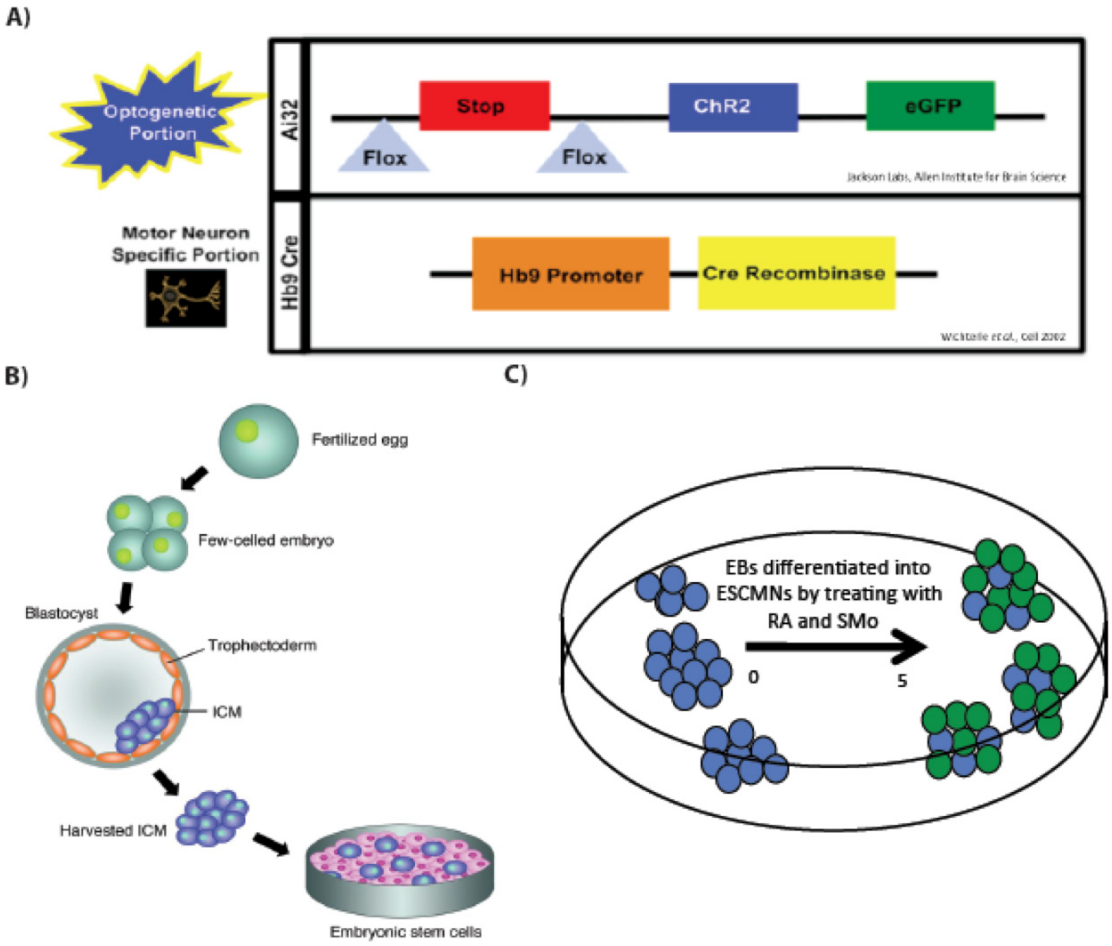
A)
Optogenetic Portion
Motor Neuron Specific Portion
Ai32
Stop
Flox
Flox
ChR2
eGFP
Jackson Labs, Allen Institute for Brain Science
Hb9 Cre
Hb9 Promoter
Cre Recombinase
Wichterle et al., Cell 2002
B)
Fertilized egg
Few-celled embryo
Blastocyst
Trophectoderm
ICM
Harvested ICM
Embryonic stem cells
C)
EBs differentiated into ESCMNs by treating with RA and SMo
0
5

Figure 3.2. Illustration showing stimulation protocol of dissociated EBs. The dissociated ChR2 ESCMNs (**A**) all were plated at low density, 15,000 cells per well, in a 37° Celsius incubator with 5% CO_2 for 48 hours, that either had blue LEDs flashing at (**B**) 100ms exposure at a frequency of.025hz or (**C**) 100ms exposure at a frequency of 0.1hz or (**D**) with out blue LEDs in total darkness.

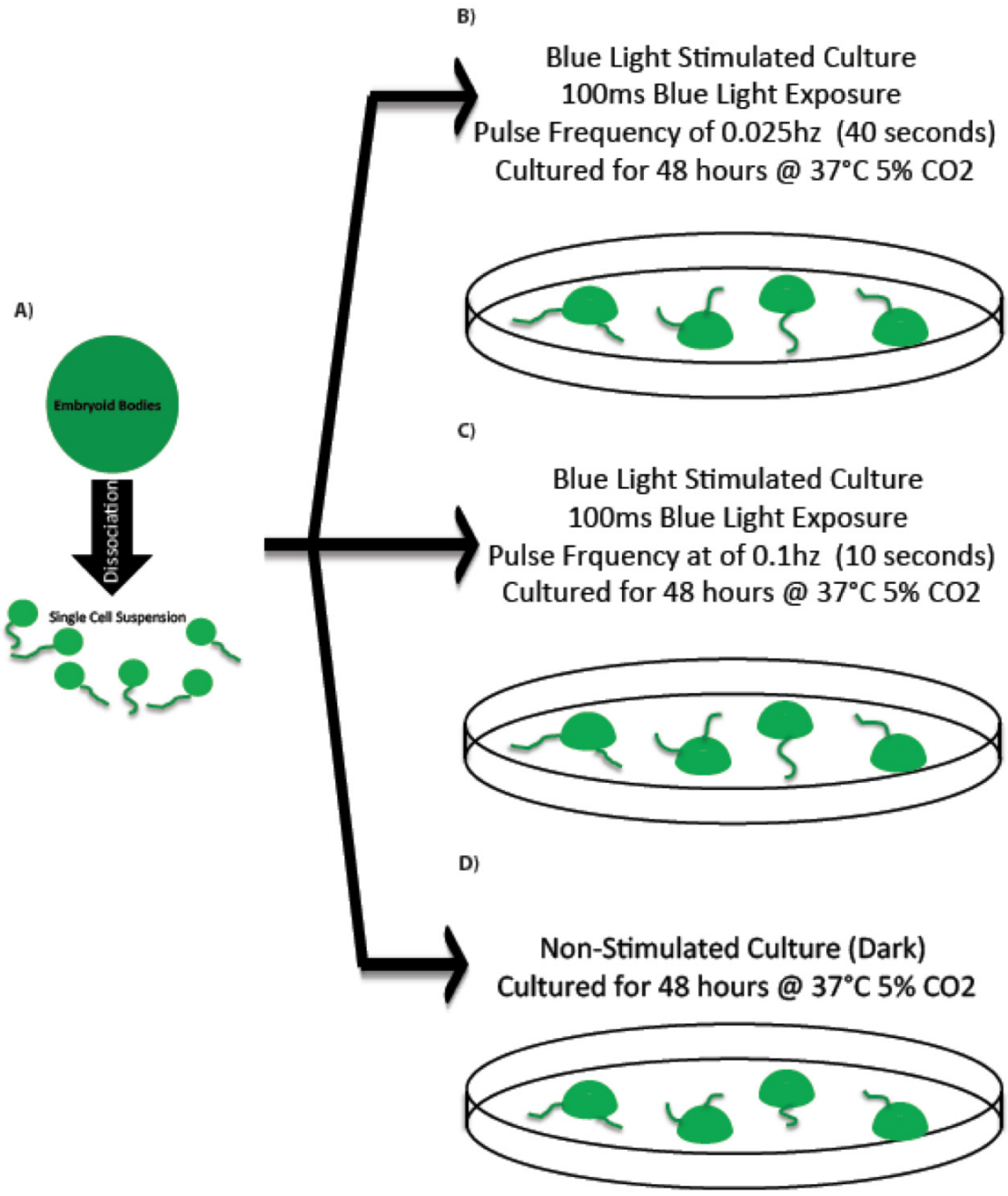
A)
Embryoid Bodies
Dissociation
Single Cell Suspension
B)
Blue Light Stimulated Culture
100ms Blue Light Exposure
Pulse Frequency of 0.025hz (40 seconds)
Cultured for 48 hours @ 37°C 5% CO2
C)
Blue Light Stimulated Culture
100ms Blue Light Exposure
Pulse Frquency at of 0.1hz (10 seconds)
Cultured for 48 hours @ 37°C 5% CO2
D)
Non-Stimulated Culture (Dark)
Cultured for 48 hours @ 37°C 5% CO2

Figure 3.3. ChR2 ESCMNs have growth characteristics comparable to ESCMNs derived from HBG3 ES cells. **A,B** ESCMNs, derived from HBG3 (**A**) and Hb9ChR2 ES cells (**B**), express GFP and have comparable neurite outgrowth 3-7 DIV. Photomicrographs to the right are inverted black and white images of the green fluorescence. Scale bar = 10 μm.

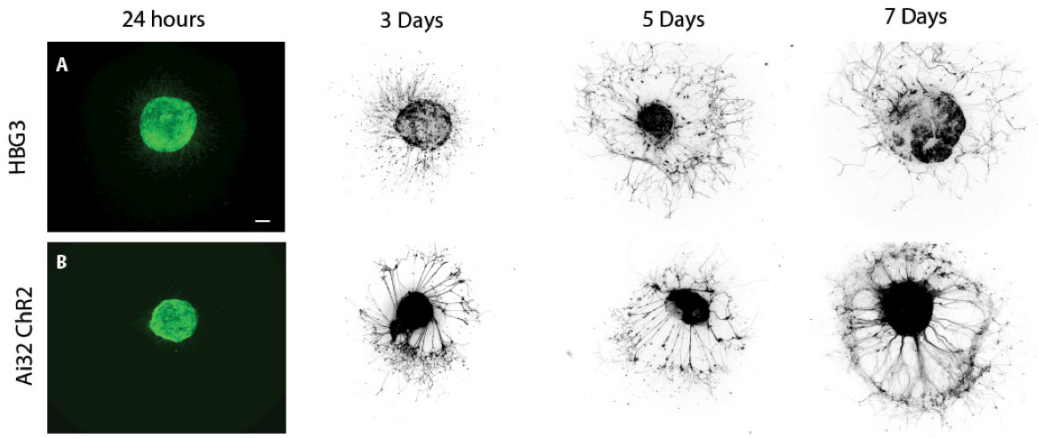
24 hours
3 Days
5 Days
7 Days
A
HBG3
B
Ai32 ChR2

Figure 3.4. ChR2 ESCMNs depolarize and fire single action potentials when depolarized by light. **A, B** Current clamp recordings of membrane potentials, from ChR2 ESCMNs cultured for 24 & 48 hours (**A**) and 1 & 2 weeks (**B**) in response to blue light pulses (blue bars). Recordings show sustained depolarizations lasting the duration of light pulses and the emergence of single action potentials at the onset of the depolarizations after 48 hours (**A**, right trace). As a result, single action potentials were elicited with each light pulse by 1 week in culture (**B**).

Light Evoked

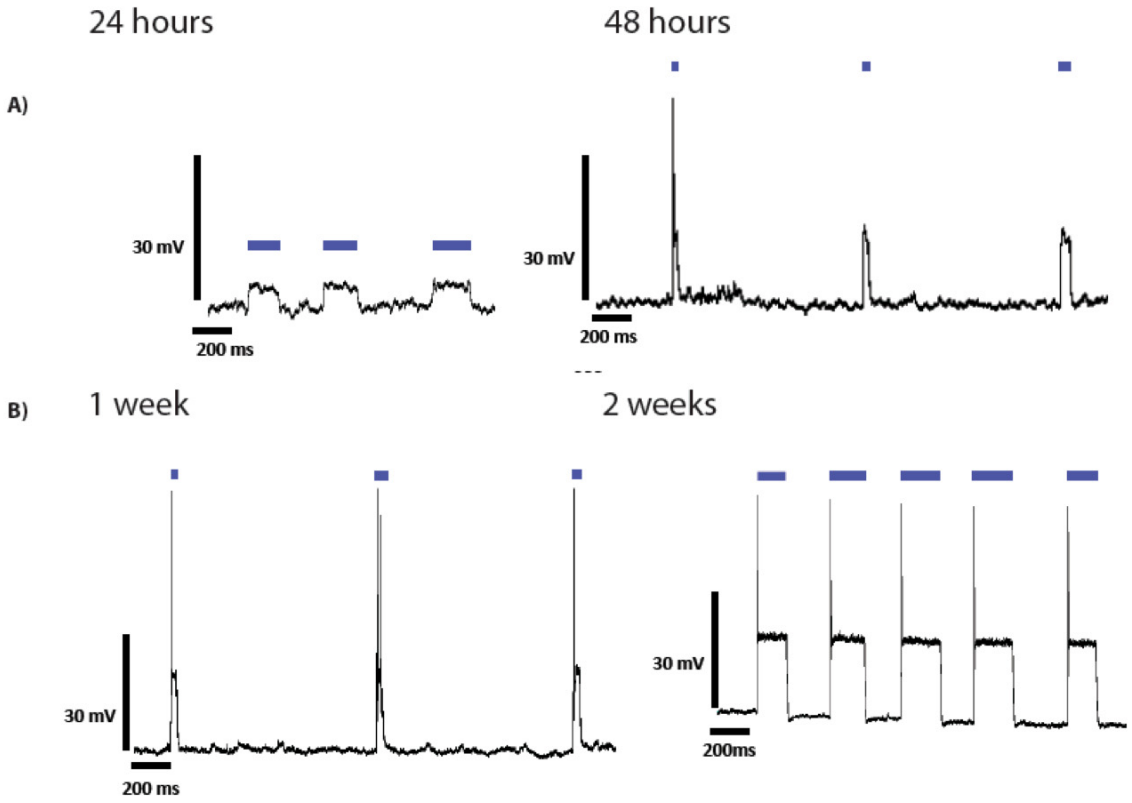

Figure 3.5. ChR2 ESCMNs develop appropriate motor neuron firing properties. **A, B** Current clamp recordings of membrane voltage in response to current injections (1000 ms duration) in ChR2 ESCMNs showing single action potentials 24 & 48 hours after plating (**A**) and repetitive firing 1 & 2 weeks after plating (**B**). 80pA (**B**, left) and 100pA (**B**, right) of depolarizing current evoked maximum firing frequencies 1 & 2 weeks after plating. **C**, 20 pA of depolarizing current evoked a single action potential in ChR2 ESCMNs after 1 week in culture. **D**, Plot of instantaneous firing frequency versus time during a single current pulse, demonstrating spike frequency adaptation in 2-week-old ChR2 ESCMNs.

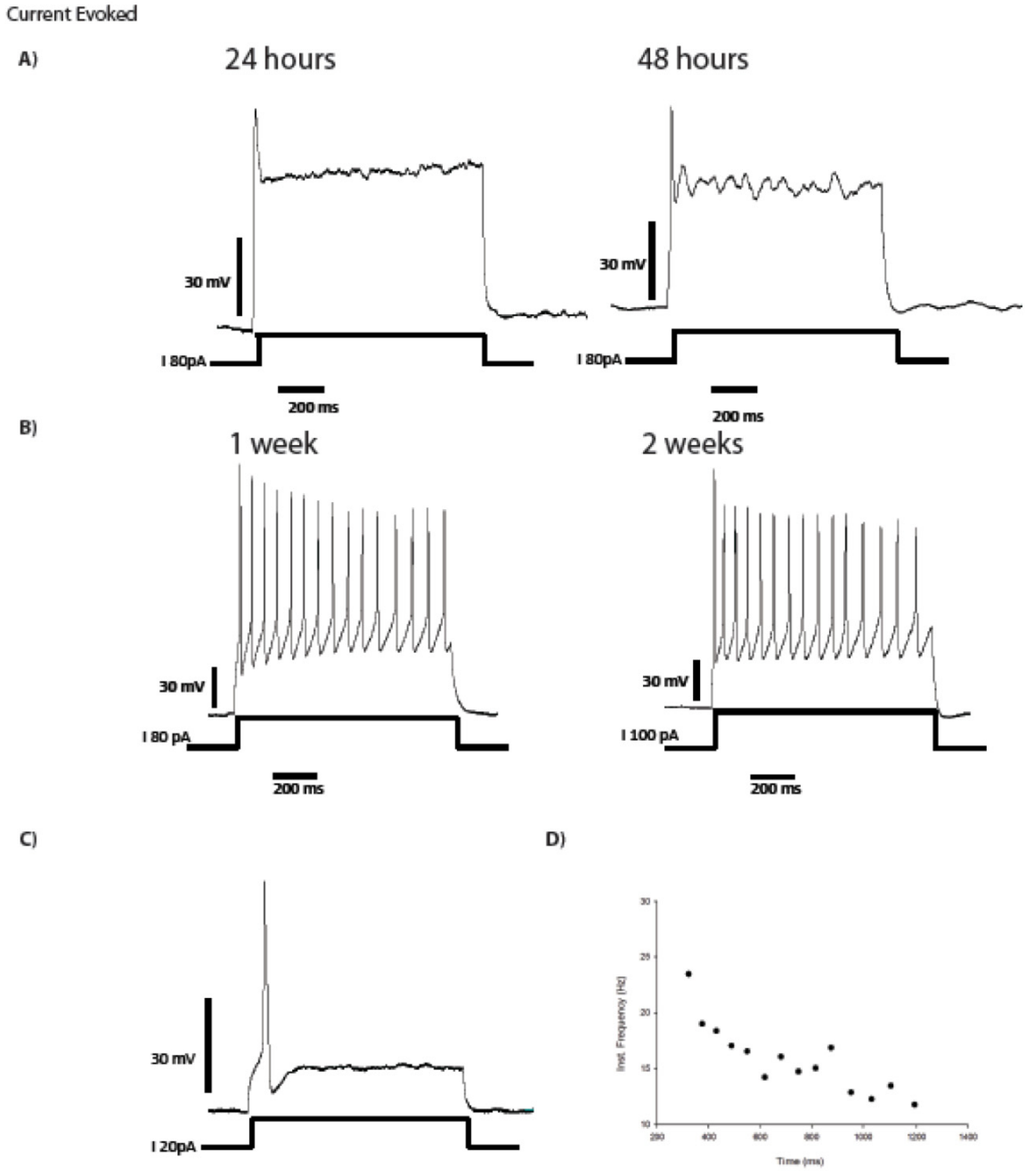
Current Evoked
A)
24 hours
48 hours
30 mV
I 80pA
200 ms
30 mV
I 80pA
200 ms
B)
1 week
2 weeks
30 mV
I 80 pA
200 ms
30 mV
I 100 pA
200 ms
C)
D)
30 mV
I 20pA
Inst. Frequency (Hz)
Time (ms)

Figure 3.6. Light-activation of ChR2 ESCMNs enhances neurite growth and complexity. **A**, Typical examples of ChR2 ESCMNs cultured in the dark (non-stimulated), or light-activated at 0.1 or 0.025 Hz for 48 hours starting 3 hours after plating. **B**, Growth parameters quantified included combined neurite lengths (blue dotted-line), distance from cell body of the longest neurite (red dotted-line) and number of neurite branches (green numbers). **C-E**, 0.1 and 0.025 Hz light pulse stimulation of ChR2 ESCMNs significantly increased combined neurite lengths (**C**), longest neurite distance (**D**) and neurite numbers (**E**) compared to motor neurons grown in the dark (***$p<0.001$; Mann-Whitney Rank Sum Test). Photomicrographs in **A, B** are black and white, inverted images of GFP.

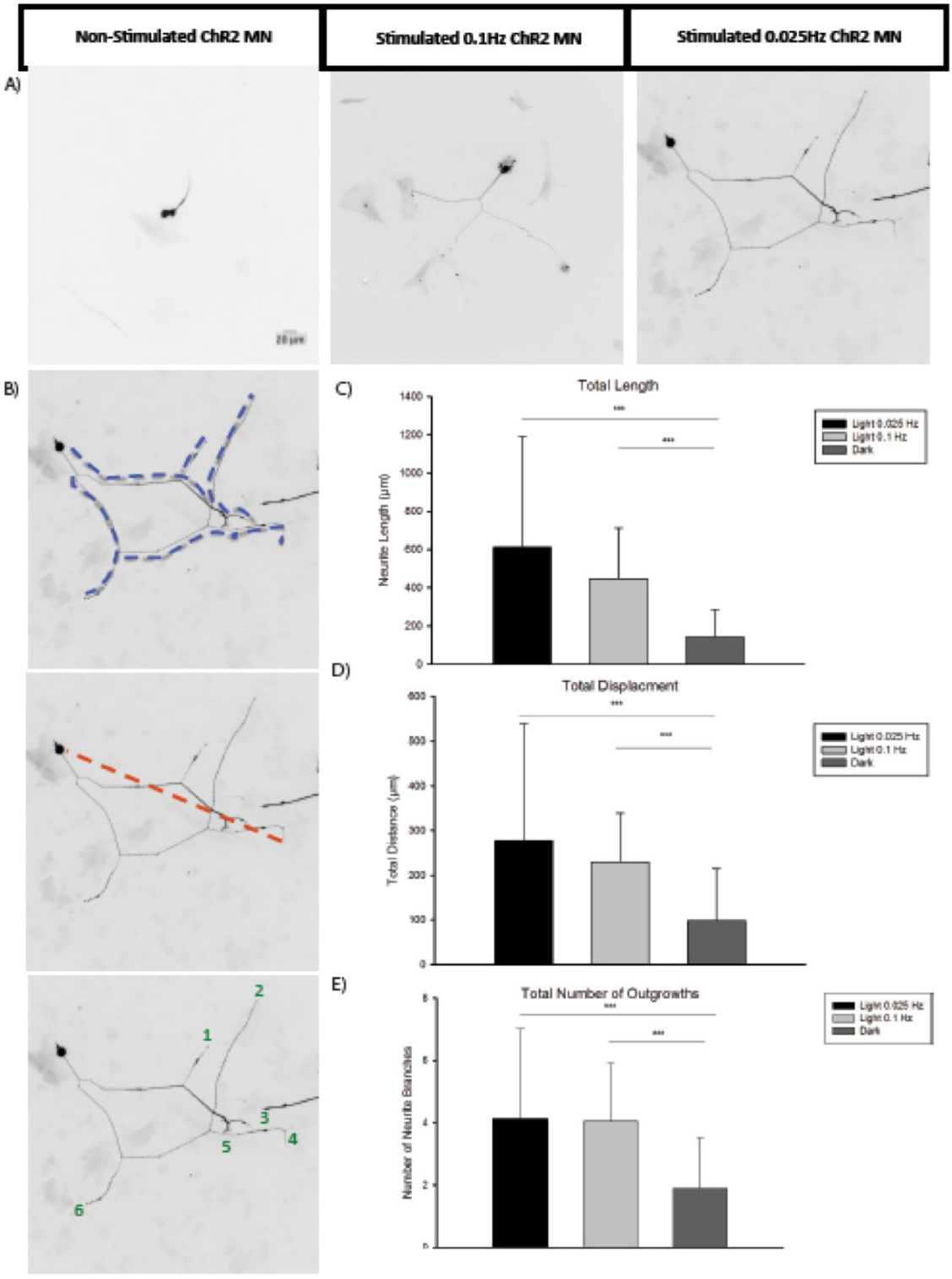
Non-Stimulated ChR2 MN
Stimulated 0.1Hz ChR2 MN
Stimulated 0.025Hz ChR2 MN
A)
B)
C)
D)
E)
Total Length
Neurite Length (µm)
Light 0.025 Hz
Light 0.1 Hz
Dark
Total Displacment
Total Distance (µm)
Total Number of Outgrowths
Number of Neurite Branches
1
2
3
4
5
6

Figure 3.7. Activity induced changes in neurite morphology are attenuated when action potentials are blocked with TTX. **A**, Typical examples of ChR2 ESCMNs cultured in the dark (non-stimulated), or light-activated at 0.025 Hz for 48 hours in the presence of TTX (2.5 μM), starting 3 hours after plating. **B-D**, Exposure to TTX eliminated morphological differences between light-stimulated and non-stimulated ChR2 ESCMNs with respect to total length (**B**), longest neurite distance (**C**), and number of neurite branches (**D**). Values from Figure 3.6 are shown for comparison.

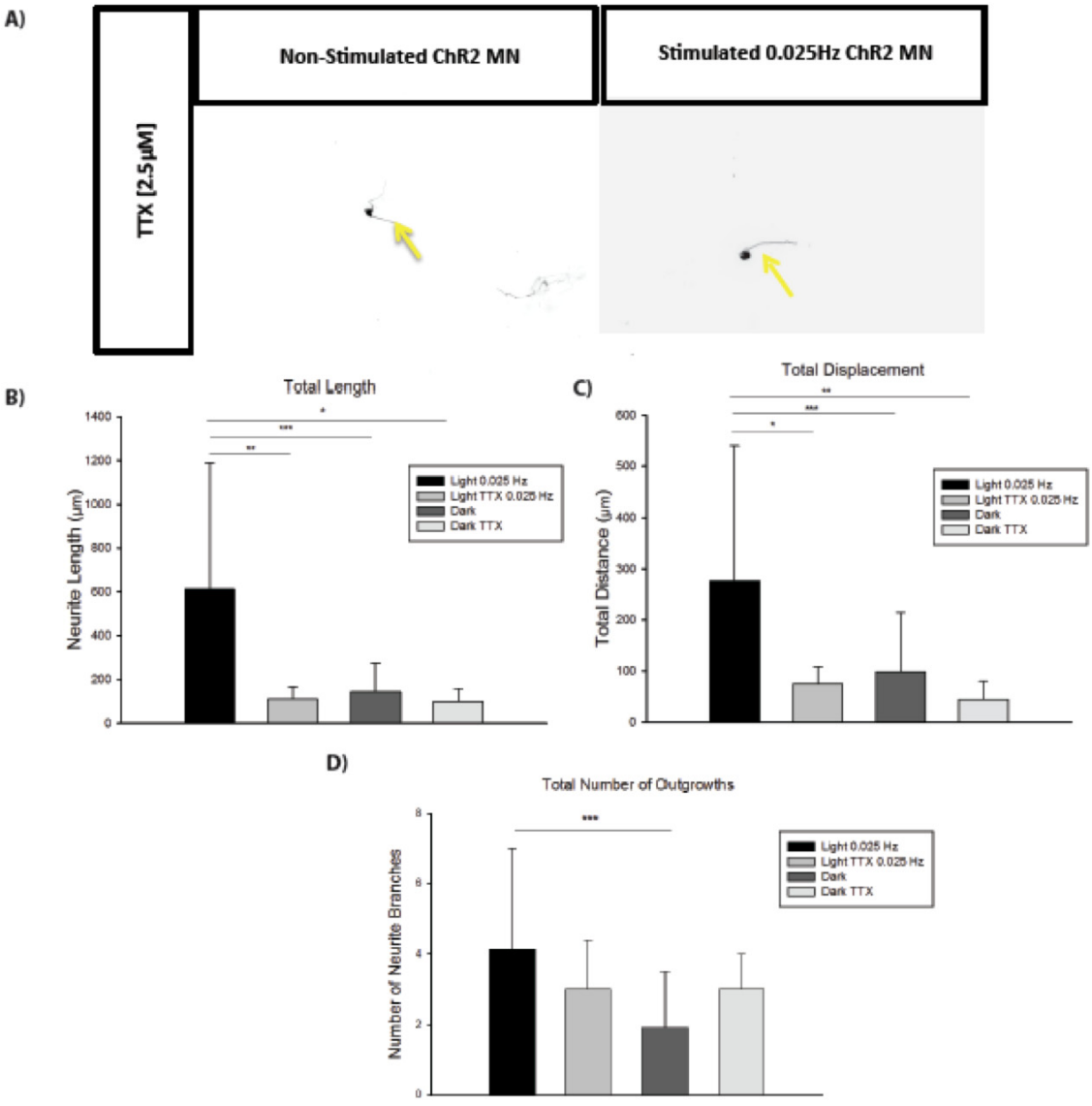
A)
TTX [2.5μM]
Non-Stimulated ChR2 MN
Stimulated 0.025Hz ChR2 MN
B)
Total Length
Neurite Length (μm)
Light 0.025 Hz
Light TTX 0.025 Hz
Dark
Dark TTX
C)
Total Displacement
Total Distance (μm)
D)
Total Number of Outgrowths
Number of Neurite Branches

Figure 3.8. SDS gel electrophoresis and immunoblot analysis of NCAM isoforms, and degree of polysialylation, of light-stimulated and non-stimulated ChR2 ESCMNs in culture. **A**, Depolysialylation protein homogenates from ChR2 ESCMN cultures that were optically stimulated (0.025 Hz) or non-stimulated for 2 DIV contain the 180- and 140 kDa NCAM isoform (lanes 2 & 4). In contrast, polysialylated NCAM (PSA-NCAM) from the same cultures was detected as a diffuse band running between 180-240 kDa (lanes 1 & 3). Both PSA-NCAM and individual NCAM isoforms are more highly expressed in the light stimulated cultures. **B-D**, Band intensity analysis showed a significant increase in the amount in PSA-NCAM (**B**), total NCAM (**C**) and individual NCAM isoforms (**D**) compared to the non-stimulated cultures (***$p<0.001$, Student t-test).

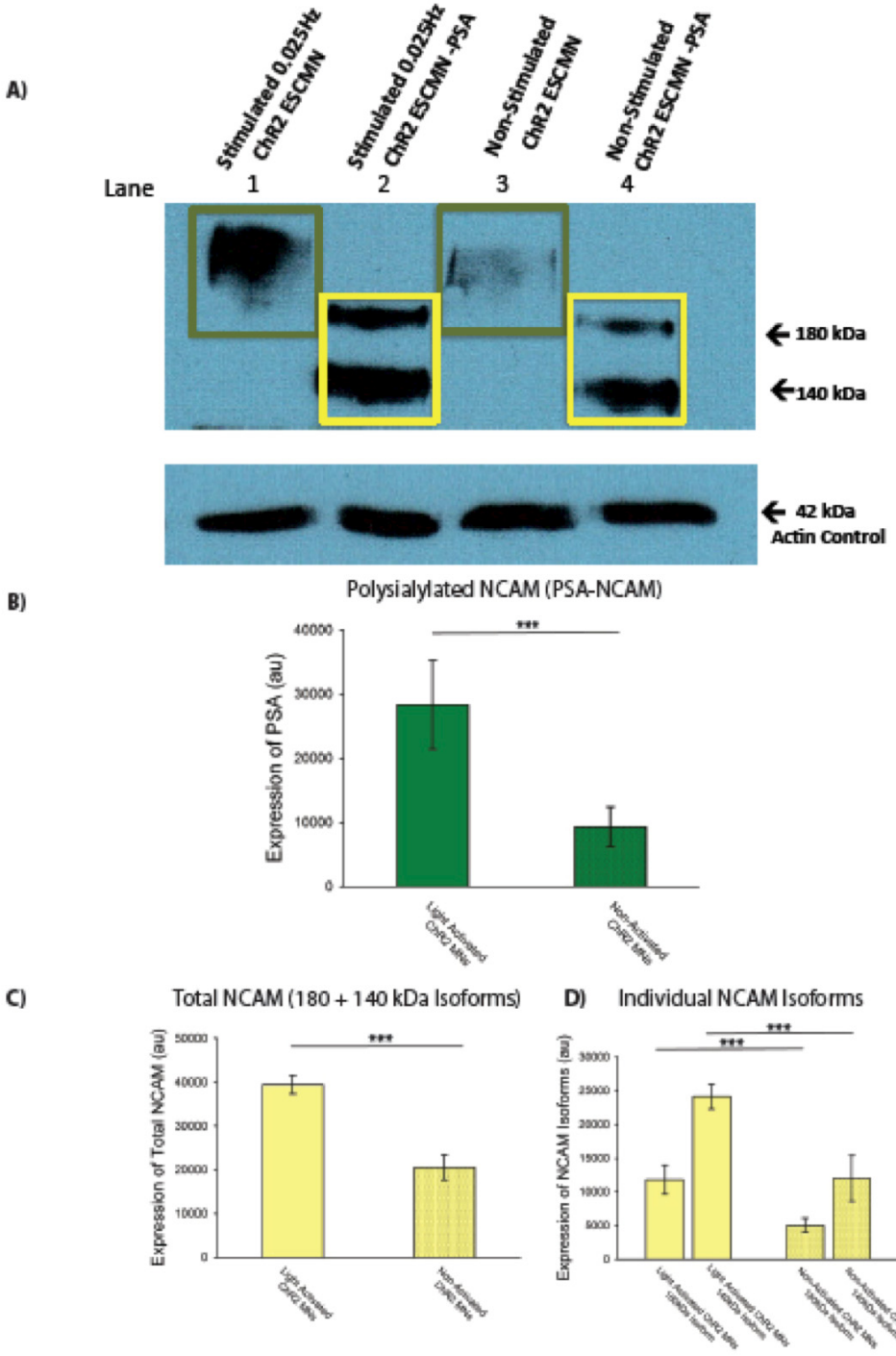
A)
Stimulated 0.025Hz ChR2 ESCMN
Stimulated 0.025Hz ChR2 ESCMN -PSA
Non-Stimulated ChR2 ESCMN
Non-Stimulated ChR2 ESCMN -PSA
Lane
1
2
3
4
180 kDa
140 kDa
42 kDa
Actin Control
B)
Polysialylated NCAM (PSA-NCAM)
Expression of PSA (au)
***
Light Activated ChR2 MNs
Non-Activated ChR2 MNs
C)
Total NCAM (180 + 140 kDa Isoforms)
Expression of Total NCAM (au)
***
D)
Individual NCAM Isoforms
Expression of NCAM Isoforms (au)
***
***

Figure 3.9. Enhanced neurite growth and branching complexity are attenuated when PSA is removed from NCAM. **A**, Cartoons of NCAM showing the 5 extracellular immunoglobulin-like (black omega structures) and 2 fibronectin type III-like (green cylinders) domains. The 180- and 140-kDa isoforms have specific intracellular domains, that regulate growth by interacting with specific cytoskeletal elements. PSA (yellow barbs) attaches to the 1st immunoglobulin domain. Endo-N rapidly degrades the PSA moiety of NCAM (right cartoon). **B-D**, Removal of PSA with Endo-N significantly reduced the total length of the motor neurons in the stimulated condition ($p<0.001$). The motor neurons without PSA that were light stimulated were still significantly longer then the non-stimulated cells with and without PSA ($p<0.001$). The removal of PSA in the non-stimulated condition did not have a significant affect to the total length of the ChR2 ESCMN (**B**). The removal of PSA in the light stimulated cells significantly reduced axon displacement compared to cells with PSA that were stimulated ($p<0.05$). ChR2 ESCMN without PSA still had greater displacement then those non-stimulated with or without PSA ($p<0.001$). Removal of PSA in the dark did not cause a significant difference in displacement between the two conditions (**C**). No significant differences were seen within the same condition regardless of the presence or removal of PSA. The stimulated motor neurons without PSA had significantly more neurite branches than those cells that were in the dark with PSA ($p<0.05$) and without PSA ($p<0.012$). The MN without PSA in the stimulated and non-stimulated condition were significantly different from each other ($p<0.05$) (**D**) (Mann-Whitney Rank Sum Test used throughout). [* $p<0.05$, ** $p<0.01$, *** $p<0.001$]

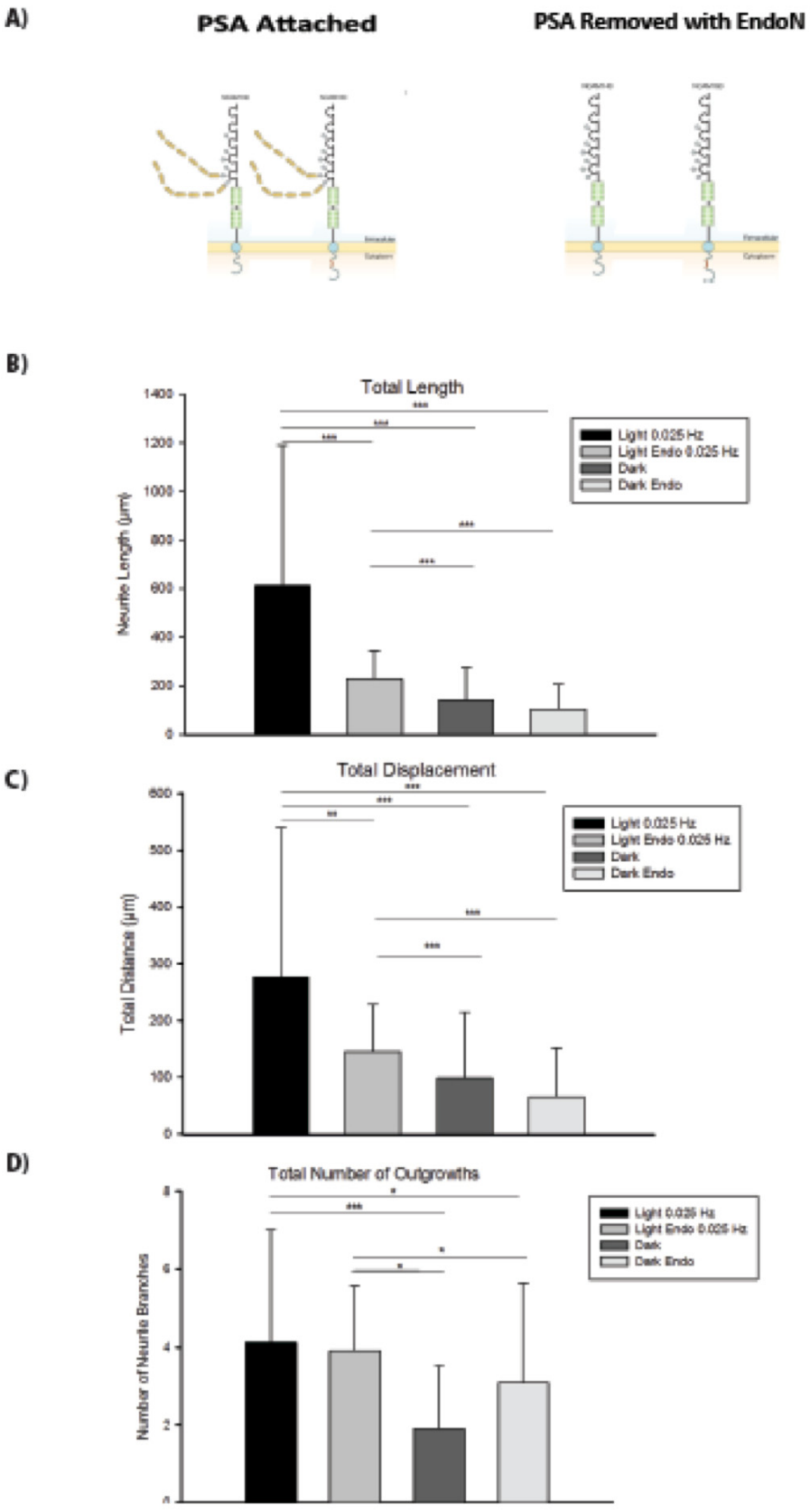
A)
PSA Attached
PSA Removed with EndoN
B)
Total Length
Neurite Length (µm)
Light 0.025 Hz
Light Endo 0.025 Hz
Dark
Dark Endo
C)
Total Displacement
Total Distance (µm)
Light 0.025 Hz
Light Endo 0.025 Hz
Dark
Dark Endo
D)
Total Number of Outgrowths
Number of Neurite Branches
Light 0.025 Hz
Light Endo 0.025 Hz
Dark
Dark Endo

CHAPTER 4: THE ROLE OF ACTIVITY IN DISEASE

Introduction

An additional embryonic stem cell line was created in which the motor neurons express the SOD1G93A mutation in addition to ChR2. Both the 'WT' and the SOD1 expressing ChR2 ESCMNs were able to form functional neuromuscular junctions in vitro when plated on embryonic chick myotubes. ChR2 ESCMNs are capable of successful neurotransmission visualized by post-synaptic recordings in the muscle, in response to wide range of light exposure and frequency patterns. A scale was created, The Contraction Intensity (CI) Index, to be able to quantify the degree of contraction elicited as result of a single light pulse. This scale allows for indirect quantification of the degree of innervation over time in the co-cultures. Using the CI index we are able to show the detrimental effect of imposing activity on SOD1 ChR2 motor neurons, as it seems to increase the rate of muscle denervation. Finally we show that removing motor neurons from the network within embryoid body causes them to take longer to innervate muscle fibres initially and prolongs innervation in SOD1 cultures. These results demonstrate the potential role activity plays in motor neuron disease.

Contribution Statement

I would like to acknowledge Matthew Mackenzie and Udy Mackenzie for myotube preparation. I would also like to acknowledge Cindee Leopold and Simone Laforest for technical assistance with stem cell culture maintenance and mouse husbandry, respectively.

Results

Generation of ESCMNs expressing ChR2 and misfolded SOD1 protein

In Chapter 3 we generated ESCMNs expressing ChR2 to examine to what extent light-evoked depolarizations regulate neurite growth and the expression of axonal guidance molecules such as NCAM and its PSA moiety. In this chapter we will explore whether this technology can be used to characterize the development, and later stability, of neuromuscular junctions in co-cultures containing muscle fibres and wild-type motor neurons or motor neuron habouring a genetic mutation causing ALS (i.e. SOD1G93A mutation). The wild-type ESCMNs used in this chapter were derived from the Hb9ChR2 ES cells described in Chapter 3. To generate GFP^+ ESCMNs harbouring a SOD1G93A mutation we first crossed mice expressing both Cre recombinase under the control of the HB9 promoter and a loxP-flanked STOP cassette upstream of the ChR2(H134R)-EYFP fusion gene (Nagel *et al.,* 2005) with SOD1G93A mice (Gurney et al., 1994; reviewed by Julien and Kirz, 2006) (Figure 4.1A). This breeding strategy generates mice with SOD1G93A motor neurons expressing ChR2(H134R)-EYFP. ES were harvested from these animals 2.5 days after copulation and expanded to yield a SOD1 Hb9ChR2 ES cell line. Motor neurons derived from this ES cell line, using a standard RA/SAG differentiation protocol (Wichterle et al., 2002; Miles et al., 2004), are referred to as SOD1 ChR2 ESCMNs. PCR was used to detect the Cre and YFP transgenes (data not shown) in the ES cells while Westernblot analysis was used to detect misfolded SOD1 mutant protein. As shown in Figure 4.1B, the D3H5 monoclonal antibody that specifically detects disease-associated epitopes of misfolded SOD1 (Gros-Louis et al., 2010), detects a 28 kDa band in the SOD1 ChR2 ESCMNs (Figure. 4.1B, middle lane) while the wild-type ChR2 ESCMNs did not (Figure 4.1B, left lane). An ear clip from a

SOD1G93A mouse was used as a positive control (Figure 4.1B, right lane) while actin was used as a loading control.

ChR2 ESCMNs form functional neuromuscular junctions when co-cultured with chick muscle fibres.

Co-cultures containing muscle fibres and ESCMNs were generated as described by Chipman et al., (2014) (Figure 4.1C). Briefly, myoblasts were harvested from embryonic day 10 chick embryos and cultured for 3 days during which time they fused to form multinucleated muscle fibres. After 3 DIV, spheres containing several hundred ChR2 ESCMNs or SOD1 ChR2 ESCMNs were plated on the muscle fibres in the presence of GDNF and CNTF (Figure 4.1C). Trophic support was removed from the co-cultured 7 days later. Anatomical, electrophysiological and functional analysis of the co-cultures were performed 5 to 21 days after plating the ESCMNs (Figure 4.1C).

As shown previously (Miles et al., 2004; Soundararajan et al., 2007), GFP^+ neurites from ChR2 ESCMNs contacted clusters of acytelcholine receptors (AChRs), labeled with rhodamine-conjugated to an **α**-BTX (form here on simply referred to as **α**-BTX), on the co-cultured muscle fibres 10 and 40 days after plating (Figure 4.2). However, over time, the anatomical relationship between the presynaptic neurites and the post-synaptic AChRs became more complex and intimate such that at 10 DIV the neurites were merely touching the endplates (Figure 4.2A, asterisks) while they completely overlapped the AChR clusters by 40 DIV (Figure 4.2B, arrowheads). This co-localization and increased morphological complexity shows that the ChR2 ESCMN form synaptic connections that mature over time in culture (Figure 4.2; from 10 days to over a month).

Previous studies have shown that spontaneously active ESCMNs make functional connections with muscle fibres *in vitro* (Miles *et al.,* 2004; Soundararajan *et al.,* 2007; Chipman *et al.,* 2014; Toma *et al*., 2015). To characterize evoked neurotransmission at the neuromuscular junction in this novel *in vitro* model system we performed intracellular sharp electrode recordings of muscle fibres while light activating the ChR2 ESCMNs. Putative, functional NMJs were selected for recordings by identifying GFP^+ neurites in close contact with clusters of AChRs labeled with a-BTX (Figure 4.3A). To prevent muscle contractions during light-activation, we paralyzed the muscle fibres with Benzyl Toluene Sulphonamide (BTS; an inhibitor of actin-myosin interaction) (Pinniger et al., 2005; Burton et al., 2006). ChR2 ESCMNs were visualized and stimulated using optical excitation on a Zeiss Axio Examiner Di Microscope. The NMJs chosen for recording (n=11, in 13-16 day old cultures) had AChR staining, single motor neuron co-localization (Figure 4.3A), and were able to produce a post-synaptic muscle action potential when excited by blue light. Only cells with membrane potentials <35 mV (range -38 to -43 mV) were chosen for analysis.

To ascertain whether the amplitude and/or duration of muscle action potentials were effected by the light-pulse length (i.e. duration of presynaptic depolarization), we recorded from NMJs during 500, 200 and 1 ms light pulses (Figure 4.3B). While there was clearly variability in amplitude and duration between action potentials, neither property appeared to correlate with the duration of light-pulse used to elicit the response. Furthermore, regardless of light-pulse length, only one muscle action potential was observed at the onset of the pulse (Figure 4.3B). This latter result is not surprising given that only a single motor neuron action potential was observed in our patch-clamp

recordings during light-induced depolarizations (Chapter 3). We next examined post-synaptic responses at NMJs in the absence (Figure 4.3C) and presence of light-evoked (200 ms pulse width) ESCMN depolarizations at varying frequencies (Figure 4.3D-F). Figure 4.3 shows several mEPPs (indicated by asterisks) at a synapse indicating that spontaneous vesicle cycling and neurotransmitter release is likely occurring at these synapses. The mean amplitude (0.55 ± 0.16 mV) and range from 0.24-0.94 mV (Figure 4.3I) of mEPPs recorded in this study were very similar to those recorded from chick muscle fibres co-cultured with ESCMNs (Miles et al., 2004; Chipman et al., 2014) or iPSCMNs (Toma et al., 2014).

Repetitive light pulses between 0.1 Hz (Figure 4.3D) to 1.0 Hz (Figure 4.3F) produced muscle action potentials with each motor neuron depolarization (blue arrows), although the amplitude of the action potentials waned towards the end of the 1.0 Hz burst of light (Figure 4.3; last two muscle action potentials). There was an absence of action potentials after the first light-pulse when the stimulation frequency increased above 2 Hz (data not shown). This latter result is likely due to failures in neurotransmission at the NMJ because ChR2 ESCMNs fire repetitive action potentials when stimulated with light-pulses at 2 Hz (Figure 4.3B). Overall, the muscle action potential amplitudes ranged from 1.5-8.5 mV (Figure 4.3J) with a mean amplitude of 3.49 ± 1.74 mV (Figure 4.3K). As expected, light-evoked muscle action potentials, but not mEPPs, were blocked when TTX was added to the co-cultures (Figure 4.3G) while both were absent when D-tubocurarine (50-300 μM) was present (Figure 4.3H).

Development of a novel in vitro model system to quantify changes in neuromuscular function over time

Because ChR2 ESCMNs make functional connections with muscle fibres that can be precisely controlled by light we next sought to determine whether we could adapt this model system in order to quantify changes in functional neuromuscular connections over time. We reasoned that such a model system would be ideal for rapidly screening how specific proteins or diseases modulate neuromuscular function over time. To this end, we created a 'Contraction Index (CI)' scoring system whereby the motor neurons in the co-cultures activated by a single light pulse and the number of visually contracting muscle fibres scored between 0-5 (Figure 4.4A). In this assay, a single sphere containing ~200 ChR2 ESCMNs are plated in the centre of a well on a bed of previously formed chick muscle fibres as described previously (Figure 4.1C). CI is then scored each day after 5 DIV where the maximum number of contracting muscle fibres is given a score of "5". While there is some variability between cultures, Figure 3.4 shows how CI increases from 5 DIV to reach a peak and then plateau by 10 DIV (mean ±SD; 4.6 ±0.5, n=12). By 14 DIV, the CI score remained high (4.5 ±0.68, n=12) even though growth factors were removed from the cultures 7 days previously (Figure 4.1C & 4.4B).

CI is correlated with anatomical features indicative of functional innervation.

The CI is a rapid, longitudinal test that visually quantifies changes in number of contracting muscle fibres *in vitro*. Higher CI scores are therefore analogous to stronger muscle contractions *in vivo* while lower CIs indicate less muscle fibre contraction and overall strength. Decreased muscle strength *in vivo* can result from less muscle fibre innervation due to a decline in motor neuron numbers. This condition underlies, in part, progressive muscle weakness observed in patients with ALS. Changes in the efficiency

of neurotransmission can also lead to changes in muscle strength such as occurs in myasthenia gravis where AChR number and/or function is reduced. To determine whether CI scores correlate with anatomical features indicative of muscle fibre innervation, such as motor axon and AChR numbers, we fixed co-cultures after 7 or 14 DIV and immunolabeled them for GFP and SV2 (to visualize axons and synaptic vesicles, respectively). The latter was performed because is well known that synaptic vesicles redistribute to the presynaptic terminal from along the axon during normal neuromuscular development (Ziv & Garner, 2004 Rev; Zakharenko *et al*., 1990). In addition, we labeled the cells with **α**-BTX to visualize AChR clusters. As shown in Figure 4.5B, the co-culture with a CI score of 5 contains fewer GFP^+ axons, **α**-BTX labeled AChRs and SV2 clusters compared to the culture with a CI score of 1. In addition, the number and size of the **α**-BTX clusters appeared larger in the co-culture with a CI score of 5. These results suggest that higher CIs have more anatomical features typically associated with a higher degree of successful function innervation.

In order to determine whether there is a systematic and predictive relationship between CI scores and axon, synaptic vesicle and AChR numbers we quantified the pixel intensities of GFP and SV2 immunofluorescence, as well as **α**-BTX, in a region of interest (ROI) surrounding the cluster of ESCMNs (Figure 4.5A). Care was taken to ensure that the ROI included all of the GFP^+ neurites, but not the ESCMN cell bodies. Pixel intensities were then plotted as arbitrary units (au) versus the CI score calculated on the day the cultures were fixed (i.e. 7 DIV, n=32 or 14 DIV, n=33) (Figure 4.6A-J). Because **α**-BTX number and size appeared to be greater at higher CIs (Figure 4.5B), we also plotted these values against CI at 7 and 14 DIV. Interestingly, we found that all five

measurements increased exponentially with CI scores such that they were well fitted to a linear regression line when plotted on a semilogarithmic scale where:

$$Y=10^{(\text{slope}*x + \text{y-intercept})}$$

The slope (± SE) of the regression lines for GFP (Figure 4.6A), SV2 (Figure 4.6B) and **α**-BTX (Figure 4.6C) pixel intensities plotted against CI after 7 DIV were 0.29 ±0.05 (range: 0.86 - 29, r^2= 0.90), 0.18 ± 0.029 (range: 0.49 - 4.8, r^2= 0.91) and 0.38 ± 0.031 (range: 0.091 – 5.5, r^2= 0.97), respectively. The slope of the regression lines fitted to the number (Figure 4.6D) and size of the a-BTX clusters (Figure 4.6E) plotted against CI after 7 DIV were 0.29 ± 0.042 (range: 30 - 520, r^2= 0.92) and 0.079 ± 0.015 (range: 30 - 74, r^2= 0.87), respectively. With the exception of the range in GFP intensity (see below), we found that the relationship between CI and pixel intensities, as well as **α**-BTX number and size, at 14 DIV were remarkably similar to those recorded at 7 DIV. Figure 4.6G-J shows that the slope (± SE) of the regression lines for GFP (Figure 4.6F), SV2 (Figure 4.6G) **α**-BTX intensities (Figure 4.6H), as well as **α**-BTX cluster number (Figure 4.6I) and **α** -BTX cluster size (Figure 4.6J) were 0.31 ± 0.065 (range: 0.21 – 3.6, r^2= 0.85), 0.28 ± 0.068 (range: 0.63 - 4.9, r^2= 0.70), 0.32 ± 0.076 (range: 0.03 – 4.5, r^2= 0.82), 0.29 ± 0.027 (range: 31 - 615, r^2= 0.97), and 0.072 ± 0.018 (range: 32 – 57, r^2= 0.80), respectively when plotted against CI on semilogarithmic scales. Interestingly, GFP pixel intensities were 10-fold lower at each CI after 14 DIV (Figure 4.6F) compared to those recorded at 7 DIV (Figure 4.6A) indicating that the 14 day cultures contained less motor axons. However, because the slopes were similar (i.e. 0.29 ± 0.05 and 0.31 ± 0.065 at 7 and 14 DIV, respectively), these results suggest that the same number of muscle fibres were innervated in cultures with the same CI at both time points. The decrease in GFP

intensity, therefore, likely reflects a loss of motor axons over time in culture that did not functionally innervate muscle fibres. Taken together, these results show that CI can be used to quantify differences in functional innervation *in vitro* and predict how this level of function correlates with motor axon, synaptic vesicle and AChR numbers.

CI scores differ between WT and SOD1 ChR2 ESCMNs over time.

As shown in Figure 4.4B, the CI scores increase from approximately 2.5 at 5 DIV to plateau at 4.5 after 10-14 DIV for WT. This observation indicates that the average number of functionally innervated muscle fibres increases between 5-10 DIV, after which time it remains stable for at least 4 more days even though the number of GFP^+ axons in the culture decreases over the same time period (compare Figure 4.6A with 4.6F). Theses results suggest that the axons with functional NMJs remain stable for at least 14 DIV. NMJ instability, or the withdrawal of motor axons from endplates, has been observed in animal models of ALS (Frey et al., 2000; Fischer et al., 2004) and in patients with the disease (Piotrkiewicz and Hausmanowa-Petrusewicz, 2013). Furthermore, motor axon withdrawal appears to occur prior to motor neuron cell death in ALS (Gould et al., 2006). To determine whether this phenomena 1) occurs in culture and 2) is reflected by changes in CI scores we co-cultured SOD1 ChR2 ESCMNs with chick muscle fibres and quantified CIs over 14 days (n=4). Figure 4.7A shows that WT and SOD1 ChR2 ESCMNs generated similar CI scores at 5 DIV (2.4 ± 1.5, n=12 and 2.0 ± 1.6, n=12, respectively). Interestingly, SOD1 ChR2 ESCMNs, not only generated CI scores that were lower than their WT counterparts over the next 9 days, their CIs actually declined in value after 10-12 DIV (Figure 4.7A). By 14 DIV, the CI score of the SOD1 ESCMNs was only 2.4 ± 1.1 (n=12) while the CI of their WT counterparts was significantly higher

at 4.5 ± 0.6 (n=12) (t-test, $p<0.001$). These results suggest that, unlike WT ESCMNS, SOD1 ChR2 ESCMNs were loosing their synaptic connections with muscle fibres over time. This loss could be due to axon withdrawal and/or motor neuron cell death. To determine whether SOD1 ESCMNs were dying more rapidly than WT ESCMNs in culture we plated both cell types on muscle fibres and counted motor neuron numbers after 4 and 12 DIV. Figure 4.7B shows that the number of SOD1 ESCMNs at both time points were comparable to WT motor neurons suggesting that the decrease in CI after 12 DIV was likely due to axon withdrawal rather than motor neuron cells death. Taken together, these results indicate that the CI in vitro model system accurately mimics one of the key neuromuscular phenotype observed in ALS, namely the withdrawal of motor axons from the NMJ prior to cell death.

Optically stimulating SOD1 ChR2 ESCMNs co-cultures causes CI scores to decrease over time

Numerous studies on animal models of ALS (Frey et al., 2000) and in patients with the disease (Theys et al., 1999) have shown that the most active, 'slow' motor neurons are the last motor neurons to die. This observation has led to the hypothesis that activity may promote motor neuron survival in ALS (Dal-Bello-Haas et al., 2007; Pupillo et al., 2014; Dal Bello-Haas and Florence, 2013). To determine whether enhanced motor neuron activity results in better functional outcomes in our CI model of neuromuscular function we co-cultured a single embyroid body containing ~200 WT or SOD1 ChR2 ESCMNs with muscle fibres for 14 DIV as described previously. Similar to our previous studies, we started optically stimulated the cultures after several hours after plating at 0.025 Hz with blue LEDs. As shown in Figure 4.8A, optically stimulated WT ChR2

ESCMNs (open circles, n=12) generated the same CI scored as non-stimulated (filled circles, n-12) WT cultures over 14 DIV. In contrast, and contrary to our expectation, optically stimulating SOD1 ChR2 ESCMNs (Figure 4.8B, open circles, n=12) caused a rapid and significant decrease in CI compared to non-stimulated SOD1 ESCMNs (Figure 4.8B, filled circles, n=12). By 14 DIV, the stimulated SOD1 ChR2 ESCMNs had a significantly lower CI score of 1.0 ±1.0 compared to non-stimulated SOD1 motor neurons (2.4 ±1.0 (t-test, p=0.0027). In summary, contrary to the general hypothesis that neural activity promotes better motor neuron survival in ALS we found that enhanced activity accelerates disease progression disease *in vitro*.

WT and SOD1 ChR2 ESCMNs exhibit different CI scores when plated as dissociated cells compared to when they are cultured as a cluster within an embryoid body.

Previous studies have shown that ESCMNs receive excitatory input from glutamatergic interneurons in culture (Mile et al., 2004) and that this input produces a neural network leading to muscle fibre depolarization that can be blocked pharmacologically with TTX (Chipman *et al*., 2014). Therefore, the decline in CI, observed in the SOD1 ChR2 ESCMN cultures, could be regulated, at least in part, by neural activity in the SOD1 motor neurons. We tried to eliminate GFP^- interneurons from our cultures using FACS, but were unable to do so due to the low level of fluorescence exhibited by the ChR2 ESCMNs, see discussion. Consequently, we decided to culture ChR2 ESCMNs at a low density with the assumption that neural networks would be less likely to form under such conditions. As such, embryoid bodies containing WT or SOD1 ChR2 ESCMNs were dissociated and (75,000) cells/well were plated onto chick muscle fibres. The CI of the co-cultures were then scored and compared to similar cultures

containing non-dissociated ESCMNs (i.e. same values shown in Figure 4.7A). Figure 4.9A shows that dissociated WT ChR2 ESCMNs had CIs that were significantly lower ($p<0.01$) than those generated by ESCMNs cultured as embryoid bodies at all time points examined. Interestingly, CI values from the dissociated WT cultures also appeared to plateau from 11- 14 DIV (Figure 4.9A), although the mean (3.0 ± 0.0, n=12) remained significantly lower than that recorded from the WT cultures (mean = 4.5 ± 0.6, n= 12) plated with motor neurons as embryoid bodies (t-test, $p<0.001$). These results suggest that ESCMNs cultured as embryoid bodies innervate more muscle fibres than dissociated motor neurons. Interestingly**,** like their WT counterparts, dissociated SOD1 ChR2 ESCMNs generated increasing higher CI scores between 5-10 DIV (Figure 4.9B, open circles), although they were still significantly lower than CIs exhibited by SOD1 motor neurons that were cultured as embryoid bodies (Figure 4.9B, filled circles) over the same time period. However, unlike the EB cultures, the CIs generated by the dissociated SOD1 ChR2 ESCMNs cells did not decrease after 9 DIV (Figure 4.9B). In fact, the CI scores plateaued from 10-20 DIV such that by 20 DIV the mean CI score was 2.3 ± 0.5 (n=12) (Figure 4.9B, open circles). This value is significantly higher than that observed for SOD1 ESCMNs cultured as embroid bodies (t-test, $p<0.001$). Taken together, these results suggest that the decline in CI observed by SOD1 ChR2 ESCMNs, cultured as embryoid bodies is regulated, at least in part, by imposed neural activity resulting from the neural network.

Chapter 4 Figures

Figure 4.1. Techniques used to generate mice expressing SOD1G93A and motor neuron specific ChR2 as well as the ESCMN/chick muscle fibre co-cultures. **A**, Mice, heterozygous for $HB9^{cre}$ and a floxP-flanked STOP cassette upstream of ChR2(H134R)-EYFP fusion gene (Ai32), were crossed with SOD1G93A mice to generate SOD1 mice expressing motor neuron specific ChR2. **B**, Western blot analysis, using an antibody that recognizes misfolded SOD1 (i.e. D3H5), shows that SOD1 ChR2 ESCMNs express SOD1G93A (middle lane) while wild-type ChR2 ESCMNs do not (left lane). Ear clip (EC) protein homogenate from a SOD1G93A mouse was used as a positive control (right lane). Actin was used as a loading control. **C**, ChR2 ESCMN/muscle fibre co-cultures were generated by first culturing E10 chick myoblasts until they formed multinucleated muscle fibres. After ~3 DIV, a single EB containing ESCMNs were plated onto the muscle fibres and the culture supplemented with trophic factors (Glial-Derived Neurotrophic Factor and Ciliary Neurotrophic Factor) for 7 DIV. Trophic support was removed after 10 DIV in order to promote synaptogenesis at NMJs.

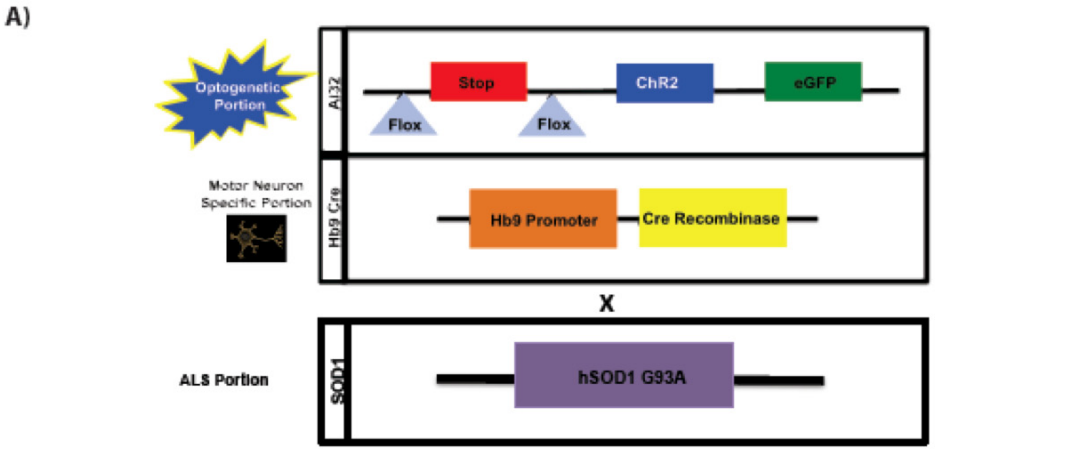

HB9xChannelrhodopsinxSOD1 (SOD1 ChR2 ESCMN)

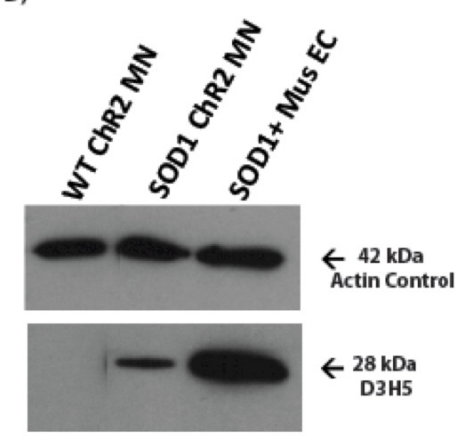

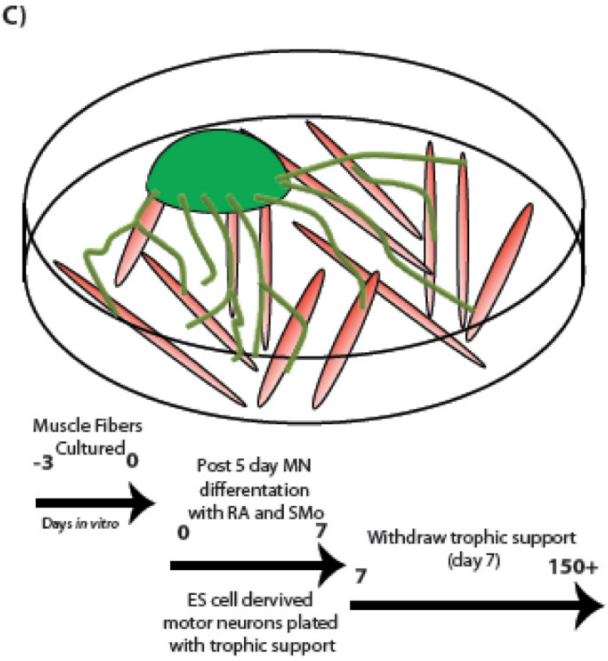

Figure 4.2. ChR2 ESCMNs form connections with the muscle fibres in vitro. **A,B** GFP^+ neurites from ESCMNs connect with a-BTX labeled AChRs after 10 (**A**) and 40 DIV (**B**). Motor neurons labeled with GFP after 10 DIV (**A**-left) have thin processes extending to AChR clusters on the muscle (**A**, center, yellow asterisks). The merged imaged (**A**-right) shows minimal overlap between motor terminal and AChR clusters. Motor axons appear thicker 40 DIV (**B**) and overlap more completely with the AChR clusters (**B**, center, yellow arrowheads).

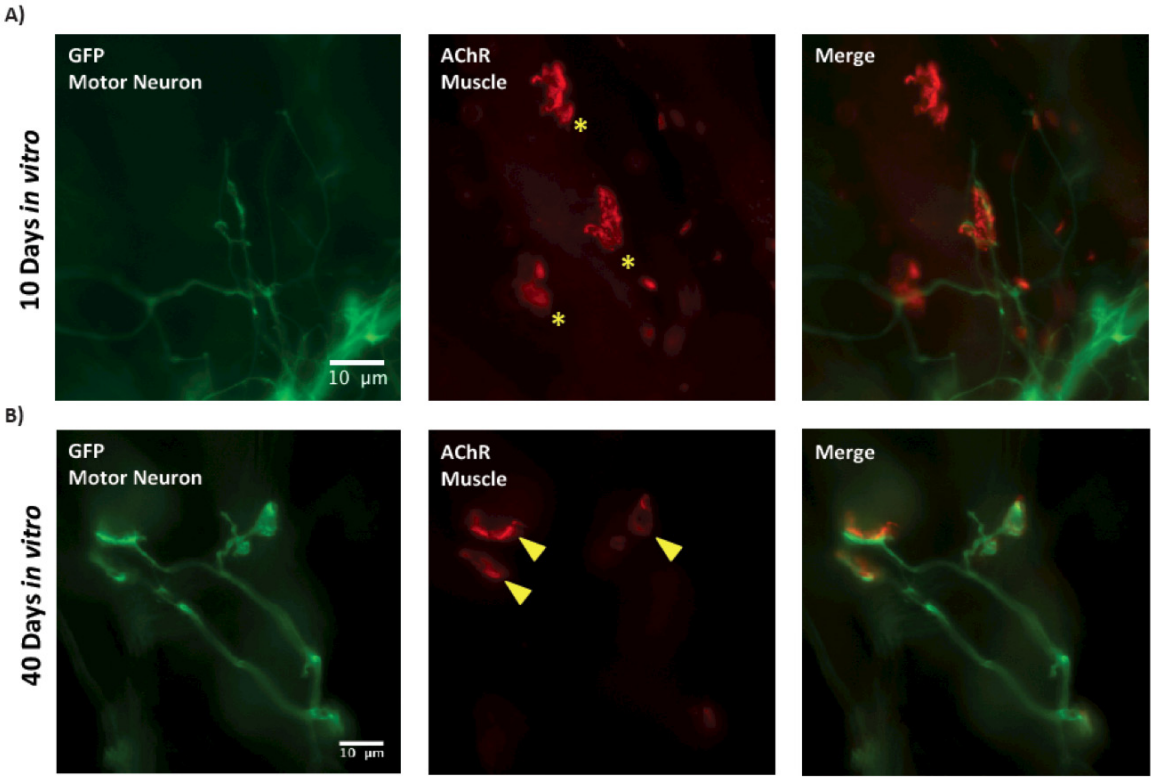
A)
10 Days in vitro
GFP
Motor Neuron
10 µm
AChR
Muscle
Merge
B)
40 Days in vitro
GFP
Motor Neuron
10 µm
AChR
Muscle
Merge

Figure 4.3 ChR2 ESCMNs form functional NMJs when co-cultured on chick myofibres. (**A**) Innervated endplates were identified by AChR staining (red) in contact with a single GFP^+ axon (green) and impaled with a sharp electrode for intracellular recordings (white lines showing electrode placement) (Chipman et al., 2014). **B**, Various blue light exposure times were pulsed over ChR2 ESCMNs (500ms, 200ms and 1ms) each showing similar endplate potentials (EPPs). **C**, Baseline recording pre-optical stimulation showing no EPPs but several miniature end plate potentials (mEPPs) denoted by (*). **D,E,F**, Traces showing 3 stimulation protocols, EPPs evoked by a single light pulses (blue arrows) at a frequencies of 0.1hz (**D**), 0.5 hz (**E**), 1 hz (**F**) and mEEPs denoted by (*). Note EPPs are elicited at a 1:1 ratio with light pulses administered. **G**, EPPs can be inhibited by bath application of 25uM TTX, various stimulation protocols were tried (blue arrows) to in order to elicit EPPs, only mEEPs were recorded (*). **H**, Spontaneous events were inhibited by bath application of D-tubocurarine 50uM, note absence of mEPPs in trace. **I,** Plot showing the frequency of mEPP amplitudes in 4 representative ChR2 ESCMNs, note the maximum amplitude does not surpass 0.9mV with an average of 0.55mV (**K**-black bar). **J**, Plot showing the frequency of EPP amplitudes in the same 4 representative cells with the maximum being 10.75mV and an average amplitude of 3.5mV (**K**-grey bar).

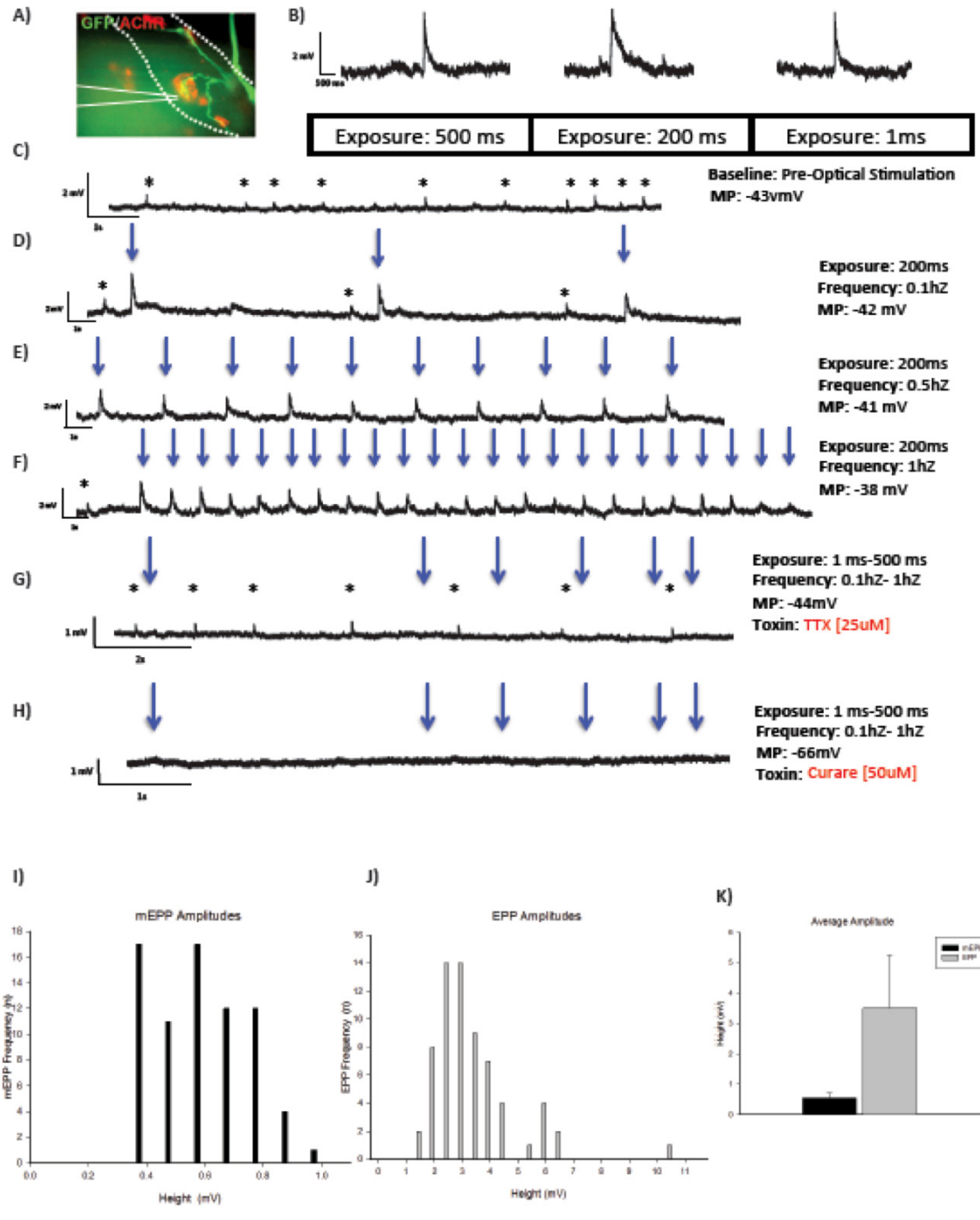
A)
GFP/AChR
B)
Exposure: 500 ms
Exposure: 200 ms
Exposure: 1ms
C)
Baseline: Pre-Optical Stimulation
MP: -43vmV
D)
Exposure: 200ms
Frequency: 0.1hZ
MP: -42 mV
E)
Exposure: 200ms
Frequency: 0.5hZ
MP: -41 mV
F)
Exposure: 200ms
Frequency: 1hZ
MP: -38 mV
G)
Exposure: 1 ms-500 ms
Frequency: 0.1hZ- 1hZ
MP: -44mV
Toxin: TTX [25uM]
H)
Exposure: 1 ms-500 ms
Frequency: 0.1hZ- 1hZ
MP: -66mV
Toxin: Curare [50uM]
I)
mEPP Amplitudes
mEPP Frequency (Hz)
Height (mV)
J)
EPP Amplitudes
EPP Frequency (Hz)
Height (mV)
K)
Average Amplitude
Height (mV)

Figure 4.4 The degree of muscle contraction elicited from ChR2 ESCMNs can be scored using the Contraction intensity index. **A**, An illustration showing the contraction intensity index, the ESCMNs (green) plated on muscle fibres (black outlined tubular structures), contracting muscle fibres are shown in red. **B**, CI scores from ChR2 ESCMNs plotted between 5-14 DIV. Growth factor supplementation (red text above graph) is present for first two days of scoring and withdrawn at 8 DIV.

A)

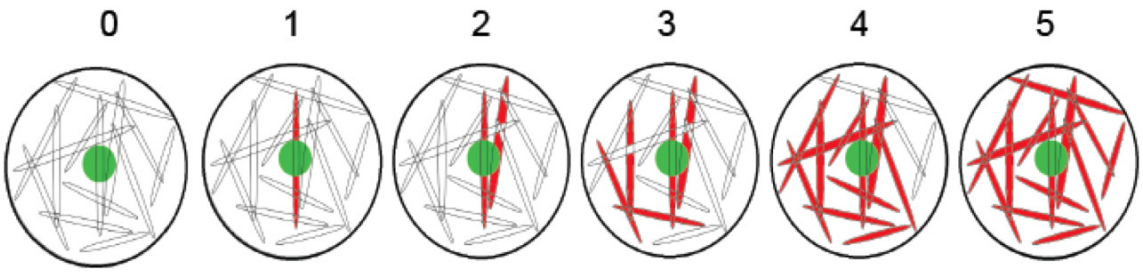
0
1
2
3
4
5

B)

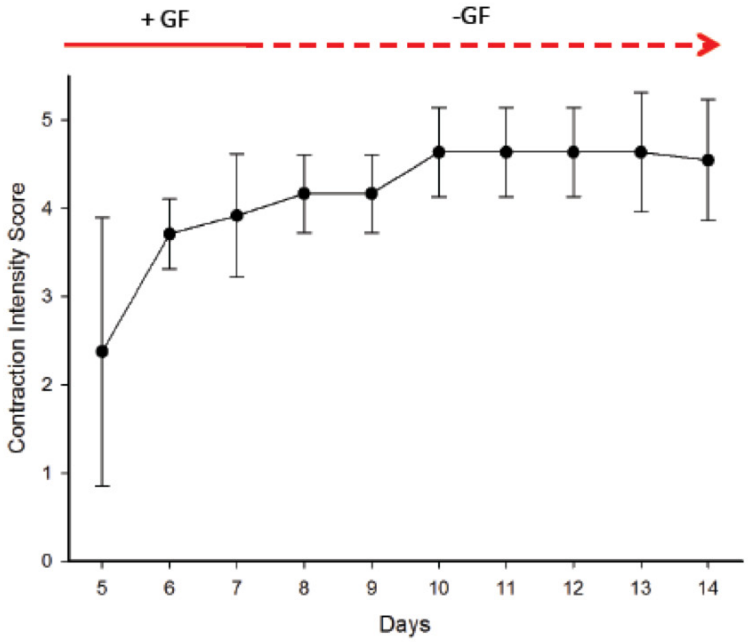
+ GF
-GF
Contraction Intensity Score
0
1
2
3
4
5
5
6
7
8
9
10
11
12
13
14
Days

Figure 4.5 A CI score is able to correlate behavior to distinct anatomy in vitro. **A**, An illustration showing the region quantified (yellow dotted line) in the co-cultures (**B**) 2 representative cultures after 7 DIV with either a CI score of 1 (left column) or a CI score of 5 (right column). **i**, Showing GFP staining with only a single GFP positive neurite in the CI score of 1 (left), many GFP positive axons in the culture with a CI score of 5 (right). **ii**, Very few and small AChR positive regions stained in the culture with a CI score of 1 (left) compared to much larger and increased amount of AChR positive regions seen in the culture with a CI score of 5 (right). **iii**, Very few regions of synaptic vesicle staining in the culture with a CI score of 1 (left-blue arrowheads), compared to several clustered regions in the culture with CI score of 5 (right-blue arrowheads). Note the higher amounts of staining in all cases in the culture with a CI of 5. (Scale bar= 20μm)

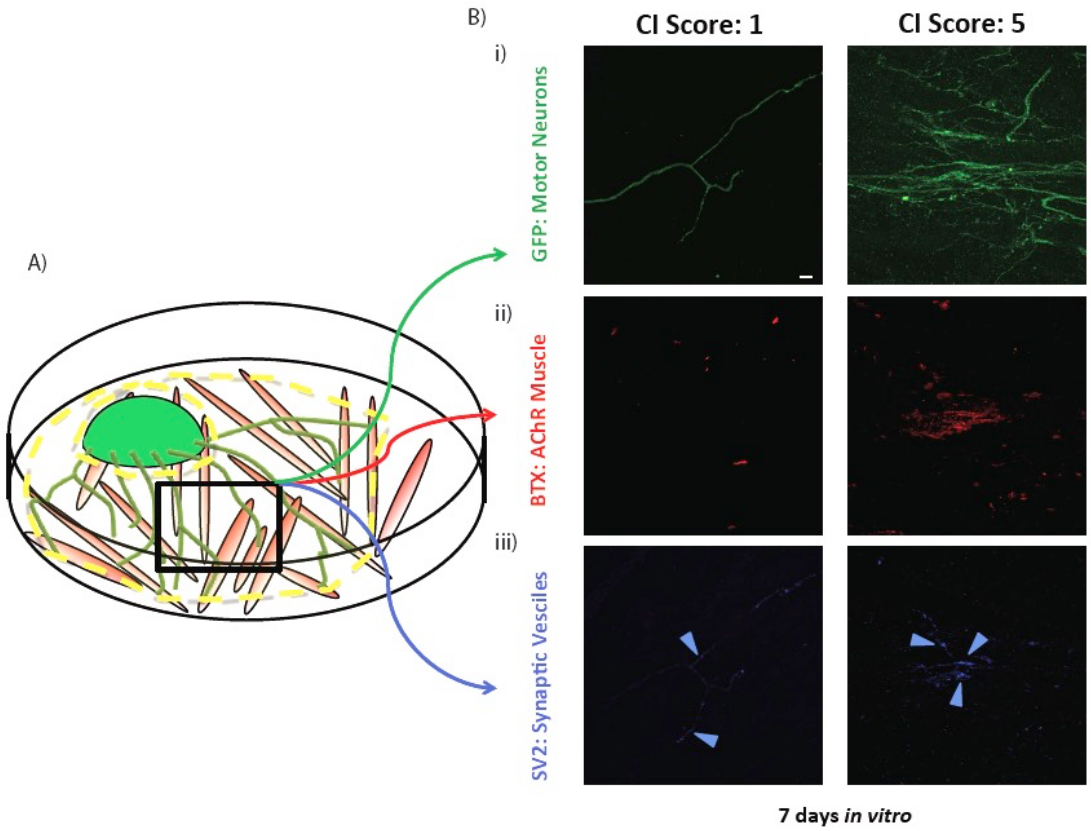
A)
B)
i)
ii)
iii)
CI Score: 1
CI Score: 5
GFP: Motor Neurons
BTX: AChR Muscle
SV2: Synaptic Vesciles
7 days *in vitro*

Figure 4.6 Behavioral-anatomical correlates can be plotted on a semi-logarithmic scale. Cultures after either 7 DIV (**A-E**) or 14 DIV (**F-J**) were scored, staining intensity quantified and plotted on a semilogarithmic scale where $Y=10^{(slope*x + y\text{-}intercept)}$. **A-J,** The slope (± SE) of the regression lines for GFP, SV2 and a-BTX pixel intensities were plotted against CI score. After 7 DIV pixel intensities of GFP (**A**), SV2 (B) and a-BTX (**C**) were 0.29 ±0.05 (range: 0.86 - 29, r^2= 0.90), 0.18 ±0.029 (range: 0.49 - 4.8, r^2= 0.91) and 0.38 ±0.031 (range: 0.091 – 5.5, r^2= 0.97), respectively. The slope of the regression lines fitted to the number (**D**) and size of the a-BTX clusters (**E**) plotted against CI after 7 DIV were 0.29 ±0.042 (range: 30 - 520, r^2= 0.92) and 0.079 ±0.015 (range: 30 - 74, r^2= 0.87), respectively. With the exception of the GFP staining intensities the relationships seen after 14 DIV were similar to those after 7 DIV. With pixel intensities of GFP (**F**), SV2 (**G**) and a-BTX (**H**) along with a-BTX cluster number (**I**) and a-BTX cluster size (**J**) being 0.31 ±0.065 (range: 0.21 – 3.6, r^2= 0.85), 0.28 ±0.068 (range: 0.63 - 4.9, r^2= 0.70), 0.32 ±0.076 (range: 0.03 – 4.5, r^2= 0.82), 0.29 ±0.027 (range: 31 - 615, r^2= 0.97), and 0.072 ±0.018 (range: 32 – 57, r^2= 0.80), respectively.

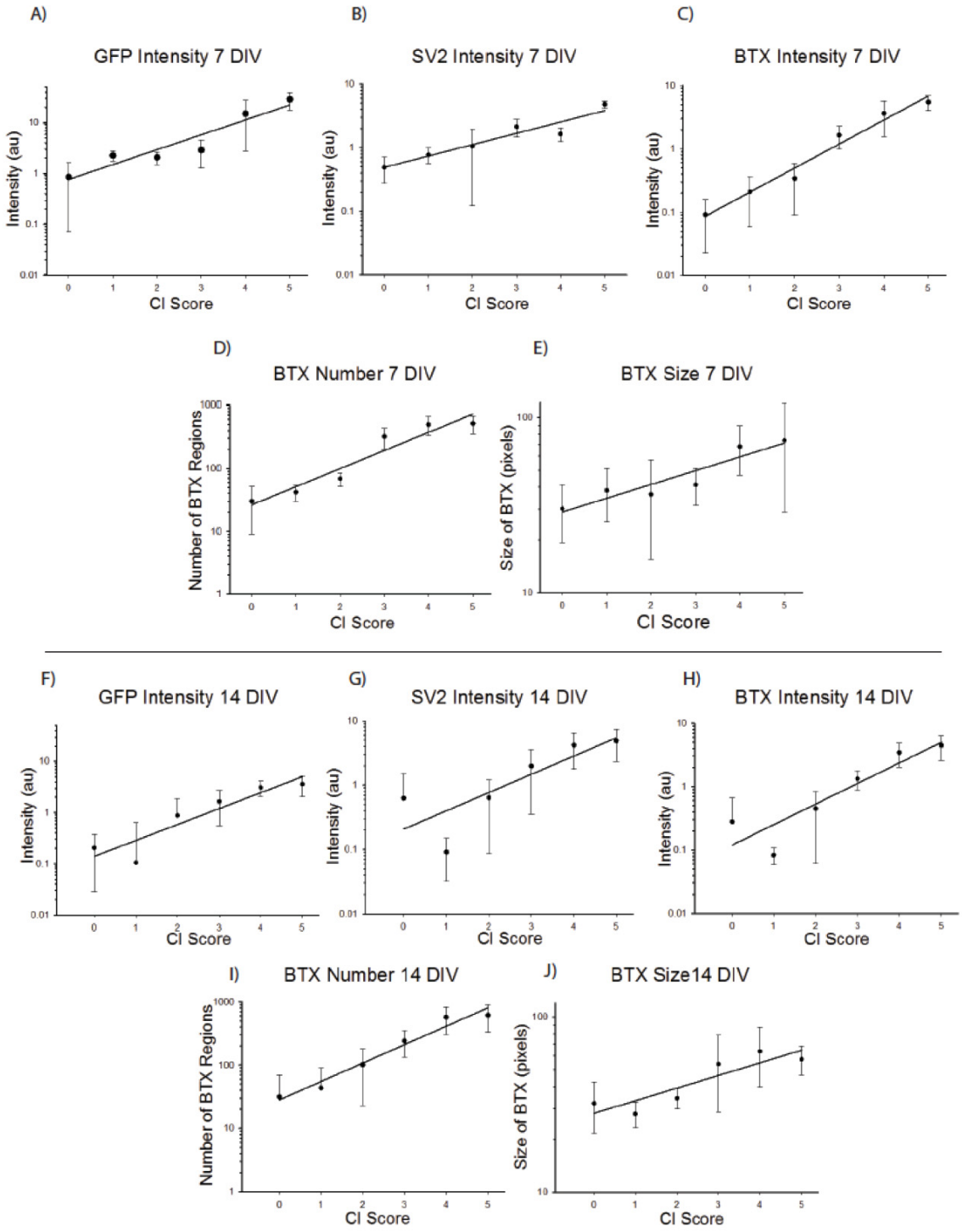
A)
GFP Intensity 7 DIV
Intensity (au)
CI Score
B)
SV2 Intensity 7 DIV
Intensity (au)
CI Score
C)
BTX Intensity 7 DIV
Intensity (au)
CI Score
D)
BTX Number 7 DIV
Number of BTX Regions
CI Score
E)
BTX Size 7 DIV
Size of BTX (pixels)
CI Score
F)
GFP Intensity 14 DIV
Intensity (au)
CI Score
G)
SV2 Intensity 14 DIV
Intensity (au)
CI Score
H)
BTX Intensity 14 DIV
Intensity (au)
CI Score
I)
BTX Number 14 DIV
Number of BTX Regions
CI Score
J)
BTX Size14 DIV
Size of BTX (pixels)
CI Score

Figure 4.7 WT ChR2 ESCMN co-cultures steadily increase in CI scores and remain stable whereas there is only a small increase followed by a decline in CI scores in SOD1 ChR2 ESCMNs co-cultures, the decrease is not due to cell death. **A**, A plot showing both non-stimulated 'WT' ChR2 ESCMNs (filled in circles) and SOD1 ChR2 ESCMNs (open circles) scored over 5-14 DIV. Note the gradual increase and plateau in the WT ESCMNs whereas SOD1 do increase as well and then significantly decrease in scores after 9 DIV. **B**, A bar graph showing survival of SOD1 ESCMNs co-cultured with chick muscle fibres after 4 and 12 DIV, compared to healthy HBG3 ESCMNs. Note the decline in CI score seen with the SOD1 after 12 DIV (**A**), yet the total number of cells is not significantly different compared to 4 DIV in (**B**). [Paired T-test * $p<0.05$, ** $p<0.01$, *** $p<0.001$)]

A)

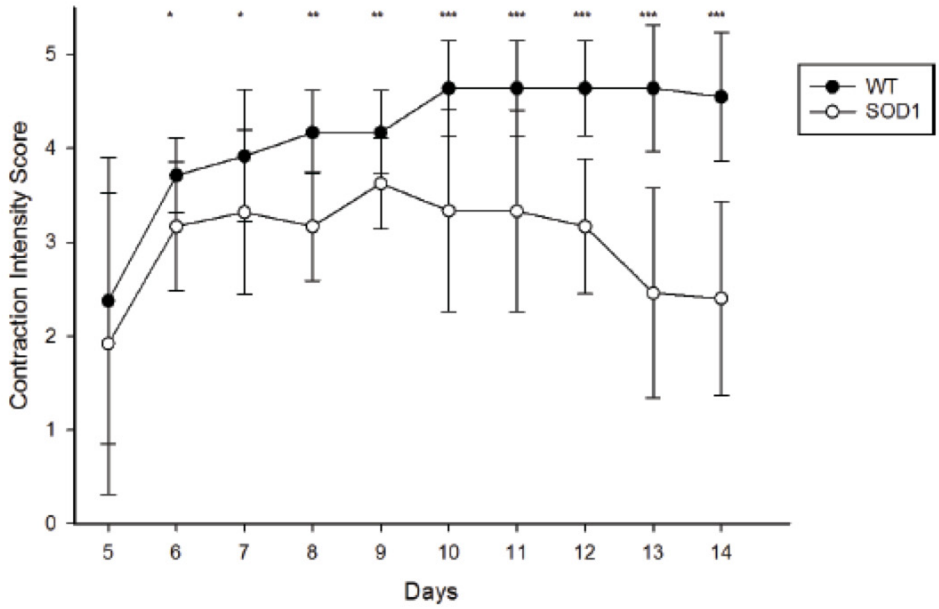
Contraction Intensity Score
Days
WT
SOD1
0
1
2
3
4
5
6
7
8
9
10
11
12
13
14

B)

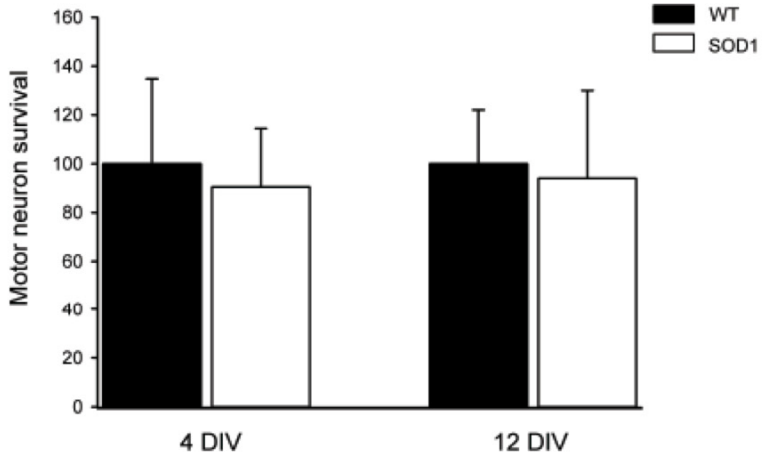
Motor neuron survival
WT
SOD1
0
20
40
60
80
100
120
140
160
4 DIV
12 DIV

Figure 4.8 Stimulating WT ChR2 ESCMNs does not affect CI scores, whereas stimulating SOD1 ESCMNs co-cultures causes an accelerated decline in scores. **A**, A plot of both non-stimulated (filled in circles) or stimulated at 0.1hz (open circles) ChR2 ESCMNs plated as EBs, scored over 5-14 DIV. Note the similarity of the two curves. **B**, A plot of both non-stimulated (filled in circles) or stimulated at 0.1hz (open circles) SOD1 ChR2 ESCMNs plated as EBs, scored over 5-14 DIV. Note the significant decrease in stimulated SOD1 cultures from after 7 DIV. [Paired T-test * $p<0.05$, ** $p<0.01$, *** $p<0.001$)]

A)

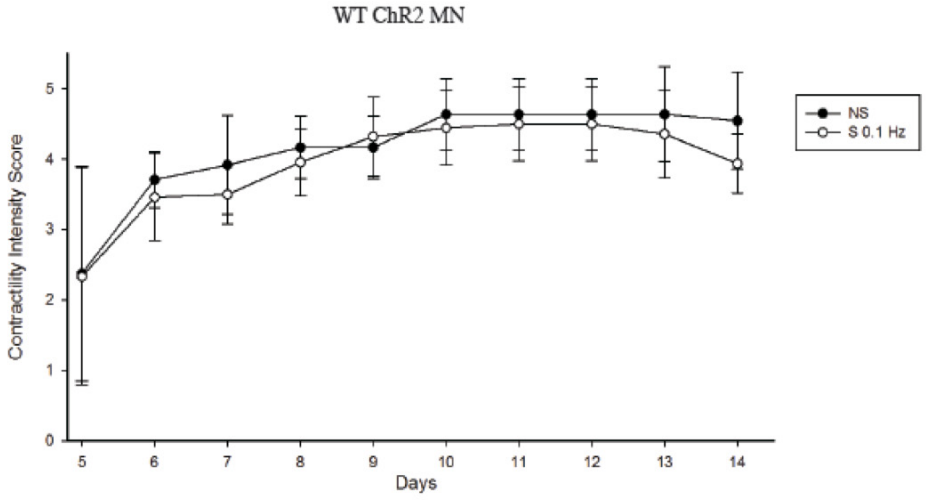
WT ChR2 MN
Contractility Intensity Score
Days
NS
S 0.1 Hz

B)

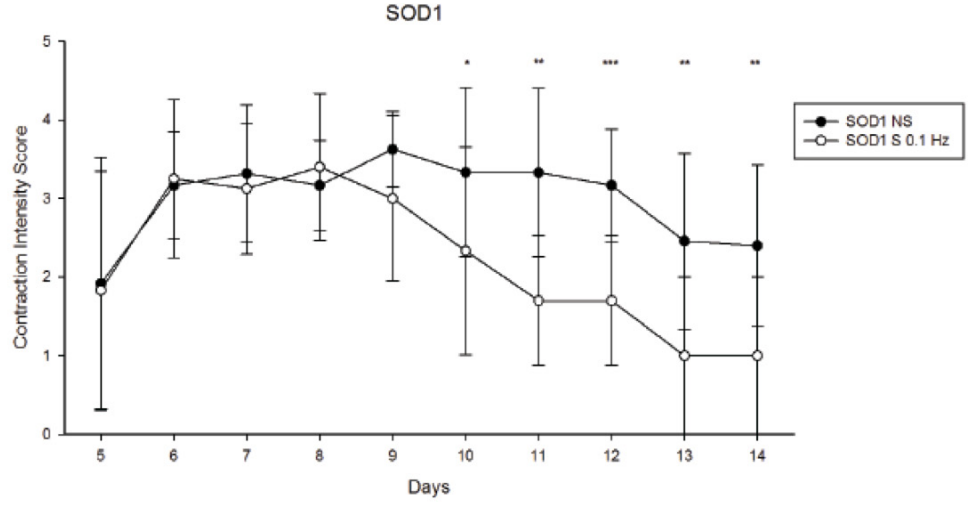
SOD1
Contraction Intensity Score
Days
SOD1 NS
SOD1 S 0.1 Hz

Figure 4.9 WT ChR2 ESMNs plated as EBs have higher CI scores and become reactive to light stimulation sooner then WT ChR2 ESMNs plated as dissociated cells. Dissociated SOD1 ChR2 ESCMNs compared to those plated as EBs maintain their maximum scores. **A**, A plot showing non-stimulated ChR2 ESCMNs plated as either EBs (closed circles) or dissociated (open circles) from 5-15 DIV. Note the dissociated cultures are significantly weaker overall and only reach a CI score of ~3. **B**, A plot showing non-stimulated SOD1 ChR2 ESCMNs plated as either EBs (closed circles) or dissociated (open circles) from 5-15 DIV. Note the significant differences between the two plating conditions in the SOD1 cultures. The EBs decrease in CI score after 9 DIV whereas dissociated SOD1 cultures appear to be weaker overall yet once they plateau after 10 DIV they do not drop off in scores. [Paired T-test * $p<0.05$, ** $p<0.01$, *** $p<0.001$)]

A)

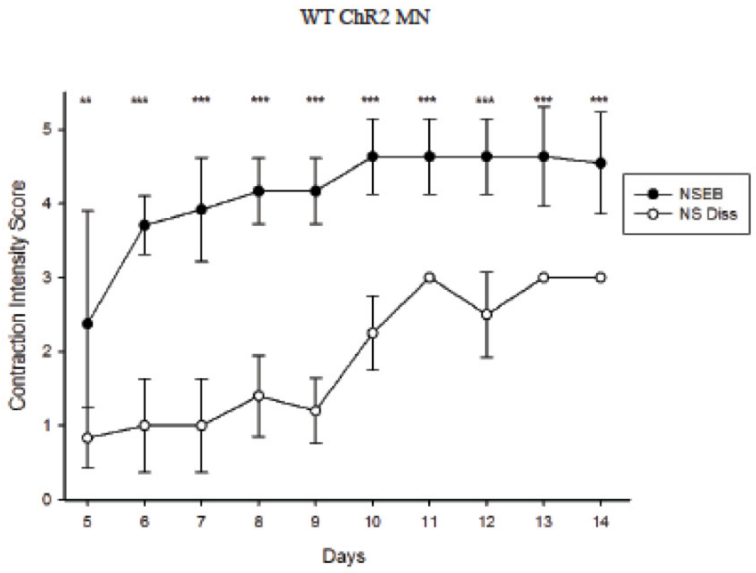
WT ChR2 MN
Contraction Intensity Score
Days
NSEB
NS Diss

B)

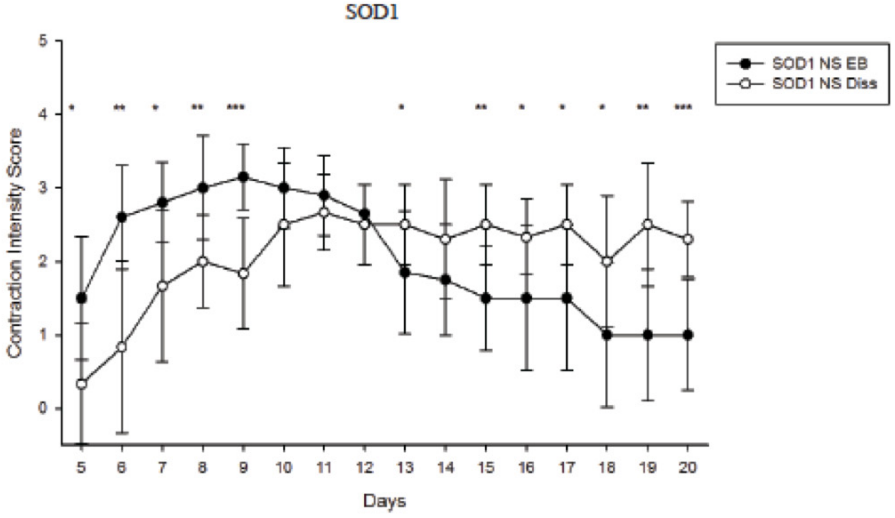
SOD1
Contraction Intensity Score
Days
SOD1 NS EB
SOD1 NS Diss

CHAPTER 5: DISCUSSION

Chapter 3 Summary

ChR2 expressing ESCMNs were reliably generated and resemble previously studied ESCMNs. Whole-cell current clamp recordings demonstrated that ChR2 ESCMNs fire a single action potential in response to light. By plating ESCMNs at low a density the affects of activating the motor neurons with light during development could be analyzed. Results showed that activity plays a role in the early development of these ChR2 ESCMNs, with enhanced outgrowth and guidance molecules expression.

Chapter 4 Summary

In addition to the ChR2 ESCMNs, SOD1 ChR2 ESCMNs were created in order to model ALS in vitro. When ESCMNs were plated on muscle, they make connections that mature over time and successfully elicit muscle contraction in response to a blue light pulse. Synapse stability in both WT and SOD1 co-cultures was analyzed using the Contraction Intensity Index. Results showed how activity increased rate of denervation in SOD1 co-cultures.

Isolation of a pure motor neuron population - The FACS Saga

Both motor neuron and muscle recordings with ESCMNs have demonstrated the presence of intrinsic firing within the EB (Miles et al., 2004; Chipman et al., 2014). To lessen the probability of glutamatergic synapses on the motor neurons, ChR2 ECS EBs were dissociated and plated at a low-density. This allowed for only imposed activity (blue light pulses) to be influencing the ESCMNs development. This technique of low density plating has been used previously with retinal ganglion cells (RGC) such that the

experimental outcomes are not likely due to synaptic or autocrine effects (Goldberg et al., 2002).

We used fluorescence-activated cell sorting (FACS) in an attempt to isolate a pure population of the GFP^+ motor neurons. If successful, this would eliminate other cells within the EBs that could influence the development of motor neurons. However, after an exorbitant amount of time and resources it was not possible to FACS the ChR2 ES cell line. The reason for this is likely due to the fact that the fluorescence emitted from the ChR2 ESCMNs is not bright. The failure to sort was not due to the fact that the motor neurons 'die' when they pass through the laser, as post-FACS they have been plated down and survived weeks in vitro, capable of eliciting EPPs in muscle (not shown).

The ChR2 is membrane-bound in our ESCMNs, not cytoplasmic, resulting in the GFP expression to appear dim and patchy. Whereas ESCMNs (e.g. HBG3 ESCMNs) that have a cytoplasmic GFP expression appear homogenously green. The patchy green expression of GFP linked ChR2 has previously been exhibited in hippocampal neurons, making it seem characteristic to the channel's expression pattern (Xiang et al., 2005).

The HBG3 cell line shown in Figure 3.3, has cytoplasmic GFP expression, making the cells 'easier to sort.' The differing expression patterns can be easily seen using high magnification confocal images of the total cell, as shown in Supplemental Figure 1A-D; Appendix 1. A central cross-sectional image of the cells shows the HBG3 ESCMNs are homogenously green, whereas the ChR2 line has GFP expression solely around the parameter (Supplemental Figure 1A-D; Appendix 1). The patchy GFP expression of the ChR2 ESCMNs resulted in low post-FACS purity.

FACS analysis shows that the level of GFP fluorescence intensity detected is an entire logarithmic value lower in the ChR2 ESCMNs compared to the HBG3 ESCMNs (Supplemental Figure 1-graphs). It is likely that the low level of GFP detected in the ChR2 ESCMNs is negligibly different from the low underlying level of autofluorescence detected in GFP^- cells. This low level of fluorescence resulted in a non-pure final population. This is empirically represented in pie charts shown in Supplemental Figure 1. The HBG3 cell line pre-sort sample is only 22% GFP^+, and post-FACS 94% positive, compared to the ChR2 cell line pre-sort is only 16% GFP^+ and post-FACS 22% positive, barely an increase at all.

Bryson and colleagues recently used a ChR2 expressing ES cell line in which the motor neurons had magnetic beads in them allowing them to be easily sorted via magnetic activated cell sorting (MACS) (2014). The line was originally created to improve sorting efficiency and signal-to-background ratio resulting in a purer population of motor neurons (Machado et al., 2014). Using a similar cell line would allow for our guidance molecule experiments to potentially show greater effects as a result of activity as the sample would not be diluted by other cells types. The dim GFP expression is the reason why all immunohistochemical experiments done using the ChR2 ESCMNs were always stained again for GFP, as the endogenous signal is not strong enough to be reliable for post-hoc analysis.

ChR2 ESCMN Firing Properties

Our results illustrate that ChR2 ESCMNs develop the ability to fire a single action potential from a single light pulse. As shown in Figure 3.4, there is a clear sustained depolarization for the remainder of the light pulse duration; however, this does not seem

to be enough to drive the cell over the threshold to fire continuously. The amount of depolarization induced by light increases from ~5 mV at 24 hours to >15 mV after 1-2 weeks in vitro, demonstrating that the degree of depolarization increases as the ESCMNs mature.

It should be noted that the level of depolarization reached with current injection, in order for a single action potential to fire is ~14-20 mV. Whereas the amount of depolarizing current required for multiple action potentials to fire is >30 mV. This possibly indicates that a depolarization above 30 mV is needed in order to cause multiple action potentials firing. A future experiment would be to see whether ChR2 ESCMNs would fire repetitive action potentials in response to light stimulation after several more weeks in vitro. To see whether the depolarization elicited from light would pass about the 30 mV threshold, allowing multiple action potentials.

Two recent studies using ChR2 expressing mouse and human ESCMNs (Bryson et al., 2014, Steinbeck et al., 2016); demonstrate that motor neurons are capable of repetitively firing action potentials from optical depolarization. However, in Steinbeck et al., their motor neurons were over 30 DIV, much more mature compared to the ones used in this study (2016). These findings provide proof-of-principle for the future experiment outlined above, to recording from more mature motor neurons to see whether they develop the capability to fire repetitive action potentials from light depolarization.

Bryson et al., generated mouse ESCMNs that expressed both ChR2 and glial-derived neurotrophic factor (GDNF), a neurotrophic factor known to promote long-term survival (2014). They demonstrated that ChR2 motor neurons were able to produce a single action potential-like spike response at 3 DIVs similar to what we demonstrated at 2

DIV. However, after 7 and 14 DIV stimulating their motor neurons with light caused them to fire repetitively at 40 Hz and 75 HZ, respectively each with only a few failures (Bryson et al., 2014). There are several potential reasons for their ability to fire repetitive action potentials; this could be due to the expression of GDNF in the cells. It would be interesting to modify our ESCMNs to express GDNF inherently in addition to ChR2 and see whether motor neurons would develop the ability to fire repetitively in response to light by 7 DIV. Further, their motor neurons were not dissociated at the point of recording and their EBs were plated on astrocytes, both being favourable growth conditions for ESCMNs to thrive in.

Finally, Bryson and colleagues used a more efficient method to express ChR2 in their motor neuron population, whereas our Cre genetics method is not 100% effective in excising STOP, resulting in a non-ubiquitous ChR2 expression. Additionally our breeding method used to create the ChR2 ES stem cells used a heterozygote mouse (only harbouring one of the alleles of interest) this potentially could have resulted in a decreased expression of ChR2 compared to those seen in Bryson et al. It would be interesting to quantify the amount of ChR2 present in the cells with western blotting and breed mice again this time to create a homozygote for our alleles, potentially doubling the amount of expression of ChR2. To see if with a new breeding strategy i) how much the ChR2 protein levels are increased and ii) if this increase is enough to drive the cell past depolarization threshold causing repetitive action potentials in response to light stimulation.

ESCMNs morphological complexity, as shown in Figure 3.6, and adhesion molecule levels, as shown in Figure 3.8, can be altered as a result of optical stimulation.

It would be extremely interesting to see whether chronic light stimulation alters ChR2 ESCMN's intrinsic firing properties as well. Aspects that would be quantified include: firing frequency, firing threshold, half-width of the action potentials elicited from both current/light depolarization and depolarization height. Preliminary data suggests that activity may play a role in causing the ChR2 ESCMNs to develop more mature firing properties at earlier time-points in vitro. In connection to the experiments proposed above, it would be worth seeing if stimulating the ChR2 ESCMNs resulted in a higher level of depolarization would this then causing them to fire multiple action potentials in response to a light stimulus. Finally, in order to define the source of the sustained depolarization seen from light stimulation recordings cultures should be treated with TTX as the final recording. This would demonstrate what degree of the depolarization is TTX sensitive (as result of sodium channels) and what portion is exclusively ChR2.

Outgrowth Experiments

Light stimulation during development increased ChR2 ESCMNs morphological complexity, shown in Figure 3.6. The three parameters that were quantified: total neurite length, total displacement and number of neurite branches. In addition, future experiments could also quantify soma areas, as this too has been used as a measure of increased cell growth (Takazawa et al., 2012). This could be used an indicator of cell death at the cell body. It would be important when trying to determine the site of disease-initiated cell death in motor neuron diseases. Measuring soma size of ESCMNs could allow for identification of motor neuron subtypes. Similar to this study several others have shown increasing neuronal activity by either pharmacological or electrical stimulation increases the rate of axonal arborization or axon growth *in vitro* and *in vivo*

by stabilizing growing branches (Rashid and Cambray-Deakin, 1992; Cohen-Cory, 1999; Fields et al., 1990).

Activity has been shown to increase the density of trophic receptors on the surface of both RCGs and hippocampal neurons (Meyer-Franke et al., 1998; Du et al., 2000; Goldberg et al., 2002). These findings suggest that electrical activity increases the amount of CNS axon outgrowth in response to trophic factors. The ChR2 ESCMNs are very responsive to trophic support and withdrawal, either promoting large amounts of healthily outgrowth or cell death, respectively (data not shown). As such, all cultures are plated with trophic support for the first 7 days, as outlined in the methods section and previously shown in Soundararajan et al. (2007). A potential mechanism for the increased growth seen in optically stimulated cells is an up regulation of trophic receptors on their surface, allowing them to receive more trophic support during development and therefore promoting increased outgrowth.

The ability to selectively stimulate motor neurons through ChR2 with light is a more advantageous stimulation method compared pharmacological methods or passing current through an entire culture, both of which could have residual affects on other nearby cells. Landmesser's lab has successfully demonstrated that activity can modulate axon pathfinding and targeting (Hanson and Landmesser, 2004, 2006; Kastanenka and Landmesser 2010, 2013). A future experiment based on the series of Landmesser experiments would be to perform an in ovo application of this study's outgrowth experiments. This would be done by transplanting ChR2 ESCMNs into chicken embryos, as previously described by Soundararajan et al., 2006 and stimulating them as they grow out of the neural tube. Their outgrowth could then be compared to previous ESCMN

(Soundararajan et al., 2006) or IPSCMN transplant experiments (Toma et al., 2015) to see whether simulation augments ChR2 ESCMNs growth and targeting. Preliminary data suggests that ChR2 ESCMNs can survive transplantation and chronic stimulation resulting in enhanced outgrowth into the periphery.

Both NCAM isoforms (140kDa and 180kDa) detected in this study using western blotting are known to be highly expressed by ESCMNs, as shown in Soundararajan et al. (2006) and Chipman et al. (2014). This study found that activity altered total NCAM (doubled in stimulated cells) and PSA-NCAM (tripled in stimulated cells) as shown in Figure 3.8. Previously it has been shown that knocking out NCAM in motor neurons reduces their total axon length compared to NCAM expressing motor neurons, as shown in Chipman Thesis (2012), Figure 4.3. In addition, both NCAM180kDa and NCAM140kDa contain a specific domain that is known to participate in synaptic vesicle recruitment during repetitive stimulation at the mouse NMJ (Polo-Parada et al., 2005). Both the 180 and 140 NCAM isoforms were significantly increased in stimulated cells. It would be interesting to see whether this increase results in enhanced vesicle recruitment to the presynaptic terminal resulting in a higher value of quantal content in chronically stimulated cells.

Studies from Lynn Landmesser's lab have shown that activity during development alters expression patterns of polysialylated NCAM but not the NCAM itself (Hanson and Landmesser, 2004; Tang et al., 1992, 1994). The same group was able to use in ovo electroporated ChR2 to drive neural activity to counter the effects of picrotoxin (used to silence neural activity). In doing so PSA levels were restored in motor axons however, there was no effect on NCAM (Hanson and Landmesser, 2006).

Similarly, the present study found that activity altered PSA-NCAM expression, as shown in Figure 3.8B. However, we also found that NCAM expression in stimulated cells increased, as shown in Figure 3.8C, indicating that in stimulated motor neurons, there is not only more PSA added to every NCAM molecule, but there is also an increase in total NCAM molecule production. Compared to the in ovo system used in the Landmesser experiments, the advantage of our in vitro optogenetic model is that we are able to selectively activate motor neurons, whereas these studies could have been activating both sensory and motor neurons. In the Hanson experiments, it is possible that NCAM levels are being affected in motor neurons but not the sensory neurons, diluting the affect measured, as they only show a slight increase in NCAM in the stimulated cells that is not significant (Hanson and Landmesser, 2006).

Tang and colleagues in 1992 demonstrated that enzymatic removal of PSA from NCAM with EndoN, results in motor axon path finding errors, a phenomenon comparable to this study's findings that removing PSA from ChR2 ESCMNs results in truncated growth patterns, as shown in Figure 3.9. PSA is a large negatively charged molecule that when bound to NCAM decreases NCAM-NCAM interactions along with other cell-adhesive interactions, and instead promotes the growth and defasciculating of PSA-bearing axons (Rutishauser and Landmesser, 1996). When PSA is added to NCAM, the growth cones on motor axons are primed to more actively respond to guidance molecules such as EphA and EphB1 present in the limb (Kastanenka and Landmesser, 2010). Soundararajan and colleagues in 2010 demonstrated that the mouse ES cells differentiate into motor neurons that exclusively innervate epaxial muscles otherwise known as medial motor column motor neurons (MMCMNs). Endogenous MMCMNs

express fibroblast growth factor receptor 1 (FGFR1) and selectively extend axons towards the epaxial trophin FGF8, as do the ES cell derived MMCMNs (Soundararajan et al., 2010). As the present study used the same differentiation protocol, it would be an interesting future experiment to see if primed (having extra PSA added to them) stimulated motor neurons respond with more outgrowth towards to FGF8 in vitro, possibly requiring a lower concentration than non-stimulated cells. This could have potential applications in nerve regeneration research.

Post-synaptic recordings

Intracellular recordings confirmed successful neurotransmission at the NMJ in WT ChR2 ESCMNs, as shown in Figure 4.3. More specifically, it was demonstrated that ChR2 ESCMNs produce similar EPPs irrespective of light pulse exposure time and that EPPs can be consistently recorded up to 1 Hz. Our in vitro model system is advantageous for studying neurotransmission, by being able to precisely, yet non-invasively, evoke an action potential in motor neurons and easily record a response in the muscle. The evoked responses were blocked with TTX, allowing only spontaneous events to occur (mEPPs). Previous studies have shown similar amplitudes of both EPPs and mEPPs in ESCMNs (Miles et al., 2004, Chipman et al., 2014) and in iPSCMNs (Toma et al., 2015). This study is the first to be able to evoke a response by directly activating the motor neuron; previous studies have used glutamate or non-precise depolarizing current and defined EPPs based on amplitude range (Kandel et al., 2000; Miles et al., 2004; Chipman et al., 2014). It should be noted that the average EPP amplitude recorded (3.5mV- Figure 4.3) in these experiments were substantially less compared to those recorded in vivo of 17 mV at 4-6 weeks of age that increases to 24 mV from 12-15 weeks of age (Rocha et al., 2013).

Besides the obvious difference of in vitro versus in vivo, the cells used for recordings were more mature than our cultures and current was used to depolarize motor neurons instead of light.

Quantal content is the number of synaptic vesicles that fuse with the presynaptic membrane as a result of a single action potential (Kandel, 2000). It would be interesting to determine the quantal content in our co-culture system by recording after both 7 and 14 DIV, as done by Chipman et al., 2014. If the value increases over time, this would demonstrate that ChR2 ESCMNs possesses the ability to gradually refine neurotransmission as they mature in vitro. An additional future experiment would be to perform intracellular recordings on stimulated ChR2 ESCMN co-cultures. To determine if consistently stimulating these cultures can influence neurotransmission seen through changes in the post-synaptic recordings.

ChR2 ESCMNs are able to fire repetitively up to a frequency of 1 Hz before EPPs start to decrease in both consistency and amplitude, as shown in Figure 4.3F. A recent paper introduced an in vitro model system using human ESCMNs expressing ChR2 and found that, similar to our recordings, that motor neurons can consistently fire 100% of the time at a frequency of 0.2 Hz light pulses (Steinbeck et al., 2016). However, unlike our ESCMNs, they are able to maintain 100% repetitive light induced firing up to 2 Hz (Steinbeck et al., 2016). It should be noted that these motor neurons are more mature (35 DIV) then the ChR2 ESCMNs at the time of recording. Further, they demonstrate that their cells were able to fire up to a frequency of 10 Hz with a 65 ± 23% rate of consistency (Steinbeck et al., 2016). This illustrates that, although their cells can fire repetitively, they do have a repetitive firing limit. The failure to record EPPs above 1 Hz

could be due to the fact that the synaptic vesicle dynamics in the ChR2 ESCMNs after 14 DIV are not mature enough. Pursuing FM4-64 dye recordings, similar to what was shown by Chipman et al. (2014), would allow for a better understanding of the synaptic vesicle dynamics at the NMJ over time. It would be interesting to perform intracellular recordings on ChR2 ESCMN co-cultures after 30 DIV, to see whether at a later time point they are capable of firing at higher frequencies similar to Steinbeck et al. (2016).

The work of Steinbeck and colleagues (2016) is particularly impressive as they generated human ESCMNs expressing ChR2. However, it is important to remember the value of a mouse ESCMN co-culture system as it can be rapidly generated (a 5 day differentiation protocol compared to 30+ days in human). This demonstrates validity for using our system for primary proof-of-concept studies and large-scale drug screens (see below).

The next step: SOD1 ChR2 ESCMN intracellular recordings

SOD1 mice display changes of neuromuscular transmission prior to disease onset (Souayah et al., 2012; Rocha et al., 2013). Specifically, that pre-symptomatic SOD1 mice displayed reduced ability to consistently fire EPPs at high frequencies of stimulation (Souayah et al., 2012). SOD1 G93A mice have increased EPP amplitudes together with a greater quantal content before disease onset (Rocha et al., 2013). An appropriate follow-up experiment to these two studies would be to perform intracellular recordings on the SOD1 ChR2 ESCMNs at 7 days in vitro ("pre-symptomatic", before CI scores start to drop off), and then again at 12 days when they are "symptomatic" when CI scores steadily decrease. It would be interesting to see whether subtle differences could be detected in the our in vitro model i.e. increased EPP amplitude or deceased ability to

consistently fire, this would first: i) provide validation of accurate disease modeling and ii) allow for simplified screening of dysfunction that occurs in a minimalized environment.

Behavioral-Anatomical correlates with CI

We were able to establish distinct anatomical differences for each of the CI scores at both 7 and 14 DIV (Figure 4.5), these relationships can be plotted on a semi-logarithmic scale, as shown in Figure 4.6. An appropriate series of future experiments would be to look at the anatomical-behavioural correlates of stimulated ChR2 ESCMNs. It would be interesting to see i) whether there is greater neurite outgrowth in stimulated cultures or ii) does stimulating cultures cause more of a distinction in the anatomy seen for each CI score.

Pursuing these experiments with SOD1 ChR2 ESCMN co-cultures would be extremely worthwhile, as they could highlight the reason why strong CI scores never develop in SOD1 co-cultures even before disease onset, shown in Figure 4.8. Additionally, the anatomy of both stimulated and non-stimulated SOD1 ChR2 ESCMNs would allow for a better illustration of the NMJ as ALS progresses in vitro and a better understand of the role activity plays in the disease. Whether, i) the amount of motor axons in SOD1 cultures are as dense as WT cultures, or ii) if not, are SOD1 motor axons retracting/degenerating before motor neuron itself dies, or iii) and if so, when does this occur. This evidence would support the "dying-back hypothesis" where retrograde degeneration of the axon occurs starting at the NMJ (Frey et al., 2000; Hegedus et al., 2007l Hegedus et al., 2008; Marcuzzo et al., 2011).

The Contraction Intensity Index: potential limitations

The Contraction Intensity Index as shown in Figure 4.4 allows for quantification of the degree of muscle contraction elicited from a single light pulse. This scoring system was conceptualized similar to the Basso, Beattie and Bresnahan (BBB) locomotor scale used to assess motor behaviour (Basso et al., 1995). As with any newly created system, there are always limitations that arise, and in the case of the Contraction Intensity Index there are two: the variation in the size of EBs and the scoring method used for dissociated ESCMNs. The differentiation protocol used consistently yields motor neurons; however, the percentage of motor neurons within a given EB can vary anywhere from 15-22% (as outlined in chapter 3-results), meaning that there could be more motor neurons within an EB in one well-being scored compared to another. For example, one EB could be 22% motor neurons, giving a CI score of five meanwhile, the well next to it on the same day could potentially only contain 15% motor neurons, and result in a CI score of three. This factor could account of some of the variations in CI scores at different time points.

Another potential limitation with the scoring system is that it was created to score EBs plated on muscle fibres where the EB is in the center allowing for clear visualization of surrounding muscles only within the field of view. Using the CI index to score dissociated cultures is trickier, as dissociated cultures do not have a central region that one can focus on to score due to the spread-out distribution of motor neurons over the muscle. This means that at least 3 different regions need to be scored followed by an averaging of the scores. Often different scores can be obtained from all three regions surveyed, due to an uneven distribution of dissociated motor neurons and also because the cultures do not always elicit the same degree of contraction from the first to the third

pulse of light. Despite the issues outlined above, we believe the system is able to offer a reliable way to score the degree of contraction intensity over time in vitro.

The advantages of an optogenetic *in vitro* co-culture system

This novel in vitro model has significant potential in the field of neurobiology as it requires a short amount of time to establish, is able to specifically depolarize motor neurons using light and it being mouse derived, allowing for numerous transgenic possibilities. This novel model-system has the potential for clinical applications such as rapid drug screening and could be a future direction for the field of functional electrical stimulation. In addition, it provides a system for modeling the NMJ during motor neuron disease, which will allow for a better understanding of the poorly known disease mechanism in ALS.

Cell-type specific current free depolarization

Previous to this study, nerve-muscle in vitro co-culture systems used electrical currents to depolarize motor neurons. Issues associated with passing high currents through cultures include temperature changes, electrode corrosion, cellular damage and potential unwanted stimulation of the nearby muscles (Plenk, 2011). Optogenetics allows us to selectively and non-invasively activate our cells of interest avoiding the issues listed above.

Clinically, functional electrical stimulation (FES) has been proven to help restore function to paralyzed limbs (Popovic, 2014). FES however can lead to tissue damage and pain associated with passing electrical current through skin. Using optical stimulation instead of current avoids these harmful side-effects and provides a more selective stimulation technique. As a result, optogenetic stimulation may be used to replace FES as

a form of therapy after spinal cord injury in the future (Mallory et al., 2015). Although more research is needed for the potential application of our model as a patient therapy for motor neuron diseases, optical stimulation has already been shown to promote functional recovery in a stoke mouse model (Cheng et al., 2014). More recently the benefits of ChR2 stimulation was shown in mice by stimulating a denervated muscle daily resulting in attenuation of muscle atrophy (Magown et al., 2015).

Drug Screening

Rapid pre-clinical drug screens can be done using the CI Index paired with the ChR2 SOD1 ESCMN co-cultures, as the CI score serves as an indication of the degree of functional innervation or the health of the NMJ. Novel drugs would first be tested on healthy WT ChR2 ESCMN co-cultures, ensuring they do not promote irregular cell-death or muscle denervation before testing on SOD1 ChR2 ESCMNs. Drug screens can be performed on SOD1 co-cultures either i) pre-symptomatically (before CI scores drop) to prevent onset or ii) after onset (as CI scores are decreasing) to attempt to prolong NMJ function.

This system is ideal for drug screening, as it provides medium to test in the culture dish before testing on animals, and ultimately, human patients. Some of the benefits of cell culture experiments are that they are not as expensive and require less ethics paperwork compared to in vivo and human studies. Additionally, drug screenings using our model could accommodate in high volumes allowing for multiple drugs to be tested and high numbers of ‘subjects’ in each experimental condition. Recruiting a high volume of patients, or alternatively, getting the ethics board to approve novel drug testing on hundreds of animals is unlikely and highly time consuming. In comparison to the

creation of human ESCMNs, our mouse ESCMNs differentiate after 5 days in vitro whereas human cell lines have differentiation protocols spanning ~30 days. Therefore, our system provides a time-efficient, cost-saving and high-volume method for testing novel drugs.

Determining the role of activity in ALS

Our in vitro system can be used to better understand motor neuron disease progression and a way to tease out whether activity accelerates or attenuates motor neuron cell death in ALS. Once disease onset has occurred, there is controversy within the literature whether exercise should be prescribed to patients, or be entirely avoided since a high-activity lifestyle has been implicated with developing ALS (Mallory et al., 2015, Pupillo et al., 2014; Dal Bello-Haas and Florence, 2013). Clinical studies have demonstrated that moderate aerobic exercise is not detrimental to ALS patients (Bello-Haas et al., 2007; Dorry et al., 2001 Pupillo et al., 2014; Dal Bello-Haas and Florence, 2013*)*. Mouse studies have also shown benefits after SOD1 G93A mice were subjected to moderate daily exercise (Deforges et al., 2009; Kirkinezos et al., 2003; Kasper et al., 2005; Deforges et al., 2009). However, it is still not clear whether exercise may cause motor neurons in ALS to remain healthier longer. The benefits from activity have been correlated with a discovery from the mid-1990s demonstrating that short aerobic workouts in animals boosts levels of neurotrophins that act as protective substances in both the brain and spinal cord (Neeper et al., 1995). In contrast, we found that activating our SOD1 ChR2 ESCMN co-cultures caused CI scores (degree of innervation) to decrease more rapidly than those non-stimulated, as shown in Figure 4.8B.

Previous work demonstrated that SOD1 G93A ESCMNs die in culture as the disease progresses over weeks when supplemented with trophic support; however, once trophic support is withdrawn, these cells die rapidly (DiGiorgio et al., 2007; Yang et al., 2013). It is important to note that in the current study, trophic support was withdrawn after 7 DIV, the day before the rapid decrease in scores of the stimulated SOD1 co-cultures was observed. This led to the theory that the more rapid decrease in CI score was associated with trophic withdrawal. Previous work has shown neuronal activation causes an up regulation in the number of cell-surface trophic receptors (Meyer-Franke et al., 1998; Du et al., 2000; Goldberg et al., 2002), potentially causing the stimulated motor neurons to be more sensitive to the removal of these factors. As non-stimulated SOD1 ESCMNs eventually decrease in scores as well, it appears that the trophic withdrawal paired with constant activation accelerates the inevitable denervation. A future experiment to test this hypothesis would be to continue trophic support until 14 DIV and see whether at this time both stimulated and non-stimulated cultures similarly decrease in scores. Theoretically, the activity should not have as detrimental of an effect without the trophic withdrawal.

The decrease in CI scores in stimulated SOD1 co-cultures could also be due to the fact that the stimulation protocol of this study is too rigorous (every 10 seconds for 14 days) to equate to "moderate aerobic activity" shown to be beneficial in both animal and human studies. If the protocol was altered to stimulate co-cultures for several hours a day only, or to stimulate once every couple minutes instead of seconds, this could potentially mimic a more moderate level of exercise. Taken together, it seems as though consistent activity in the form of light-driven ESCMN activation is detrimental, causing the rate of

denervation to increase in SOD1 ChR2 ESCMNs compared to non-stimulated (non-exercised) cells.

Interestingly, when the SOD1 ChR2 ESCMNs were removed from the intrinsic firing network within the EB, by dissociation, less denervation was seen, as shown in Figure. 4.9. This finding is consistent with the conclusion above; that activity, in this case the intrinsic activity within the EB, is detrimental to the degree of muscle innervation over time in ALS co-cultures. Taken together, these results were unexpected as many studies indicate that exercise is beneficial in ALS. A set of follow-up experiments to those seen in Figure 4.9, would be to stimulate both dissociated WT ChR2 ESCMN and SOD1 ChR2 ESCMN co-cultures to see the effects on their CI scores and determine whether we will see the same rapid decrease in the cells post-trophic withdrawal or if there will be no affect at all.

The types of motor units innervating skeletal muscle are divided functionally into three subtypes: fast fatigable (FF), fast fatigue resistant (FR), and slow twitch (S) (Purves et al., 2001). In ALS, it has been demonstrated that FF motor units used to produce quick powerful bursts of speed are more susceptible to the disease than S type motor units (Frey et al., 2000; Hegedus et al., 2007, 2008; Kanning et al., 2010; Vinsant et al., 2013). It would be interesting to see whether this aspect of the disease could be replicated using our model, where the larger more easily fatigable motor units would have their motor axons withdrawing first. If this were the case it would further validate our model system as an accurate recapitulation of ALS, providing even more proof of principle for using this system for rapid-drug screening.

The stimulation protocol used for CI scoring experiments always began hours after plating, before cells made any post-synaptic contacts. Therefore the activity is affecting both the development and initial NMJ formation along with the continued survival and maintenance of the ESCMNs in co-culture. If stimulation began after 4-5 DIV, once post-synaptic connections were established, it would be interesting to see whether at this point, introducing activity would have a different affect than what we have shown in Figure 4.8.

The next step for in vitro modeling

The field of stem cell research is infinitely expanding, pun intended and the potential for modeling diseases in vitro has increased ever since Takahashi and Yamanaka discovered the specific conditions that would allow for adult cells to be 'reprogrammed' to a stem-cell like state, known as induced pluripotent stem cells (IPSCs) (2006). In addition, human embryonic stem cells have been created and reprogrammed into motor neurons (Lee et al., 2007; Li et al., 2005) that are well suited for studying the pathophysiology causing ALS. Motor neurons can now be derived from somatic cells collected from patients with ALS (Wainger et al., 2014; Kiskinis et al., 2014). Further these motor neurons have been shown to mimic endogenous motor neurons (Bilican et al., 2012; Son et al., 2011). Following the identification of clinically relevant phenotypes using our mouse ESCMN model these molecules can be next tested in vitro using human motor neurons derived from ALS patients, this being the step before testing on animals and eventually human patients.

Final Conclusions

Our results demonstrate that activity with respect to development is beneficial as it promotes growth and increases the expression of growth-promoting molecules. Future experiments are needed in order to determine whether ChR2 ESCMNs can either develop the ability to fire multiple action potentials in response to light or whether a different breeding strategy is needed in order to increase ChR2 expression. ChR2 ESCMNs can be incorporated into a functional in vitro model system and with SOD1 ChR2 ESCMNs this system can be used for disease modeling. It seems as though motor neurons early in development can be easily influenced by activity, whereas later in development when healthy cells are more focused on maintenance there does not seem to be an affect however, in diseased cells imposing activity seems to speed up disease progression. Taken together, this thesis introduces a novel model system to study cellular mechanisms underlying activity-dependent modulation of motor neuron development and disease.

REFERENCES

A

Albright, T. D., Jessell, T. M., Kandel, E. R., & Posner, M. I. (2000). Neural Science: A Century of Progress and the Mysteries that Remain. Neuron, 25(1).

Alaynick WA., Jessell TM., Pfaff SL. (2011) SnapShot: spinal cord development. Cell 146:178.

Anderson, A. A., Kendal, C. E., Garcia-Maya, M., Kenny, A. V., Morris-Triggs, S. A., Wu, T., Saffell, J. L. (2005). A peptide from the first fibronectin domain of NCAM acts as an inverse agonist and stimulates FGF receptor activation, neurite outgrowth and survival. Journal of Neurochemistry J Neurochem, 95(2), 570-583.

Arber, S., Han, B., Mendelsohn, M., Smith, M., Jessell, T. M., & Sockanathan, S. (1999). Requirement for the Homeobox Gene Hb9 in the Consolidation of Motor Neuron Identity. Neuron, 23(4), 659-674.

Arenkiel, B. R. et al. In vivo light-induced activation of neural circuitry in transgenic mice expressing channelrhodopsin-2.Neuron 54, 205–218 (2007).

Avila, O., Drachman, D., & Pestronk, A. (1989). Neurotransmission regulates stability of acetylcholine receptors at the neuromuscular junction. Journal of Neuroscience, 9(8), 2902-2906.

B

Basso, D. M., Beattie, M. S., & Bresnahan, J. C. (1995). A Sensitive and Reliable Locomotor Rating Scale for Open Field Testing in Rats. Journal of Neurotrauma, 12(1), 1-21.

Bamann, C., Kirsch, T., Nagel, G. & Bamberg, E. Spectral characteristics of the photocycle of channelrhodopsin-2 and its implication for channel function. J Mol Biol 375, 686–694 (2008).

Bello-Haas, V. D., & Florence, J. M. (2013). Therapeutic exercise for people with amyotrophic lateral sclerosis or motor neuron disease. Cochrane Database of Systematic Reviews Reviews.

Bello-Haas VP, Florence JM, Kloos AD, Scheirbecker J, Lopate G, Hayes SM. (2007) A randomized controlled trial of resistance exercise in individuals with ALS. Neurology 68(23):2003-7

Benjumeda I, Escalante A, Law C, Morales D, Chauvin G, Muca G, Coca Y, cuquez J, Lopez-Bendito G, Kania A, Martinez L, Herrera E (2013) Uncoupling of EphA/ephrinA Signaling and Spontaneous Activity in Neural Circuit Wiring. J Neurosci 33:18208–18218.

Bensimon, G., Lacomblez, L., Meininger, V. & The ALS/Riluzole Study Group (1994) A controlled trial of riluzole in amyotrophic lateral sclerosis. N. Engl. J. Med. 330, 585–591.

Bezakova, G., Rabben, I., Sefland, I., Fumagalli, G., & Lomo, T. (2001). Neural agrin controls acetylcholine receptor stability in skeletal muscle fibers. Proceedings of the National Academy of Sciences, 98(17), 9924-9929.

Bhat S., Silberberg DH. (1986) Oligodendrocyte cell adhesion molecules are related to neural cell adhesion molecule (N-CAM). J Neurosci 6: 3348-3354

Bilican, B., Serio, A., Barmada, S.J., Nishimura, A.L., Sullivan, G.J., Carrasco, M., Phatnani, H.P., Puddifoot, C.A., Story, D., Fletcher, J., Park, I.H., Friedman, B.A., Daley, G.Q., Wyllie, D.J., Hardingham, G.E., Wilmut, I., Finkbeiner, S., Maniatis, T., Shaw, C.E., Chandran, S., 2012. Mutant induced pluripotent stem cell lines recapitulate aspects of TDP-43 proteinopathies and reveal cell-specific vulnerability. Proc. Natl. Acad. Sci. U.S.A. 109, 5803–5808.

Black, M. A., Deurveilher, S., Seki, T., Marsh, D. R., Rutishauser, U., Rafuse, V. F., & Semba, K. (2009). Role of polysialylated neural cell adhesion molecule in rapid eye movement sleep regulation in rats. European Journal of Neuroscience, 30(11), 2190-2204.

Borodinsky LN, Root CM, Cronin JA, Sann SB, Gu X, Spitzer NC (2004) Activity dependent homeostatic specification of transmitter expression in embryonic neurons. Nature 429:523–530.

Borowska, J., Jones, C. T., Zhang, H., Blacklaws, J., Goulding, M., & Zhang, Y. (2013). Functional Subpopulations of V3 Interneurons in the Mature Mouse Spinal Cord. Journal of Neuroscience, 33(47), 18553-18565.

Boyden, E. S., Zhang, F., Bamberg, E., Nagel, G. & Deisseroth, K.Millisecond-timescale, genetically targeted optical control of neural activity. Nat Neurosci 8, 1263–1268 (2005).

Briscoe, J., and Ericson, J. (2001). Specification of neuronal fates in the ventral neural tube. Curr. Opin. Neurobiol. 11, 43–49.

Briscoe, J., Susse;, L., Serup, P., Hartigan O'Connor, D., Jessell, T., Ruenstein, J., & Ericson, J. (1999). The specification of neuronal identity by graded sonic hedgehog signalling. Seminars in Cell & Developmental Biology, 10(3), 353-362.

Bryson, J. B., Machado, C. B., Crossley, M., Stevenson, D., Bros-Facer, V., Burrone, J., Greensmith, L., Lieberam, I. (2014). Optical Control of Muscle Function by Transplantation of Stem Cell-Derived Motor Neurons in Mice. Science, 344(6179), 94-97.

Burke RE (1994) Physiology of motor units. In: Myology (Engel AG, Franzini-Armstrong C, eds), pp 464–484. New York: McGraw-Hill.

Bruton, J., Pinniger, G. J., Lannergren, J., & Westerblad, H. (2006). The effects of the myosin-II inhibitor N-benzyl-p-toluene sulphonamide on fatigue in mouse single intact toe muscle fibres. Acta Physiologica Acta Physiol, 186(1), 59-66.

Buskirk, D. R., Thiery, J., Rutishauser, U., & Edelman, G. M. (1980). Antibodies to a neural cell adhesion molecule disrupt histogenesis in cultured chick retinae. Nature, 285(5765), 488-489.

C

Castillo, J. D., & Katz, B. (1954). Quantal components of the end-plate potential. The Journal of Physiology, 124(3), 560-573.

Chater, T. E., Henley, J. M., Brown, J. T. & Randall, A. D. Voltage- and temperature-dependent gating of heterologously expressed channelrhodopsin-2. J Neurosci Methods 193, 7–13 (2010).

Cheng, M. Y., Wang, E. H., Woodson, W. J., Wang, S., Sun, G., Lee, A. G., . . . Steinberg, G. K. (2014). Optogenetic neuronal stimulation promotes functional recovery after stroke. Proceedings of the National Academy of Sciences, 111(35), 12913-12918.

Chernyshova, Y., Leshchyns'ka, I., Hsu, S., Schachner, M., & Sytnyk, V. (2011). The Neural Cell Adhesion Molecule Promotes FGFR-Dependent Phosphorylation and Membrane Targeting of the Exocyst Complex to Induce Exocytosis in Growth Cones. Journal of Neuroscience, 31(10), 3522-3535.

Chipman, P. H. (2012). The regulation of synaptic efficacy at regreneation and cultured neuromuscular junctions. Dalhousie University.

Chipman PH., Toma JS., Rafuse VF. (2012) Generation of motor neurons from pluripotent stem cells. Prog Brain Res. 201: 313-331.

Chipman, P. H., Zhang, Y., & Rafuse, V. F. (2014). A Stem-Cell Based Bioassay to Critically Assess the Pathology of Dysfunctional Neuromuscular Junctions. PLoS ONE, 9(3).

Cleveland DW, Rothstein JD (2001) From Charcot to Lou Gehrig: deciphering selective motor neuron death in ALS. Nat Rev Neurosci 2:806–819.

Coble NO, Maloney FP. Interdisciplinary rehabilitation of multiple sclerosis and neuromuscular disorders. In: Maloney FP, Burks JS, Ringel SP editor(s). Effects of Exercise in Neuromuscular Disease. New York: JB Lippincott, 1985:228-38.

Cohen-Cory S. (1999) BDNF modulates, but does not mediate, activity-dependent branching and remodeling of optic axons arbors in vivo. J Neurosci. 19:996-10003.

Crisp SJ, Evers JF, Bate M (2011) Endogenous Patterns of Activity Are Required for the Maturation of a Motor Network. Journal of Neuroscience 31:10445–10450.

Crown, E.D., Ye, Z., Johnson, K.M., Xu, G.-Y., McAdoo, D.J., Westlund, K.N. & Hulsebosch, C.E. (2005) Upregulation of the phosphorylated form of CREB in spinothalamic tract cells following spinal cord injury: relation to central neuropathic pain. Neurosci. Lett., 384, 139–144.

Crossin, K. L., Edelman, G., & Cunningham, B. (1984). Mapping of three carbohydrate attachment sites in embryonic and adult forms of the neural cell adhesion molecule. The Journal of Cell Biology, 99(5), 1848-1855.

Cunningham BA, Hemperly JJ, Murray BA, Prediger EA, Brackenbury R, Edelman GM (1987) Neural cell adhesion molecule: structure, immunoglobulin-like domains, cell surface modulation, and alternative RNA splicing. Science 236:799–806

Czaplinski, A., Yen, A.A., Simpson, E.P., Appel, S.H. (2006) Slower disease progression and prolonged survival in contemporary patients with amyotrophic lateral sclerosis: is the natural history of amyotrophic lateral sclerosis changing? Arch. Neurol. 63, 1139–1143.

D

Dal Bello-Haas VP, Florence JM, Kloos AD, Scheirbecker J, Lopate G, Hayes SM. (2007) A randomized controlled trial of resistance exercise in individuals with ALS. Neurology. 68(23):2003-7.

Dal Bello-Haas, V. D., & Florence, J. M. (2013). Therapeutic exercise for people with amyotrophic lateral sclerosis or motor neuron disease. Cochrane Database of Systematic Reviews Reviews.

Danilenko, M., Coffman, F. D., & Studzinski, G. P. (2012). Differentiation of Somatic Cells, Stem Cells and Stem Cell Variants: In Vitro Models. ELS.

Dantes, M., & Mccomas, A. (1991). The extent and time course of motoneuron involvement in amyotrophic lateral sclerosis. Muscle & Nerve Muscle Nerve, 14(5), 416-421.

Davis-Dusenbery, B. N., Williams, L. A., Klim, J. R., & Eggan, K. (2014). How to make spinal motor neurons. Development, 141(3), 491-501.

Deisseroth, K. (2015). Optogenetics: 10 years of microbial opsins in neuroscience. Nature Neuroscience Nat Neurosci, 18(9), 1213-1225.

Deforges, S., Branchu, J., Biondi, O., Grondard, C., Pariset, C., Lécolle, S., . . . Charbonnier, F. (2009). Motoneuron survival is promoted by specific exercise in a mouse model of amyotrophic lateral sclerosis. The Journal of Physiology, 587(14), 3561-3572.

Deshpande, D.M., Kim, Y.S., Martinez, T., Carmen, J., Dike, S., Shats, I., Rubin, L.L., Drummond, J., Krishnan, C., Hoke, A., Maragakis, N., Shefner, J., Rothstein, J.D., Kerr, D.A., 2006. Recovery from paralysis in adult rats using embryonic stem cells. Ann. Neurol. 60, 32–44.

Demarque M, Spitzer NC (2010) Activity-Dependent Expression of Lmx1b Regulates Specification of Serotonergic Neurons Modulating Swimming Behavior. Neuron 67:321–334.

Di Giorgio FP, Boulting GL, Bobrowicz S, Eggan KC (2008) Human embryonic stem cell-derived motor neurons are sensitive to the toxic effect of glial cells carrying an ALS-causing mutation. Cell Stem Cell 3:637-648.

Di Giorgio, F. P., Carrasco, M. A., Siao, M. C., Maniatis, T., & Eggan, K. (2007). Non–cell autonomous effect of glia on motor neurons in an embryonic stem cell–based ALS model. Nature Neuroscience Nat Neurosci, 10(5), 608-614.

Dityatev A, Dityateva G, Sytnyk V, Delling M, Toni N, Nikonenko I, Muller D, Schachner M (2004) Polysialylated neural cell adhesion molecule promotes remodeling and formation of hippocampal synapses. J Neurosci 24:9372–9382.

Durston, A.J., van der Wees, J., Pijnappel, W.W., and Godsave, S.F. (1998). Retinoids and related signals in early development of the vertebrate central nervous system. Curr. Top. Dev. Biol. 40, 111–175.

Du, J., Feng, L., Yang, F., & Lu, B. (2000). Activity- and Ca 2 -Dependent Modulation of Surface Expression of Brain-Derived Neurotrophic Factor Receptors in Hippocampal Neurons. J Cell Biol The Journal of Cell Biology, 150(6), 1423-1434.

E

Eckhardt M, Bukalo O, Chazal G, Wang L, Goridis C, Schachner M, Gerardy-Schahn R, Cremer H, Dityatev A. (2000) Mice deficient in the polysialyltransferase ST8SiaIV/PST-1 allow discrimination of the roles of neural cell adhesion molecule protein and polysialic acid in neural development and synaptic plasticity. J Neurosci 20: 5234-5244

Edvardsen, K., Chen, W., Rucklidge, G., Walsh, F. S., Obrink, B., & Bock, E. (1993). Transmembrane neural cell-adhesion molecule (NCAM), but not glycosyl-phosphatidylinositol-anchored NCAM, down-regulates secretion of matrix metalloproteinases. Proceedings of the National Academy of Sciences, 90(24), 11463-11467.

Edwards, C., & Frisch, H. L. (1976). A model for the localization of acetylcholine receptors at the muscle endplate. Journal of Neurobiology J. Neurobiol., 7(4), 377-381.

Ericson, J., Rashbass, P., Schedl, A., Brenner-Morton, S., Kawa- kami, A., van Heyningen, V., Jessell, T.M., and Briscoe, J. (1997). Pax6 controls progenitor cell identity and neuronal fate in response to graded Shh signaling. Cell 90, 169–180.

Eulenburg V, Armsen W, Betz H, Gomeza J(2005) Glycine transporters: essential regulators of neurotransmission. Trends Biochem Sci 30:325–333.

F

Fields DR, Itoh K (1996) Neural cell adhesion molecules in activity-dependent development and synaptic plasticity. Trends Neurosci 11:473–480

Fields R.D., Neale E.A., Nelson P.G. (1990) Effects of patterned electrical activity on neurite outgrowth from mouse sensory neurons. J Neurosci. 10:2950-2964.

Fischer LR, Culver DG, Tennant P, Davis AA, Wang M, et al. (2004) Amyotrophic lateral sclerosis is a distal axonopathy: evidence in mice and man. Exp Neurol 185: 232–240.

Flavell, S., Pokala, N., Macosko, E., Albrecht, D., Larsch, J., & Bargmann, C. (2013). Serotonin and the Neuropeptide PDF Initiate and Extend Opposing Behavioral States in C. elegans. Cell, 154(5), 1023-1035.

Franz CK, Rutishauser U, Rafuse VF (2005) Polysialylated neural cell adhesion molecule is necessary for selective targeting of regenerating motor neurons. J Neurosci 25:2081–2091.

Frei, T., Von Bohlen und Halbach, F., Wille, W., & Schachner, M. (1992). Different extracellular domains of the neural cell adhesion molecule (N- CAM) are involved in different functions. The Journal of Cell Biology, 118(1), 177-194.

Frey D, Schneider C, Xu L, Borg J, Spooren W, Caroni P. (2000) Early and selective loss of neuromuscular synapse subtypes with low sprouting competence in motoneuron diseases. J Neurosci 20: 2534–2542.

Fulton, B. P., & Walton, K. (1986). Electrophysiological properties of neonatal rat motoneurones studied in vitro. The Journal of Physiology, 370(1), 651-678.

G

Gao BX, Ziskind-Conhaim L (1998) Development of ionic currents underlying changes in action potential wave forms in rat spinal motoneurons. J Neurophysiol 80:3047-3061.

Goldberg, J. L., Espinosa, J. S., Xu, Y., Davidson, N., Kovacs, G. T., & Barres, B. A. (2002). Retinal Ganglion Cells Do Not Extend Axons by Default. Neuron, 33(5), 689-702.

Goldberg, J. L. (2003). How does an axon grow? Genes & Development, 17(8), 941-958.

Gordon, T., Tyreman, N., Li, S., Putman, C., & Hegedus, J. (2010). Functional over-load saves motor units in the SOD1-G93A transgenic mouse model of amyotrophic lateral sclerosis. Neurobiology of Disease, 37(2), 412-422. doi:10.1016/j.nbd.2009.10.021

Gould TW, Buss RR, Vinsant S, Prevette D, Sun W, et al. (2006) Complete Dissociation of Motor Neuron Death from Motor Dysfunction by Bax Deletion in a Mouse Model of ALS. J Neurosci 26: 8774–8786.

Goulding, M., Lanuza, G., Sapir, T., & Narayan, S. (2002). The formation of sensorimotor circuits. Current Opinion in Neurobiology, 12(5), 508-515.

Granit, R., Kernell, D., & Shortess, G. K. (1963). Quantitative aspects of repetitive firing of mammalian motoneurones, caused by injected currents. The Journal of Physiology, 168(4), 911-931.

Grossman, N. et al. High-frequency limit of neural stimulation with ChR2. (2011) Conf Proc IEEE Eng Med Biol Soc 4167–4170.

Gros-Louis, F., Soucy, G., Lariviere, R. & Julien, J.P. (2010) Intracerebroventricular infusion of monoclonal antibody or its derived Fab fragment against misfolded forms of SOD1 mutant delays mortality in a mouse model of ALS. J. Neurochem. 113, 1188–1199 (2010).

Guo X, Gonzalez M, Stancescu M, Vandenburgh HH, Hickman JJ (2011) Neuromuscular junction formation between human stem cell-derived motoneurons and human skeletal muscle in a defined system. Biomaterials 32: 9602–9611

Gunaydin, L. A. et al. Ultrafast optogenetic control. Nat Neurosci13, 387–392 (2010).

Gurney ME, Haifeng P, Chiu AY, Dal Canto MC, Polchow Y, Alexander DD, Caliendo J, Hentati A, Kwon YW, Deng H, Chen W, Zhai P, Sufit RL, Siddique T (1994) Motor neuron degeneration in mice that express a human Cu, Zn superoxide dismutase mutation. Science 264:1772–1775

H

Hata, K., Polo-Parada, L., & Landmesser, L. T. (2007). Selective Targeting of Different Neural Cell Adhesion Molecule Isoforms during Motoneuron Myotube Synapse Formation in Culture and the Switch from an Immature to Mature Form of Synaptic Vesicle Cycling. Journal of Neuroscience, 27(52), 14481-14493.

Hamshere, M., Dickson, G., & Eperon, I. (1991). The muscle specific domain of mouse N-CAM: Structure and alternative splicing patterns. Nucl Acids Res Nucleic Acids Research, 19(17), 4709-4716.

Hanson MG, Landmesser LT (2003) Characterization of the circuits that generate spontaneous episodes of activity in the early embryonic mouse spinal cord. J Neurosci 23:587–600.

Hanson, M., & Landmesser, L. T. (2004). Normal Patterns of Spontaneous Activity Are Required for Correct Motor Axon Guidance and the Expression of Specific Guidance Molecules. Neuron, 43(5), 687-701.

Hanson, M. G., & Landmesser, L. T. (2006). Increasing the Frequency of Spontaneous Rhythmic Activity Disrupts Pool-Specific Axon Fasciculation and Pathfinding of Embryonic Spinal Motoneurons. Journal of Neuroscience, 26(49), 12769-12780.

Hanson, M. G., Milner, L. D., & Landmesser, L. T. (2008). Spontaneous rhythmic activity in early chick spinal cord influences distinct motor axon pathfinding decisions. Brain Research Reviews, 57(1), 77-85.

Han, X. (2012). In Vivo Application of Optogenetics for Neural Circuit Analysis. ACS Chem. Neurosci. ACS Chemical Neuroscience, 3(8), 577-584.

Hegedus, J., Putman, C., & Gordon, T. (2007). Time course of preferential motor unit loss in the SOD1G93A mouse model of amyotrophic lateral sclerosis. Neurobiology of Disease, 28(2), 154-164.

Hegedus J, Putman CT, Tyreman N, Gordon T (2008) Preferential motor unit loss in the SOD1 G93A transgenic mouse model of amyotrophic lateral sclerosis. J Physiol 586: 3337-3351.

Heeroma JH, Plomp JJ, Roubos EW, Verhage M (2003) Development of the mouse neuromuscular junction in the absence of regulated secretion. Neuroscience 120:733–744.

Henneman, E., Somjen, G. & Carpenter, D. O. (1965). Functional significance of cell size in spinal motoneurons. J. Neurophysiol. 28, 560-580

Henneman E, Mendell LM (1991) Functional organization of the mo- toneuron pool and its inputs. Handbook of physiology: the nervous system II (Brooks H, ed), pp 423–507. Baltimore: Williams and Wilkins.

Hollyday, M. (1980). Organization of motor pools in the chick lumbar lateral motor column. J. Comp. Neurol. 194, 143–170.

Hollyday, M., and Hamburger, V. (1977). An autoradiographic study of the formation of the lateral motor column in the chick embryo. Brain Res. 132, 197–208.

Horstkorte, R., Schachner, M., Magyar, J., Vorherr, T., & Schmitz, B. (1993). The fourth immunoglobulin-like domain of NCAM contains a carbohydrate recognition domain for oligomannosidic glycans implicated in association with L1 and neurite outgrowth. The Journal of Cell Biology, 121(6), 1409-1421.

I

J

Jessell, T.M. (2000). Neuronal specification in the spinal cord: induc- tive signals and transcriptional codes. Nat. Rev. Genet. 1, 20–29.

Julien, J., & Kriz, J. (2006). Transgenic mouse models of amyotrophic lateral sclerosis. Biochimica Et Biophysica Acta (BBA) - Molecular Basis of Disease, 1762(11-12), 1013-1024.

K

Kandel, E.R., Spencer, W.A. & Brinley, F.J., Jr. (1961) Electrophysiology of hippocampal neurons. I. Sequential invasion and synaptic organization. J. Neurophysiol. 24, 225–242.

Kandel, E. R., Schwartz, J. H. & Jessell, T. M. (2000) Principles of Neural Science, Edn. 4. McGraw-Hill.

Kandel, E. R. (2000). Principles of neural science: Chapter 13 Transmitter Release. New York: McGraw-Hill, Health Professions Division.

Kania, A., Johnson, R.L., and Jessell, T.M. (2000). Coordinate roles for LIM homeobox genes in directing the dorsoventral trajectory of motor axons in the vertebrate limb. Cell 102, 161–173.

Kanning, K. C., Kaplan, A., & Henderson, C. E. (2010). Motor Neuron Diversity in Development and Disease. Annu. Rev. Neurosci. Annual Review of Neuroscience, 33(1), 409-440.

Kaspar, B. K., Frost, L. M., Christian, L., Umapathi, P., & Gage, F. H. (2005). Synergy of insulin-like growth factor-1 and exercise in amyotrophic lateral sclerosis. Annals of Neurology Ann Neurol., 57(5), 649-655.

Kastanenka, K. V., & Landmesser, L. T. (2010). In Vivo Activation of Channelrhodopsin-2 Reveals That Normal Patterns of Spontaneous Activity Are Required for Motoneuron Guidance and Maintenance of Guidance Molecules. Journal of Neuroscience, 30(31), 10575-10585.

Kastanenka, K. V., & Landmesser, L. T. (2013). Optogenetic-mediated increases in in vivo spontaneous activity disrupt pool-specific but not dorsal-ventral motoneuron pathfinding. Proceedings of the National Academy of Sciences, 110(43), 17528-17533.

Katz, B., & Miledi, R. (1968). The role of calcium in neuromuscular facilitation. The Journal of Physiology, 195(2), 481-492.

Kernell, D., & Monster, A. W. (1982). Time course and properties of late adaptation in spinal motoneurones of the cat. Exp Brain Res Experimental Brain Research, 46(2), 191-196.

Kernell, D., 2006. Why bother about motoneurons? In: Kernell, D. (Ed.), The Motoneurone and Its Muscle Fibres. Oxford University Press, Oxford, pp. 1–4.

Kiskinis, E., Sandoe, J., Williams, L., Boulting, G., Moccia, R., Wainger, B., . . . Eggan, K. (2014). Pathways Disrupted in Human ALS Motor Neurons Identified through Genetic Correction of Mutant SOD1. Cell Stem Cell, 14(6), 781-795.

Kirkinezos, I. G., Hernandez, D., Bradley, W. G., & Moraes, C. T. (2003). Regular exercise is beneficial to a mouse model of amyotrophic lateral sclerosis. Annals of Neurology Ann Neurol., 53(6), 804-807.

Kiselyov, V. V., Soroka, V., Berezin, V., & Bock, E. (2005). Structural biology of NCAM homophilic binding and activation of FGFR. Journal of Neurochemistry, 94(5), 1169-1179.

Kurtzke JF. Risk factors in amyotrophic lateral sclerosis. Advances in Neurology 1991; 56:245-70.

L

Lacomblez, L., Bensimon, G., Leigh, P. N., Guillet, P., Meininger, V. (1996) Dose-ranging study of riluzole in amyotrophic lateral sclerosis. Amyotrophic Lateral Sclerosis/Riluzole Study Group II. Lancet 347, 1425–1431.

Landmesser L. and D. G. Morris (1975) The development of functional innervation in the hind limb of the chick embryo: J. Physiol. (Lond.) 249:301-326

Landmesser, L., 1978a. The distribution of motoneurones supplying chick hind limb muscles. J. Physiol. 284, 371–389.

Landmesser, L., 1978b. The development of motor projection patterns in the chick hind limb. J. Physiol. 284, 391–414

Landmesser, L. T. (1980). The Generation of Neuromuscular Specificity. Annu. Rev. Neurosci. Annual Review of Neuroscience, 3(1), 279-302.

Landmesser, L., Dahm, L., Tang, J., & Rutishauser, U. (1990). Polysialic acid as a regulator of intramuscular nerve branching during embryonic development. Neuron, 4(5), 655-667.

Landry, D. W., & Zucker, H. A. (2004). Embryonic death and the creation of human embryonic stem cells. Journal of Clinical Investigation J. Clin. Invest., 114(9), 1184-1186.

Leshchyns'ka I, Sytnyk V, Morrow JS, Schachner M (2003) Neural cell ad- hesion molecule (NCAM) association with PKCbeta2 via betaI spectrin is implicated in NCAM-mediated neurite outgrowth. J Cell Biol 161:625– 639.

Lee, H., Shamy, G.A., Elkabetz, Y., Schofield, C.M., Harrsion, N.L., Panagiotakos, G., Socci, N.D., Tabar, V., Studer, L., 2007. Directed differentiation and transplantation of human embryonic stem cell-derived motoneurons. Stem Cells 25, 1931–1939.

Lee, S.K., and Pfaff, S.L. (2001). Transcriptional networks regulating neuronal identity in the developing spinal cord. Nat. Neurosci. 4 (Suppl.), 1183–1191.

Lee, H., Shamy, G. A., Elkabetz, Y., Schofield, C. M., Harrsion, N. L., Panagiotakos, G., . . . Studer, L. (2007). Directed Differentiation and Transplantation of Human Embryonic Stem Cell-Derived Motoneurons. Stem Cells, 25(8), 1931-1939.

Lin, J. Y., Lin, M. Z., Steinbach, P. & Tsien, R. Y. (2009) Characterization of engineered channelrhodopsin variants with improved properties and kinetics. Biophys. J. 96: 1803–1814

Lin, J. Y. (2011). A user's guide to channelrhodopsin variants: Features, limitations and future developments. Experimental Physiology, 96(1), 19-25.

Li, X., Gutierrez, D. V., Hanson, M. G., Han, J., Mark, M. D., Chiel, H., Hegemann P., Landmesser L.T., Herlitze, S. (2005). Fast noninvasive activation and inhibition of neural and network activity by vertebrate rhodopsin and green algae channelrhodopsin. Proceedings of the National Academy of Sciences, 102(49), 17816-17821.

Li, X.J., Du, Z.W., Zarnowska, E.D., Pankratz, M., Hansen, L.O., Pearce, R.A., Zhang, S.C., 2005. Specification of motoneurons from human embryonic stem cells. Nat. Biotechnol. 23, 215–221.

Liske, H., Qian, X., Anikeeva, P., Deisseroth, K., & Delp, S. (2013). Optical control of neuronal excitation and inhibition using a single opsin protein, ChR2. Nature Scientific Reports, 3.

Lohnes, D., Mark, M., Mendelsohn, C., Dolle´, P., Dierich, A., Gorry, P., Gansmuller, A., Chambon, P., 1994. Function of the retinoic acid receptors (RARs) during development (I). Craniofacial and skeletal abnormalities in RAR double mutants. Development 120, 2723–2748.

Lu, Y., Truccolo, W., Wagner, F. B., Vargas-Irwin, C. E., Ozden, I., Zimmermann, J. B., . . . Nurmikko, A. V. (2015). Optogenetically induced spatiotemporal gamma oscillations and neuronal spiking activity in primate motor cortex. Journal of Neurophysiology J Neurophysiol, 113(10), 3574-3587.

M

Machado, C. B., Kanning, K. C., Kreis, P., Stevenson, D., Crossley, M., Nowak, M., . . . Lieberam, I. (2014). Reconstruction of phrenic neuron identity in embryonic stem cell-derived motor neurons. Development, 141(4), 784-794.

Madisen, L., Mao, T., Koch, H., Zhuo, J., Berenyi, A., Fujisawa, S., . . . Zeng, H. (2012). A toolbox of Cre-dependent optogenetic transgenic mice for light-induced activation and silencing. Nature Neuroscience Nat Neurosci, 15(5), 793-802.

Magown, P., Shettar, B., Zhang, Y., & Rafuse, V. F. (2015). Direct optical activation of skeletal muscle fibres efficiently controls muscle contraction and attenuates denervation atrophy. Nature Communications Nat Comms, 6, 8506.

Mallory, G. W., Grahn, P. J., Hachmann, J. T., Lujan, J. L., & Lee, K. H. (2015). Optical Stimulation for Restoration of Motor Function After Spinal Cord Injury. Mayo Clinic Proceedings, 90(2), 300-307.

Marcuzzo S, Zucca I, Mastropietro A, de Rosbo NK, Cavalcante P et al. (2011) Hind limb muscle atrophy precedes cerebral neuronal degeneration in G93A-SOD1 mouse model of amyotrophic lateral sclerosis: a longitudinal MRI study. Exp Neurol 231: 30-37.

Markus, A., Patel, T. D., & Snider, W. D. (2002). Neurotrophic factors and axonal growth. Current Opinion in Neurobiology, 12(5), 523-531.

Marek KW, Kurtz LM, Spitzer NC (2010) cJun integrates calcium activity and tlx3 expression to regulate neurotransmitter specification. Nat Neurosci 13:944–950.

Mattis, J. et al. Principles for applying optogenetic tools derived from direct comparative analysis of microbial opsins. Nat Methods9, 159–172 (2012).

Mazhar, S., & Herbst, R. (2012). The formation of complex acetylcholine receptor clusters requires MuSK kinase activity and structural information from the MuSK extracellular domain. Molecular and Cellular Neuroscience, 49(4), 475-486.

Meyer-Franke, A., Kaplan, M. R., Pfieger, F. W., & Barres, B. A. (1995). Characterization of the signaling interactions that promote the survival and growth of developing retinal ganglion cells in culture. Neuron, 15(4), 805-819.

Miles, G. B., Yohn, D. C., Wichterle, H., Jessell, T. M., & Rafuse, V. R. (2004). Functional Properties of Motoneurons Derived from Mouse Embryonic Stem Cells. Journal of Neuroscience, 24(36), 7848-7858.

Milev P,. Maurel P., Haring M., Margolis RK., Margolis RU. (1994) TAG-1/axonin-1 is a high-affinity ligand of neurocan, phosphacan/protein-tyrosine phosphatase-zeta/beta, and N-CAM. J Biol Chem 271:15716-15723

Miller, T. M., & Heuser, J. (1984). Endocytosis of synaptic vesicle membrane at the frog neuromuscular junction. The Journal of Cell Biology, 98(2), 685-698.

Muhr, J., Graziano, E., Wilson, S., Jessell, T.M., and Edlund, T. (1999). Convergent inductive signals specify midbrain, hindbrain, and spinal cord identity in gastrula stage chick embryos. Neuron 23, 689–702.

Muller D, Wang C, Skibo G, Toni N, Cremer H, Calaora V, Rougon G, Kiss JZ (1996) PSA-NCAM is required for activity-induced synaptic plasticity. Neuron 17:413–422.

Myers CP, Lewcock JW, Hanson MG, Gosgnach S, Aimone JB, Gage FH, Lee K, F, Landmesser LT, Pfaff SL (2005) Cholinergic input is required during embryonic development to mediate proper assembly of spinal locomotor circuits. Neuron 46:37–49.

N

Nagel, G. et al. (2003) Channelrhodopsin-2, a directly light-gated cation-selective membrane channel. Proc. Natl Acad. Sci. USA 100, 13940–13945.

Nagel, G., Brauner, M., Liewald, J. F., Adeishvili, N., Bamberg, E., & Gottschalk, A. (2005). Light Activation of Channelrhodopsin-2 in Excitable Cells of Caenorhabditis elegans Triggers Rapid Behavioral Responses. Current Biology, 15(24), 2279-2284.

Neeper, S. A., Goauctemez-Pinilla, F., Choi, J., & Cotman, C. (1995). Exercise and brain neurotrophins. Nature, 373(109).

Nielsen, J., Gotfryd, K., Li, S., Kulahin, N., Soroka, V., Rasmussen, K. K., . . . Berezin, V. (2009). Role of Glial Cell Line-Derived Neurotrophic Factor (GDNF)-Neural Cell Adhesion Molecule (NCAM) Interactions in Induction of Neurite Outgrowth and Identification of a Binding Site for NCAM in the Heel Region of GDNF. Journal of Neuroscience, 29(36), 11360-11376.

Noble, M., Albrechtsen, M., Møllert, C., Lyles, J., Bock, E., Goridis, C., . . . Rutishauser, U. (1985). Glial cells express N-CAM/D2-CAM-like polypeptides in vitro. Nature, 316(6030), 725-728.

Novitch, B.G., Chen, A.I., and Jessell, T.M. (2001). Coordinate regulation of motor neuron subtype identity and pan-neuronal properties by the bHLH repressor Olig2. Neuron 31, 773–789.

O

P

Paratcha, G., Ledda, F., & Ibáñez, C. F. (2003). The Neural Cell Adhesion Molecule NCAM Is an Alternative Signaling Receptor for GDNF Family Ligands. Cell, 113(7), 867-879.

Patel, P., Kriz, J., Gravel, M., Soucy, G., Bareil, C., Gravel, C., & Julien, J. (2013). Adeno-associated Virus–mediated Delivery of a Recombinant Single-chain Antibody Against Misfolded Superoxide Dismutase for Treatment of Amyotrophic Lateral Sclerosis. Mol Ther Molecular Therapy, 22(3), 498-510.

Piotrkiewicz, M., & Hausmanowa-Petrusewicz, I. (2013). Amyotrophic lateral sclerosis: A dying motor unit? Frontiers in Aging Neuroscience Front. Aging Neurosci., 5(7).

Placzek, M., Yamada, T., Tessier-Lavigne, M., Jessell, T., & Dodd, J. (1991). Control of dorsoventral pattern in vertebrate neural development: Induction and polarizing properties of the floor plate. Development, 113(2), 105-122.

Plenk, H Jr. (2011). The Role of Materials Biocompatibility for Functional Electrical Stimulation Applications. Artificial Organs, 35(3), 237-241.

Polo-Parada, L., Bose, C., Plattner, F., & Landmesser, L. (2004). Distinct Roles of Different Neural Cell Adhesion Molecule (NCAM) Isoforms in Synaptic Maturation Revealed by Analysis of NCAM 180 kDa Isoform-Deficient Mice. Journal of Neuroscience, 24(8), 1852-1864.

Polo-Parada L, Plattner F, Bose C, Landmesser LT (2005) NCAM 180 Acting via a conserved C-terminal domain and MLCK is essential for effective transmission with repetitive stimulation. Neuron 46:917–931.

Popović, D. B. (2014). Advances in functional electrical stimulation (FES). Journal of Electromyography and Kinesiology, 24(6), 795-802.

Pinniger, G. J., Bruton, J. D., Westerblad, H., & Ranatunga, K. W. (2005). Effects of a Myosin-II Inhibitor (N-benzyl-p-toluene Sulphonamide, BTS) on Contractile Characteristics of Intact Fast-twitch Mammalian Muscle Fibres. J Muscle Res Cell Motil Journal of Muscle Research and Cell Motility, 26(2-3), 135-141.

Pupillo, E., Messina, P., Giussani, G., Logroscino, G., Zoccolella, S., Chiò, A., . . . Beghi, E. (2014). Physical activity and amyotrophic lateral sclerosis: A European population-based case-control study. Annals of Neurology Ann Neurol., 75(5), 708-716.

Purves, D., & Williams, S. M. (2001). Neuroscience. 2nd edition. Sinauer Associates.

Q

U

R

Rafuse, V. F., & Landmesser, L. (1996). Contractile activity regulates isoform expression and polysialylation of NCAM in cultured myotubes: Involvement of Ca2 and protein kinase C. The Journal of Cell Biology, 132(5), 969-983.

Rafuse VF, Polo-ParadaL, LandmesserLT (2000) Structuralandfunctional alterations of neuromuscular junctions in NCAM-deficient mice. J Neu- rosci 20:6529 – 6539.

Rafuse VF, Landmesser LT (2000) The pattern of avian intramuscular nerve branching is determined by the innervating motoneuron and its level of polysialic acids. J Neurosci 20: 1056-1065.

Ramdya, P., Lichocki, P., Cruchet, S., Frisch, L., Tse, W., Floreano, D., & Benton, R. (2015). Mechanosensory interactions drive collective behaviour in Drosophila. Nature, 519(7542), 233-236.

Rashid, N., & Cambray-Deakin, M. (1992). Effects on the growth, morphology and cytoskeleton of individual neurons in vitro. Developmental Brain Research, 67(2), 301-308.

Rieger, F., Grumet, M., & Edelman, G. (1985). N-CAM at the vertebrate neuromuscular junction. The Journal of Cell Biology, 101(1), 285-293.

Robbins, N., & Yonezawa, T. (1971). Developing Neuromuscular Junctions: First Signs of Chemical Transmission during Formation in Tissue Culture. Science, 172(3981), 395-398.

Roberts, T. F., Gobes, S. M., Murugan, M., Ölveczky, B. P., & Mooney, R. (2012). Motor circuits are required to encode a sensory model for imitative learning. Nature Neuroscience Nat Neurosci, 15(10), 1454-1459.

Rocha, M. C., Pousinha, P. A., Correia, A. M., Sebastião, A. M., & Ribeiro, J. A. (2013). Early Changes of Neuromuscular Transmission in the SOD1(G93A) Mice Model of ALS Start Long before Motor Symptoms Onset. PLoS ONE, 8(9).

Rosen DR, Siddique T, Patterson D, Figlewicz DA, Sapp P, Hentati A, Donaldson D, Goto J, O'Regan JP, Deng H, Rahmani Z, Krizus A, McKenna-Yasek D, Cayabyab A, Gaston SM, Berger R, Tanzi RE, Halperin JJ, Herzfeldt B, Van Den Bergh R (1993) Mutations in Cu/Zn superoxide dismutase gene are associated with familial amyotrophic lateral sclerosis. Nature 362:59–62.

Rutishauser, U., Hoffman, S., & Edelman, G. M. (1982). Binding properties of a cell adhesion molecule from neural tissue. Proceedings of the National Academy of Sciences, 79(2), 685-689.

Rutishauser, U. (1996). Polysialic acid and the regulation of cell interactions. Current Opinion in Cell Biology, 8(5), 679-684.

Rutishauser U, Landmesser LT (1996) Polysialic acid in the vertebrate nervous system: a promoter of plasticity in cell-cell interactions. Trends Neurosci 19:422–427.

S

Sanes, J. R., & Lichtman, J. W. (1999). Development Of The Vertebrate Neuromuscular Junction. Annu. Rev. Neurosci. Annual Review of Neuroscience, 22(1), 389-442.

Sinaki M, Mulder DW. Rehabilitation techniques for patients with amyotrophic lateral sclerosis. Mayo Clinic Proceedings 1978;53(3):173-8.

Sine, S. M. (2012). End-Plate Acetylcholine Receptor: Structure, Mechanism, Pharmacology, and Disease. Physiological Reviews, 92(3), 1189-1234.

Sockanathan, S., & Jessell, T. M. (1998). Motor Neuron–Derived Retinoid Signaling Specifies the Subtype Identity of Spinal Motor Neurons. Cell, 94(4), 503-514.

Sockanathan, S., Perlmann, T., & Jessell, T. M. (2003). Retinoid Receptor Signaling in Postmitotic Motor Neurons Regulates Rostrocaudal Positional Identity and Axonal Projection Pattern. Neuron, 40(1), 97-111.

Son, E.Y., Ichida, J.K., Wainger, B.J., Toma, J.S., Rafuse, V.F., Woolf, C.J., Eggan, K., 2011. Conversion of mouse and human fibroblasts into functional spinal motor neurons. Cell Stem Cell 9, 205–218.

Souayah N, Coakley KM, Chen R, Ende N, McArdle JJ (2012) Defective neuromuscular transmission in the SOD1 G93A transgenic mouse improves after administration of human umbilical cord blood cells. Stem Cell Rev 8: 224-228.

Soundararajan, P., Miles, G.B., Rubin, L.L., Brownstone, R.M., Rafuse, V.F., 2006. Motoneurons derived from embryonic stem cells express transcription factors and develop phenotypes characteristic of medial motor column neurons. J. Neurosci. 26, 3256–3268.

Soundararajan, P., Lindsey, B.W., Leopold, C., Rafuse, V.F., 2007. Easy and rapid differentiation of embryonic stem cells into functional motoneurons using sonic hedgehog producing cells. Stem Cells 25: 1697–1706.

Soundararajan, P., Fawcett, J.P., Rafuse, V.F., 2010. Guidance of postural motoneurons requires MAPK/ERK signaling downstream of fibroblast growth factor receptor 1. J. Neurosci. 30: 6595–6606.

Spudich, J. L. (2006). The multitalented microbial sensory rhodopsins. Trends in Microbiology, 14(11), 480-487.

Steinbeck, J., Jaiswal, M., Calder, E., Kishinevsky, S., Weishaupt, A., Toyka, K., . . . Studer, L. (2016). Functional Connectivity under Optogenetic Control Allows Modeling of Human Neuromuscular Disease. Cell Stem Cell, 18(1), 134-143.

Strickland D, Smith SA, Dolliff G, Goldman L, Roelofs R. Physical activity, trauma, and ALS: a case-control study. Acta Neurologica Scandinavica 1996;94(1):45-50.

T

Takahashi, K., & Yamanaka, S. (2006). Induction of Pluripotent Stem Cells from Mouse Embryonic and Adult Fibroblast Cultures by Defined Factors. Cell, 126(4), 663-676.

Takazawa, T., Croft, G. F., Amoroso, M. W., Studer, L., Wichterle, H., & Macdermott, A. B. (2012). Maturation of Spinal Motor Neurons Derived from Human Embryonic Stem Cells. PLoS ONE, 7(7).

Tang, J., Landmesser, L., & Rutishauser, U. (1992). Polysialic acid influences specific pathfinding by avian motoneurons. Neuron, 8(6), 1031-1044.

Thaler, J., Harrison, K., Sharma, K., Lettieri, K., Kehrl, J., and Pfaff, S.L. (1999). Active suppression of interneuron programs within developing motor neurons revealed by analysis of homeocomain factor HB9. Neuron 23, 675–687.

Theys, P. A., Peeters, E., & Robberecht, W. (1999). Evolution of motor and sensory deficits in amyotrophic lateral sclerosis estimated by neurophysiological techniques. Journal of Neurology, 246(6), 438-442. doi:10.1007/s004150050379

Thelen, K., Georg, T., Bertuch, S., Zelina, P., & Pollerberg, G. E. (2008). Ubiquitination and Endocytosis of Cell Adhesion Molecule DM-GRASP Regulate Its Cell Surface Presence and Affect Its Role for Axon Navigation. Journal of Biological Chemistry, 283(47), 32792-32801.

Thiele, T., Donovan, J., & Baier, H. (2014). Descending Control of Swim Posture by a Midbrain Nucleus in Zebrafish. Neuron, 83(3), 679-691.

Thiery JP, Brackenbury R, Rutishauser U, Edelman GM. (1977) Adhesion among neural cells of the chick embryo. II. Purification and characterization of a cell adhesion molecule from neural retina. J Biol Chem 252: 6841-6845

Thomson, J. A., Itskovitz-Eldor, J., Shapiro, S., Waknitz, M. A., Swiergiel, J. J., Marshall, V. S., & Jones, J. M. (1998). Embryonic Stem Cell Lines Derived from Human Blastocysts. Science, 282(5391), 1145-1147.

Toma, J. S., Shettar, B. C., Chipman, P. H., Pinto, D. M., Borowska, J. P., Ichida, J. K., Rafuse, V. F. (2015). Motoneurons Derived from Induced Pluripotent Stem Cells Develop Mature Phenotypes Typical of Endogenous Spinal Motoneurons. Journal of Neuroscience, 35(3), 1291-1306.

Tourovskaia, A., Li, N., & Folch, A. (2008). Localized Acetylcholine Receptor Clustering Dynamics in Response to Microfluidic Focal Stimulation with Agrin. Biophysical Journal, 95(6), 3009-3016.

Tsuchida, T., Ensini, M., Morton, S.B., Baldassare, M., Edlund, T., Jessell, T.M., and Pfaff, S.L. (1994). Topographic organization of embryonic motor neurons defined by expression of LIM homeobox genes. Cell 79, 957–970.

U

Umbach JA, Adams KL, Gundersen CB, Novitch BG (2012) Functional Neuromuscular Junctions Formed by Embryonic Stem Cell-Derived Motor Neurons. PLoS ONE 7: e36049.

University of Queensland. (2016). Using ImageJ to Quantify Blots. Retrieved March 02, 2016, from http://www.di.uq.edu.au/sparqimagejblots

V

Varoqueaux F, Sigler A, Rhee J-S, Brose N, Enk C, Reim K, Rosenmund C. (2002) Total arrest of spontaneous and evoked synaptic transmission but normal synaptogenesis in the absence of Munc13-mediated vesicle priming. Proc Natl Acad Sci USA 99:9037–9042.

Varoqueaux F, Sons MS, Plomp JJ, Brose N (2005) Aberrant morphology and residual transmitter release at the Munc13-deficient mouse neuromuscular synapse. Mol Cell Biol 25:5973–5984.

Veldink JH, Bar PR, Joosten EAJ, Otten M, Wokke JHJ, van den Berg LH. Sexual differences in onset of disease and response to exercise in a transgenic model of ALS. Neuromuscular Disease 2003;13(9):737-43.

Vitale, A.M., Wolvetang, E., Mackay-Sim, A., 2011. Induced pluripotent stem cells: a new technology to study human diseases. Int. J. Biochem. Cell Biol. 43, 843–846.

Vinsant, S., Mansfield, C., Jimenez-Moreno, R., Moore, V. D., Yoshikawa, M., Hampton, T. G., . . . Milligan, C. (2013). Characterization of early pathogenesis in the SOD1 G93A mouse model of ALS: Part II, results and discussion. Brain Behav Brain and Behavior, 3(4), 431-457.

W

Wainger, B., Kiskinis, E., Mellin, C., Wiskow, O., Han, S., Sandoe, J., . . . Woolf, C. (2014). Intrinsic Membrane Hyperexcitability of Amyotrophic Lateral Sclerosis Patient-Derived Motor Neurons. Cell Reports, 7(1), 1-11.

Whitelaw, V., and Hollyday, M. (1983). Thigh and calf discrimination in the motor innervation of the chick hindlimb following deletions of limb segments. J. Neurosci. 3, 1199–1215.

Wichterle, H., Lieberam, I., Porter, J. A., & Jessell, T. M. (2002). Directed Differentiation of Embryonic Stem Cells into Motor Neurons. Cell, 110(3), 385-397.

Wilson, S.I., and Edlund, T. (2001). Neural induction: toward a unify- ing mechanism. Nat. Neurosci. 4 (Suppl), 1161–1168.

X

Y

Yamada, T., Placzek, M., Tanaka, H., Dodd, J., & Jessell, T. (1991). Control of cell pattern in the developing nervous system: Polarizing activity of the floor plate and notochord. Cell, 64(3), 635-647.

Yamada, T., Pfaff, S. L., Edlund, T., & Jessell, T. M. (1993). Control of cell pattern in the neural tube: Motor neuron induction by diffusible factors from notochord and floor plate. Cell, 73(4), 673-686.

Yang YM, Gupta SK, Kim KJ, Powers BE, Cerqueira A, Wainger BJ, Ngo HD, Rosowski KA, Schein PA, Ackeifi CA, Arvanites AC, Davidow LS, Woolf CJ, Rubin LL (2013) A small molecule screen in stem-cell-derived motor neurons identifies a kinase inhibitor as a candidate therapeutic for ALS. Cell Stem Cell 12:713-726.

Yap, C. C., Lasiecka, Z. M., Caplan, S., & Winckler, B. (2010). Alterations of EHD1/EHD4 Protein Levels Interfere with L1/NgCAM Endocytosis in Neurons and Disrupt Axonal Targeting. Journal of Neuroscience, 30(19), 6646-6657.

Yohn, D.C., Miles, G.B., Rafuse, V.F., Brownstone, R.M., 2008. Transplanted mouse embryonic stem-cell-derived motoneurons form functional motor units and reduce muscle atrophy. J. Neurosci. 28, 12409–12418.

Z

Zakharenko, S., Chang, S., O'donoghue, M., & Popov, S. V. (1999). Neurotransmitter Secretion along Growing Nerve Processes: Comparison with Synaptic Vesicle Exocytosis. J Cell Biol The Journal of Cell Biology, 144(3), 507-518.

Zhang, H. L., & Peng, H. B. (2011). Mechanism of Acetylcholine Receptor Cluster Formation Induced by DC Electric Field. PLoS ONE, 6(10).

Zhang, F., Vierock, J., Yizhar, O., Fenno, L.E., Tsunoda, S., Kianianmomeni, A., Prigge, M., Berndt, A., Cushman, J., Polle, J., et al. (2011). The microbial opsin family of optogenetic tools. Cell 147: 1446–1457.

Zhou, H. (1993). Homophilic adhesion between Ig superfamily carcinoembryonic antigen molecules involves double reciprocal bonds. The Journal of Cell Biology, 122(4), 951-960.

Ziv, N. E., & Garner, C. C. (2004). Cellular and molecular mechanisms of presynaptic assembly Nature Reviews Neuroscience Nat Rev Neurosci, 5(5), 385-399.

APPENDIX

Supplemental Figures

Supplemental Figure 1: Inherent dim GFP expression in ChR2 ESCMNs poses issues with fluorescence activity cell sorting**.** Confocal images (**A-D**) showing the differing GFP expression patterns in HBG3 ESCMNS compared to ChR2 ESCMNS. (**A**) HBG3 ESCMN with a homogenous green appearance, (**C**) ChR2 ESCMN showing patchy GFP expression. (**B**) Center cross-section of HBG3 ESCMN showing cytoplasmic GFP expression (**D**) center cross-sectional image of ChR2 ESCMNs showing the membrane bound GFP expression with a dark cytoplasmic region. The level of GFP fluorescence intensity detected from the ChR2 ESCMNs (green region-left graph) is an entire logarithmic value lower compared HBG3 cells (green region-right graph). This yielding low purity in the sorted sample, this is shown by pie charts. HBG3 cell line pre-sort sample is only 22% GFP+ and post-FACS is 94% positive, yet the ChR2 ESCMNs start with 16% GFP+ and post-FACS are only 22% positive only a negligible increase in purity.

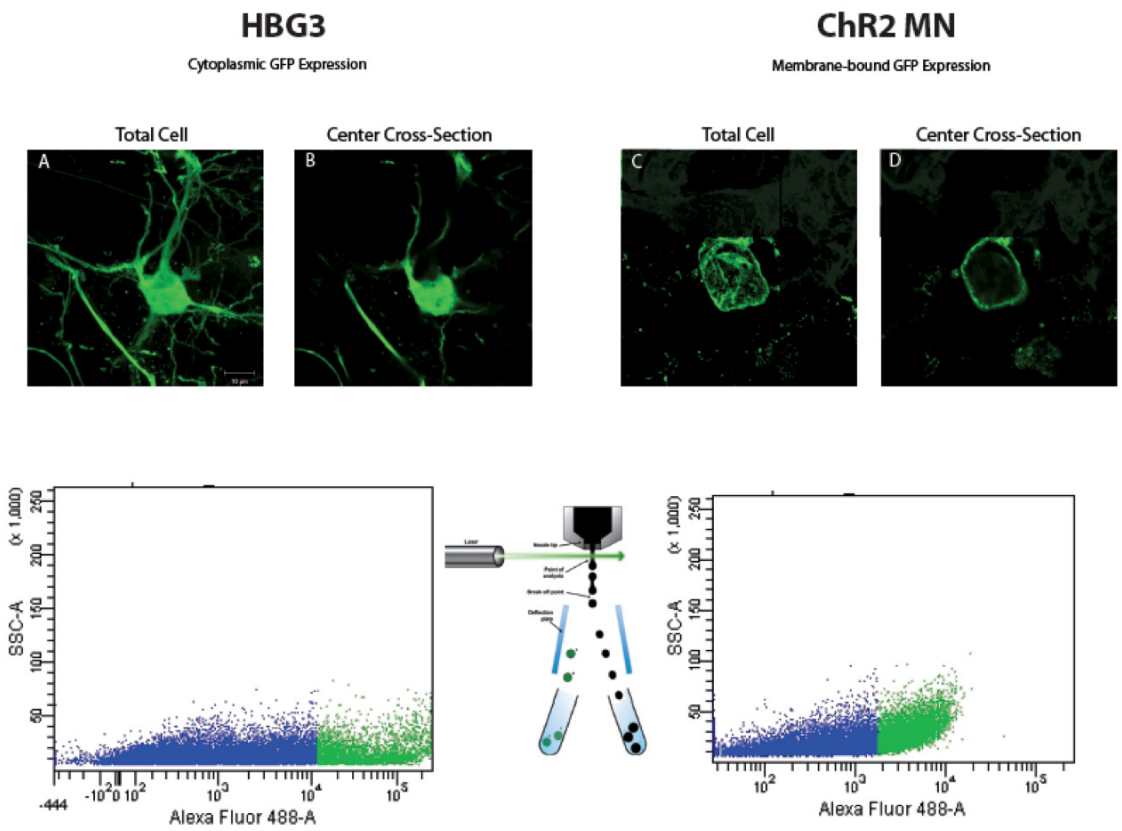
HBG3
Cytoplasmic GFP Expression
ChR2 MN
Membrane-bound GFP Expression
Total Cell
Center Cross-Section
Total Cell
Center Cross-Section
A
B
C
D
SSC-A
Alexa Fluor 488-A
SSC-A
Alexa Fluor 488-A

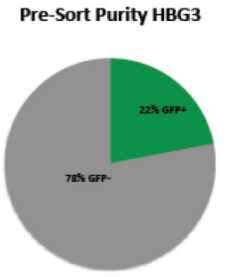
Pre-Sort Purity HBG3
22% GFP+
78% GFP-

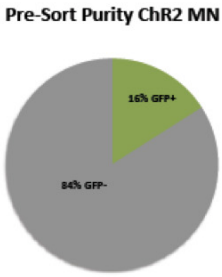
Pre-Sort Purity ChR2 MN
16% GFP+
84% GFP-

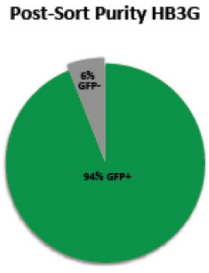
Post-Sort Purity HB3G
6% GFP-
94% GFP+

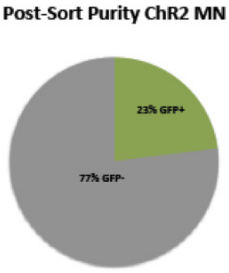
Post-Sort Purity ChR2 MN
23% GFP+
77% GFP-